TRANSPORTATION RESEARCH
RECORD

No. 1347

*Maintenance*

# Maintenance of Highway Structures

*A peer-reviewed publication of the Transportation Research Board*

TRANSPORTATION RESEARCH BOARD
NATIONAL RESEARCH COUNCIL

NATIONAL ACADEMY PRESS
WASHINGTON, D.C. 1992

**Transportation Research Record 1347**
Price: $21.00

Subscriber Category
IIIC maintenance

TRB Publications Staff
*Director of Publications*: Nancy A. Ackerman
*Senior Editor*: Naomi C. Kassabian
*Associate Editor*: Alison G. Tobias
*Assistant Editors*: Luanne Crayton, Susan Gober, Norman Solomon
*Office Manager*: Phyllis D. Barber
*Production Assistant*: Betty L. Hawkins

Printed in the United States of America

**Library of Congress Cataloging-in-Publication Data**
National Research Council. Transportation Research Board.

Maintenance of highway structures.
p. cm. — (Transportation research record, ISSN 0361-1981; no. 1347)
ISBN 0-309-05213-0
1. Bridges—Maintenance and repair. I. National Research Council (U.S.). Transportation Research Board. II. Series: Transportation research record ; 1347.
TE7.H5 no. 1347
[TG315]
388 s624'.28—dc20 92-23519
CIP

# Foreword

Proper and timely maintenance of the highway infrastructure is essential to obtaining the level of service needed by the traveling public and for commerce. Failure to identify and correct defects in a timely manner contributes to increased transportation costs and deterioration rates. This Record contains 12 papers on maintenance techniques and technologies applicable to highway structures. It should be of interest to engineers responsible for structures on the national, state, and local roadway systems.

Papers contain information on automated data collection technologies for recording bridge deficiencies, efforts to predict structure condition, vulnerability of bridges to hydraulic failure, use of radar to evaluate bridge deck conditions at highway speeds, use of high molecular weight methacrylate monomers on bridge decks, and benefits of including rebar corrosion rates in bridge deck condition surveys. Other topics are use of half-cell survey measurements to identify high potential gradients on bridges, new grouts used for bonded tendons in post-tensioned bridge structures, accelerated corrosion laboratory tests for metals, efforts to improve field measurements for structure chloride content, a calcium magnesium acetate – based deicing chemical, and infrared thermography to detect delaminations in reinforced concrete.

# Transportation Research Record 1347

## Contents

# Innovative Technology for Computer-Automated Bridge Inspection Process

S. S. KUO, THOMAS E. DAVIDSON, LEONARD M. FIJI, AND RICHARD KERR

A procedure is presented for automated data collection and reporting of bridge deficiencies. The procedure was developed under the sponsorship of the Florida Department of Transportation (FDOT). A computer program for field data collection based on FDOT's Condensed Inspection Report (CIR) was designed for a handheld computer. The program is used to input condition ratings and generate or edit comments for each bridge element on the CIR. A text-file record of the inspection is stored in the handheld computer for subsequent uploading to an office-based personal computer (PC) system. Visual information on bridge defects can be recorded with a camcorder or 35-mm camera, or by sketch. The images are digitized and stored on computer disk with an automated system developed for the PC. The PC system uses the JetForm form program to place the images and text-file inspection record onto the cover, CIR, Comprehensive Report of Deficiencies, and Image Log forms. The complete bridge inspection reports are saved to computer disks for archiving and for printing final copies on a laser printer. This automated procedure was tested in a FDOT bridge inspection district. Field inspection time was comparable with the conventional method; office time required for completion of reports was significantly reduced.

This study presents the design of a computer-automated bridge inspection system for the Florida Department of Transportation (FDOT). The purpose of the system is to increase field inspection organization and accuracy and to speed office-based report preparation. The field system uses a handheld computer, a video camera, and computer programs to aid the collection of bridge data. The office system combines a personal computer (PC), imaging equipment, and computer programs to assist report preparation and archiving.

In order to accomplish these tasks, the study includes procedures and equipment for automating bridge inspection data collection and reporting, development of data collection and reporting software, a test of the system in a FDOT bridge inspection district, and an evaluation of the inspection procedures.

## INSPECTION PROCEDURES

The proposed bridge inspection system for FDOT has two distinct parts: a field system and an office system. The field system has three tasks: to record numerical ratings of the condition of bridge components, provide an efficient method of entering narrative descriptions of bridge component defects, and visually document serious bridge component defects. The office system has four tasks: to place the bridge component condition ratings onto FDOT's Condensed Inspection Report (CIR), produce FDOT's Comprehensive Report of Deficiencies Section B narrative report describing bridge component defects, store and print photo logs of bridge component defects, and automatically integrate these sections into a bridge inspection report that can be easily archived on computer disk and printed.

The computer-automated bridge inspection system uses a portable computer programmed to be compatible with FDOT's bridge inspection reporting procedures. Past bridge inspection reports are uploaded to the portable computer from a desktop PC used to store bridge inspection data. Narrative descriptions of existing defects are edited by the inspectors. New descriptions of defects are keyed into the portable computer using a set of shorthand codes of commonly used descriptive words. Videotapes, photographs, or sketches are made of serious deficiencies and noted in the portable computer inspection program.

After all deficiencies have been documented, the inspectors enter ratings of each bridge element's condition. Descriptions of the condition of each element are displayed to the inspector before he or she enters a rating. When all ratings have been entered, the program assembles the data into files that can be transferred back to the PC at the inspection office.

On returning to the office, the inspectors download the new inspection data to the PC. A form-generation program assembles the data into a cover page, CIR, and Comprehensive Report of Deficiencies and prints these sections at the request of the inspectors. Digitizing programs request the video images, photographs, and sketches made during the inspection and convert them to formats that can be stored on the computer. Image logs containing descriptions of each defect visually documented on a bridge can then be printed at the inspectors' request.

Field work is accomplished by two-person teams. One inspector handles the portable computer while the other handles the video and photographic equipment. Tool belts and carrying cases were designed to make carrying and using the equipment easier. Small two-way radios provide communication for the inspectors if they are separated.

## FIELD EQUIPMENT

### Paravant RHC-44 Handheld Computer

FDOT specified that all field equipment be as lightweight and durable as possible. The Paravant RHC-44 is a lightweight

S. S. Kuo, Civil and Environmental Engineering Department, University of Central Florida, Orlando, Fla. 32816-4450. T. E. Davidson, Parsons DeLeuw, Inc., 2300 Maitland Center Parkway, Maitland, Fla. 32751. L. M. Fiji, California Department of Transportation, 120 South Spring Street, Los Angeles, Calif. 91012. R. Kerr, Florida Department of Transportation, Tallahassee, Fla. 32301.

handheld computer that uses removable battery-backed random access memory (RAM) cards that perform the same function as floppy disks in PCs. It is MS-DOS compatible and can be programmed in BASIC, C, FORTRAN, Ada, and Pascal.

### Sony CCD-TR5 Handycam 8-mm Camcorder

FDOT required that the camcorder chosen for the study be durable, provide clear pictures, be as small as possible, enable mounting of lights, and be usable underwater. No one camcorder meets all of these requirements, but the Sony CCD-TR5 camcorder meets most of them.

### Voice Actuated Audionic FM Transceiver

The Radio Shack Voice Actuated Audionic FM Transceiver was chosen as the communication device for this study because of its small size, economical price, and innovative design. The system has a single earpiece that functions as both a receiver and a microphone.

### Tool Belts

The portable field equipment just described can be carried easily with properly designed carrying cases and used on bridges. J.A.C. Custom Pouches of Marcellus, Michigan, used high-strength, weatherproof Cordura and polypropylene to custom make tool belts and carrying cases for the field equipment. Two special carrying cases were designed for the portable computer and camcorder.

## OFFICE EQUIPMENT

### PC

An MS-DOS PC based at the district inspection office is required to control the transfer and assembly of inspection data into a report. Because the computer-automated bridge inspection system depends heavily on computer graphics, a PC with a fast processors, large amount of internal memory, and high-quality video and storage subsystems is necessary. Figure 1 shows a schematic of the computer configuration recommended for the computer-automated bridge inspection system.

### Hewlett Packard Scanjet Plus Optical Scanner

The computer-automated bridge inspection system provides two ways to acquire images for storage on computer disk. The first of these methods uses the Hewlett Packard Scanjet Plus Optical Scanner to digitize photos and sketches. Scanned images can be saved on computer disk, displayed on a monitor, or printed.

### Sigma Designs Video Image Capture Board

The second method of acquiring images for computer storage uses the Sigma Designs Video Image Capture Board. The image capture board is an expansion card that accepts standard video signals from a video camera or video cassette recorder and digitizes frames for storage or display on a computer. Video frames can be displayed in real time on a separate television monitor or at three frames per second on the computer's video graphics array (VGA) display. In either case, frames are always captured in real time. Once captured, images can be saved in Tag Image File Format (TIFF), PC Paintbrush (PCX), or several other popular file formats.

### Hewlett Packard LaserJet Series II Printer with Intel Visual Edge Enhancement

To produce professional quality reports, a high-resolution printing device is needed. A laser printer was chosen for this study because of its ability to output high-resolution text and graphics at a relatively low cost. The laser printer selected for this study was the HP LaserJet Series II. The Intel Visual Edge Enhancement for the Series II is a set of add-on boards that enables the Series II to produce graphics with twice the quality and up to six times the speed of the Series II alone.

## FIELD DATA COLLECTION SOFTWARE

The field data collection software, which is written in Microsoft BASIC Professional Development System Version 7.0, is designed to run on the RHC-44 handheld computer. The software can also be run on any PC to enter existing data from conventional inspections before the field work. Bridge condition ratings and narrative defect descriptions are collected with the program and organized into files for transference to an office-based PC.

FDOT's CIR for static bridges organizes a bridge into six components: substructure, superstructure, deck, approach roadway, channel, and nonstructural. These components are further broken down into elements. The field data collection program is based on the structure of the CIR. Figure 2 shows the main menu of the field bridge inspection software known as BIS. BIS has built-in routines that check the validity of data entered. The program will warn the user if the data are not acceptable. The data acquisition program is divided into three components: general input, numerical condition ration (NCR) input, and comment input and generation.

The general input section handles data that relate to the cover sheet. These are the bridge numbers, date, and identification of inspectors. The software also asks the number of bridges to be inspected. Up to six bridges can be inspected simultaneously.

The NCR input section has built-in features to ensure that all components and elements are addressed. NCRs of elements that have comments in the Comprehensive Report of Deficiencies, Section B of the report, are automatically affixed with an asterisk. The user of the report then knows to

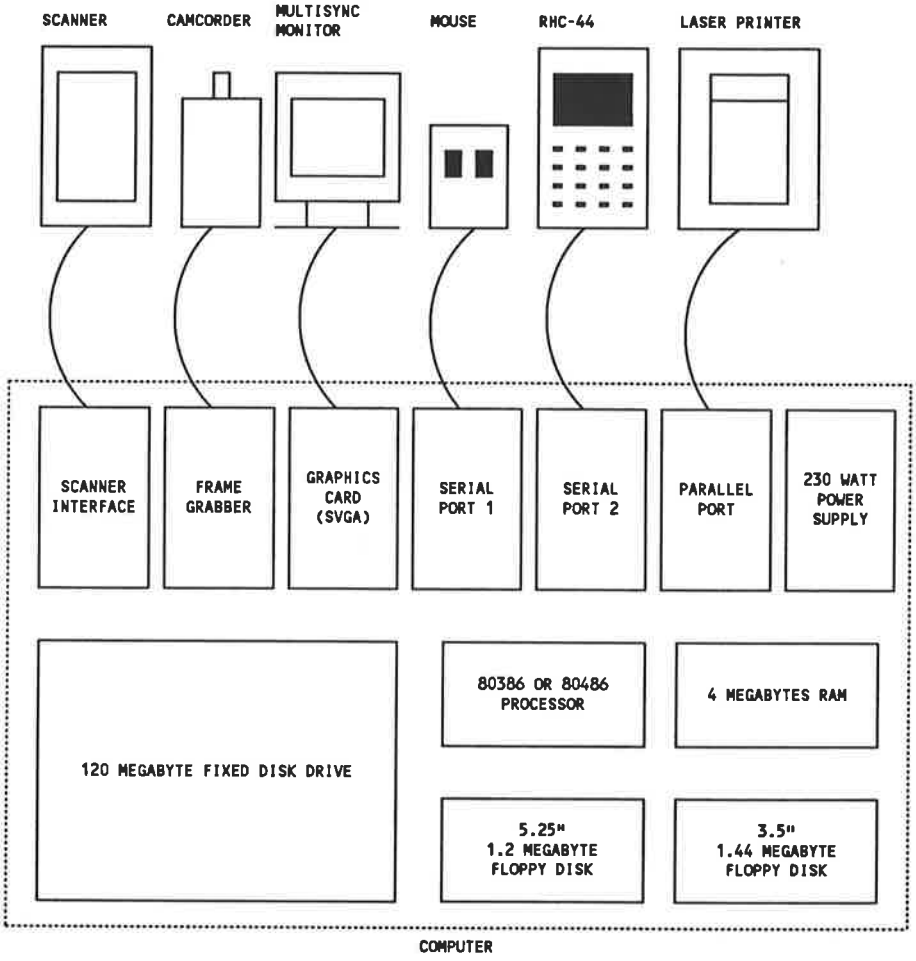


**FIGURE 1 Schematic of recommended hardware configuration for automated bridge inspection system.**

```
        BRIDGE INSPECTION PROGRAM
              MAIN  MENU

PRESS THE NUMBER OF THE ROUTINE
                                STATUS
 1  SUBSTRUCTURE        (NCR)  [   ]
 2  SUPERSTRUCTURE      (NCR)  [   ]
 3  DECK                (NCR)  [   ]
 4  APPROACH ROADWAY    (NCR)  [   ]
 5  CHANNEL             (NCR)  [   ]
 6  NON-STRUCTURAL      (NCR)  [   ]
 7  QUIT
 8  SHIFT TO ADJACENT BRIDGE
 9  COMMENTS ON ANY ELEMENT
```

**FIGURE 2 Data acquisition program main menu.**

look for a comment. An opportunity to change the NCRs assigned is also provided.

The comment input and generation section handles the generation and editing of comments on the deficiencies. New deficiencies are described and located in a standardized format. A built-in word processors provides flexibility of editing new and old comments.

At the completion of the inspection, the data are saved in a format compatible with the Jetform software. The duration of the inspection is then calculated and written to a file named TIME.LOG. The TIME.LOG file is also used to monitor the time interval of the activities for office preparation and printing of reports. Flowcharts of the bridge inspection software are shown in Figures 3–8.

## OFFICE REPORTING SOFTWARE

The office reporting software is separated into two categories: text handling software and image handling software. The text handling functions, such as data file transfer, text data editing, and text form printing, are controlled through the FDOT main menu. The image handling functions, such as video image capture, sketch and photo digitization, image editing, and image form printing are controlled from the image editing menu. The image editing menu is called from the FDOT main menu and always returns control back to the main menu.

### FDOT Main Menu

All of the office reporting functions of the computer-automated bridge inspection system are accessed through the

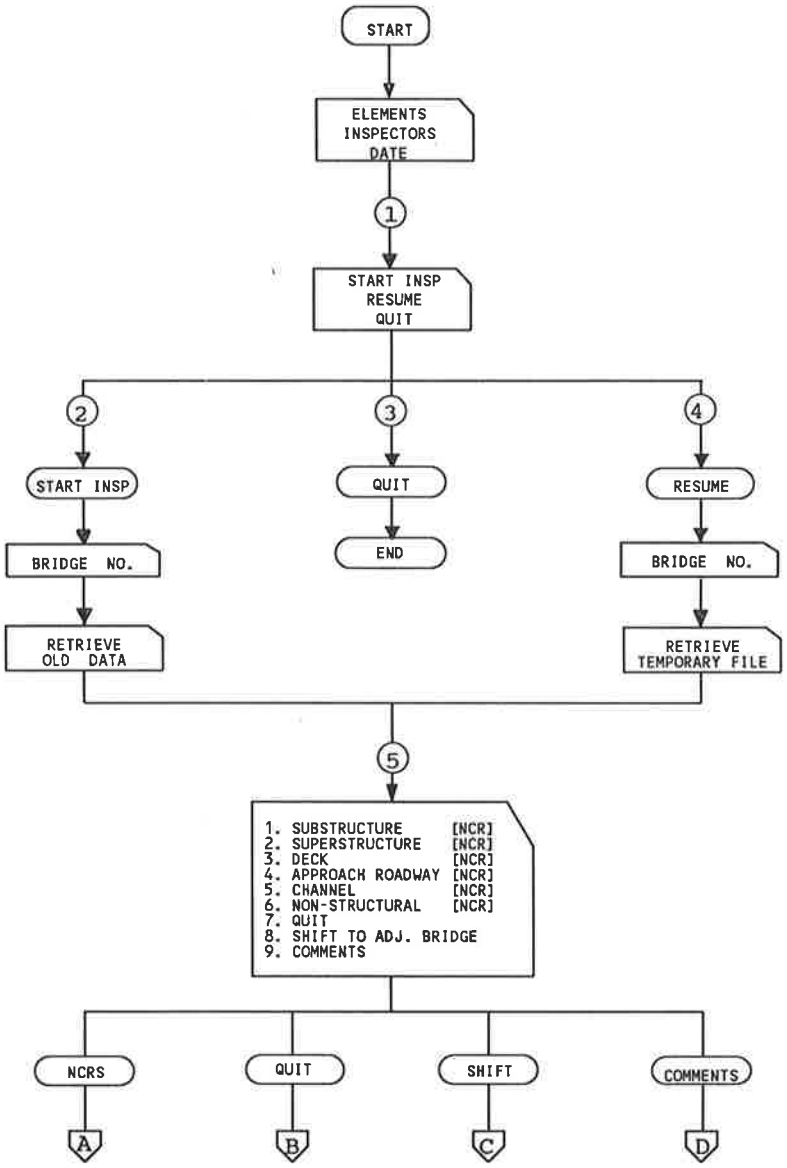


**FIGURE 3 Data acquisition flowchart, general input.**

FDOT main menu. The main menu is written in Microsoft BASIC Version 7.0. The menu brings together the large variety of commercial and original programming used to create the computer-automated bridge inspection system. A flowchart of the main menu is shown in Figure 9.

*Data Transfer*

Before a bridge is inspected with the RHC-44, the old inspection report is transferred from the PC. After returning from an inspection, inspectors must transfer updated inspection data back to the PC. Data are transferred between the RHC-44 and the PC through a serial cable connected to RS-232 ports on each computer. The FDOT main menu automates the transfer procedure. The bridge number is used to select the appropriate inspection files to transfer.

*Text Editing, Form Completion, and Printing*

Once all inspection data have been transferred to the PC, two options are available for adding comments or correcting mistakes. The first option, edit inspection data, uses a text editor called QEdit from SemWare to give access to the data in their original ASCII format. QEdit allows text to be typed, deleted, inserted, and copied, among other features. The edited file is then saved in ASCII format.

The second option for editing the inspection data, view or print cover, CIR, and Section B report, uses JetForm from Indigo Software. JetForm is a professional form design and completion program that operates with Microsoft Windows. The cover, CIR, and Section B forms were designed with JetForm. Data fields for all of the necessary inspection information were placed on the forms with JetForm's design module. The data fields are accessible through JetForm's form completion module.

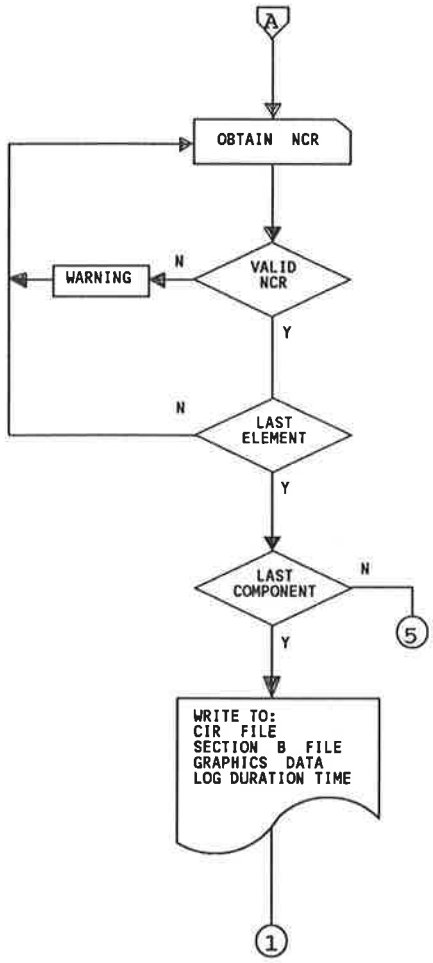


**FIGURE 4 Data acquisition flowchart, NCR input.**

The FDOT main menu calls the JetForm form completion module for the desired bridge. The form completion module uses the inspection data files for the bridge, which were structured to conform to JetForm's file format, to fill in the data fields on the forms. The data fields can then be stepped through one at a time or page by page for viewing or editing. The data files are updated with any changes or additions and saved to disk.

### Image Editing Menu

The purpose of the image editing menu is to coordinate the commercial and original software used for digitizing, annotating, and printing bridge defect images so that the process is as automated as possible. The image editing menu is a combination of two DOS batch files and a menu program written in Microsoft BASIC. Figure 10 shows a simplified block diagram of the interactions between the programs used by the image editing menu. The image editing menu allows easy access to each of the tasks involved in digitizing, editing, printing, and displaying images. The menu is accessed from FDOT main menu.

*Capturing and Converting Video Images*

Images from the camcorder are captured and converted to digital form with automated software that controls the Sigma Designs Image Capture Board. The digitized video pictures are saved in .SHW files that can be manipulated and displayed with computer software.

*Scanning Photos and Sketches*

The scanning process has been automated by a program called ScanDOT, which was specifically written for the computer-

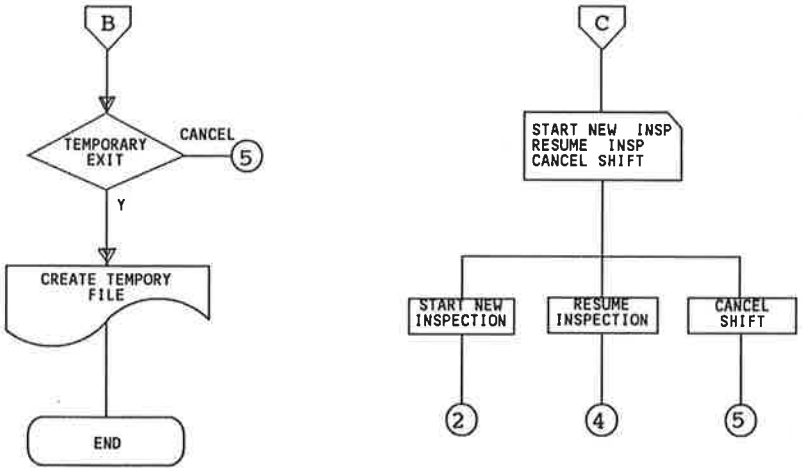


**FIGURE 5 Data acquisition flowchart, quit and shift section.**

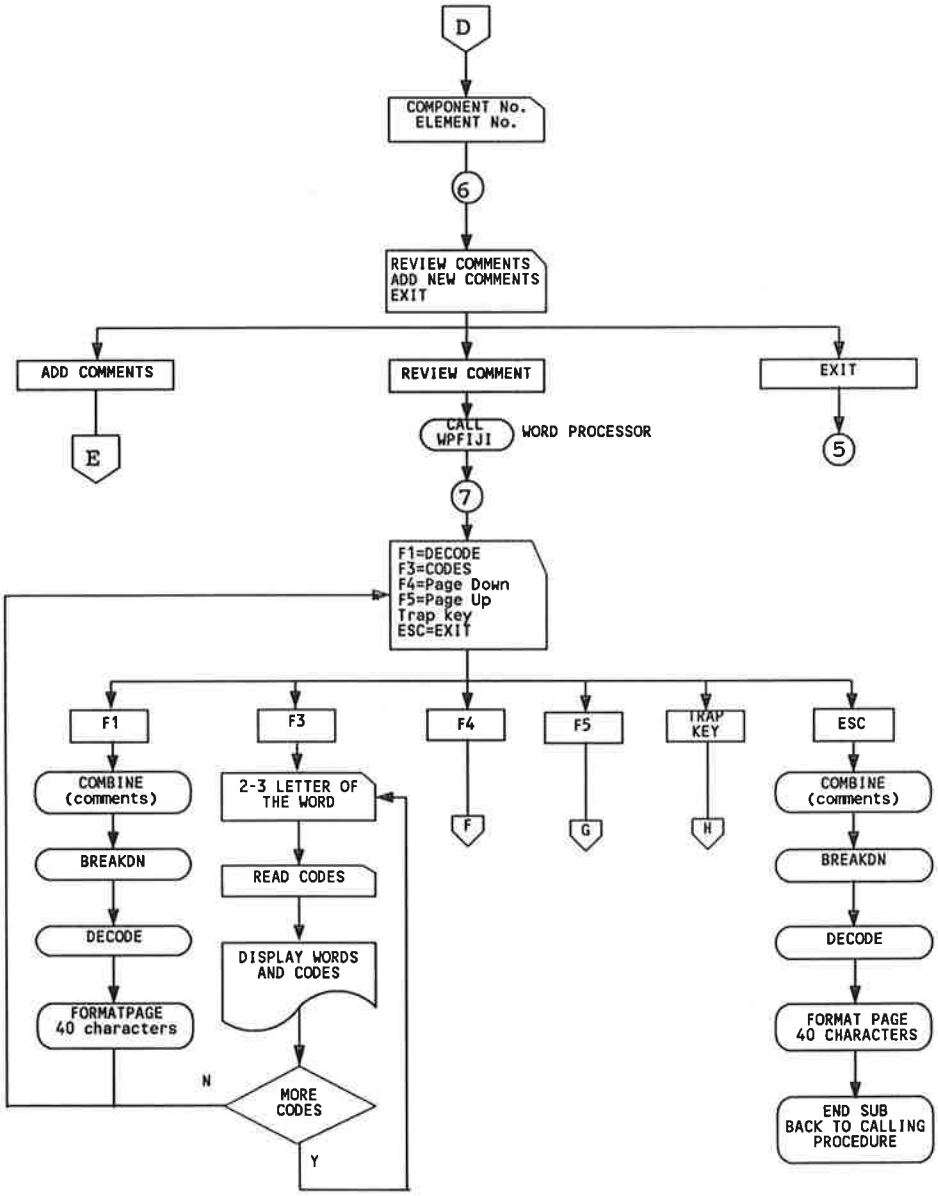


**FIGURE 6 Data acquisition flowchart, comment generation by word processor.**

automated bridge inspection system. ScanDOT reads the image-description file written by the bridge inspection program for a particular bridge and displays the descriptions for each image one by one on screen. The operator finds the picture or sketch matching the description, places it on the scanner, and begins the scan by pressing a key.

*Video Data Base of Structures*

Video images converted to the .SHW file format can be displayed on a VGA monitor by using the SHOW.COM utility program provided with the Sigma Designs Video Capture Board. A slideshow program that takes advantage of the SHOW.COM utility has been written to make the display of images easier.

*Form Utilities*

The image form utilities selection on the image menu allows three options for editing and printing image data and forms. The first option, view image forms, allows viewing of the forms as they will be printed with JetForm. The second option, edit image data, allows corrections of any typographical errors made in the field. The third option, print image forms, automatically prints out the finished image forms.

*Manually Editing and Printing Images*

PC Paintbrush IV Plus is the program used to manually edit and print photographs, sketches, and video images. The program has many sophisticated image enhancement functions if required, but is relatively easy to use.

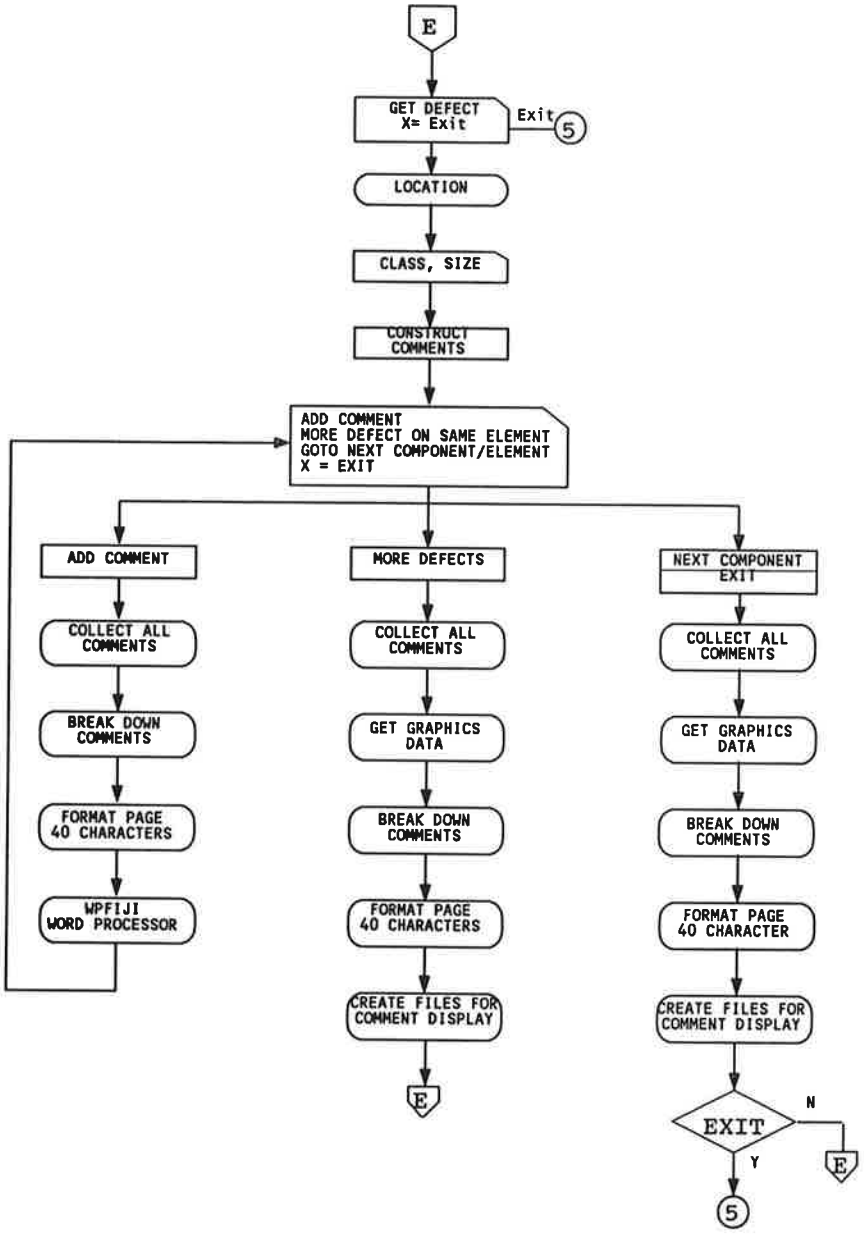


**FIGURE 7** Data acquisition flowchart, obtain defects.

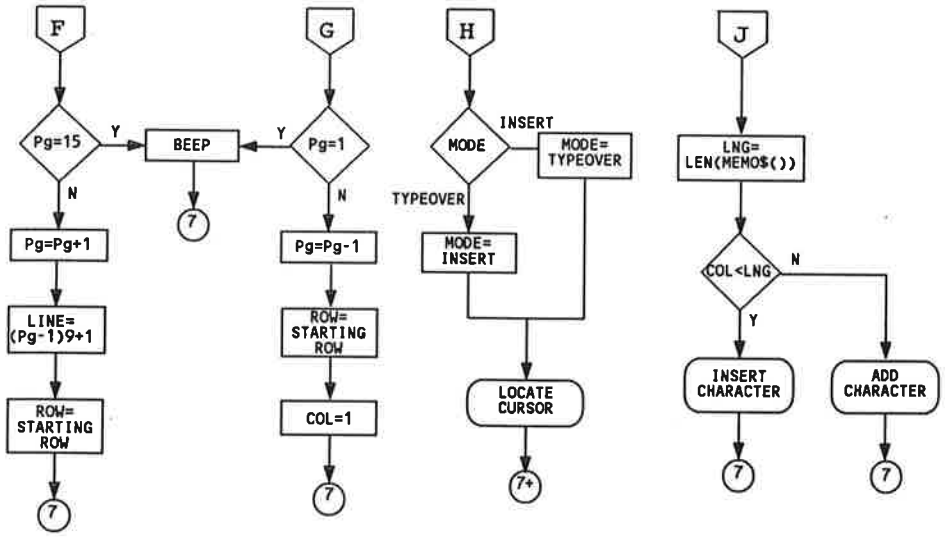


**FIGURE 8** Data acquisition flowchart, word processor editing functions.

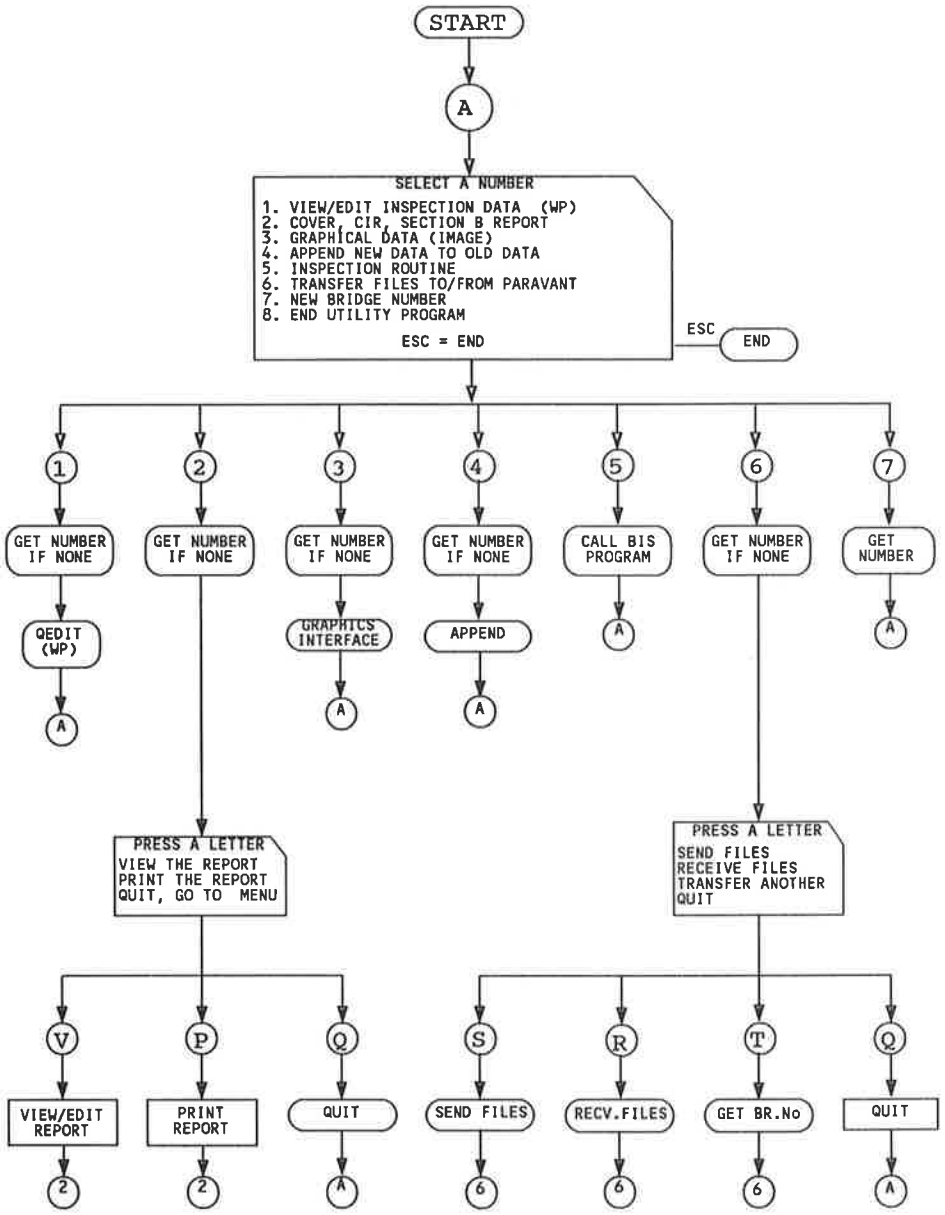


**FIGURE 9 Flowchart of utility program (FDOT main menu).**

## FIELD TESTING

Testing of the computer-automated bridge inspection system took place in FDOT's Bridge Inspection District One, which is located in the Tampa area. Experiments were undertaken 2 days a week for 8 weeks. Five bridge inspectors participated in the testing.

The field-testing procedure involved outfitting the inspectors with the automation equipment and monitoring them as they completed inspections. Completion times for the field and office procedures were recorded by the field and office computers. These times may be used in the future to compare efficiency and cost of the system with the conventional inspection procedure.

The field tests were conducted by two-person bridge inspection crews on actual bridge inspections. One member of the crew used the handheld computer; the other was responsible for the camcorder.

The bridge inspectors followed their normal inspection procedure while in the field. They entered or edited narrative descriptions of defects with the handheld computer and videotaped, sketched, or photographed major defects. After recording all defects, they would review the comments and rate each element of the bridge using the handheld computer. The time to complete these tasks was recorded by BIS. The results of the inspections are presented in Table 1.

Table 2 presents a comparison of the completion times for the automated and conventional bridge inspection procedures. The overall completion times for both methods are virtually identical (Table 2). However, office times were significantly less with the automated process. Simply comparing completion times, however, does not take into account other

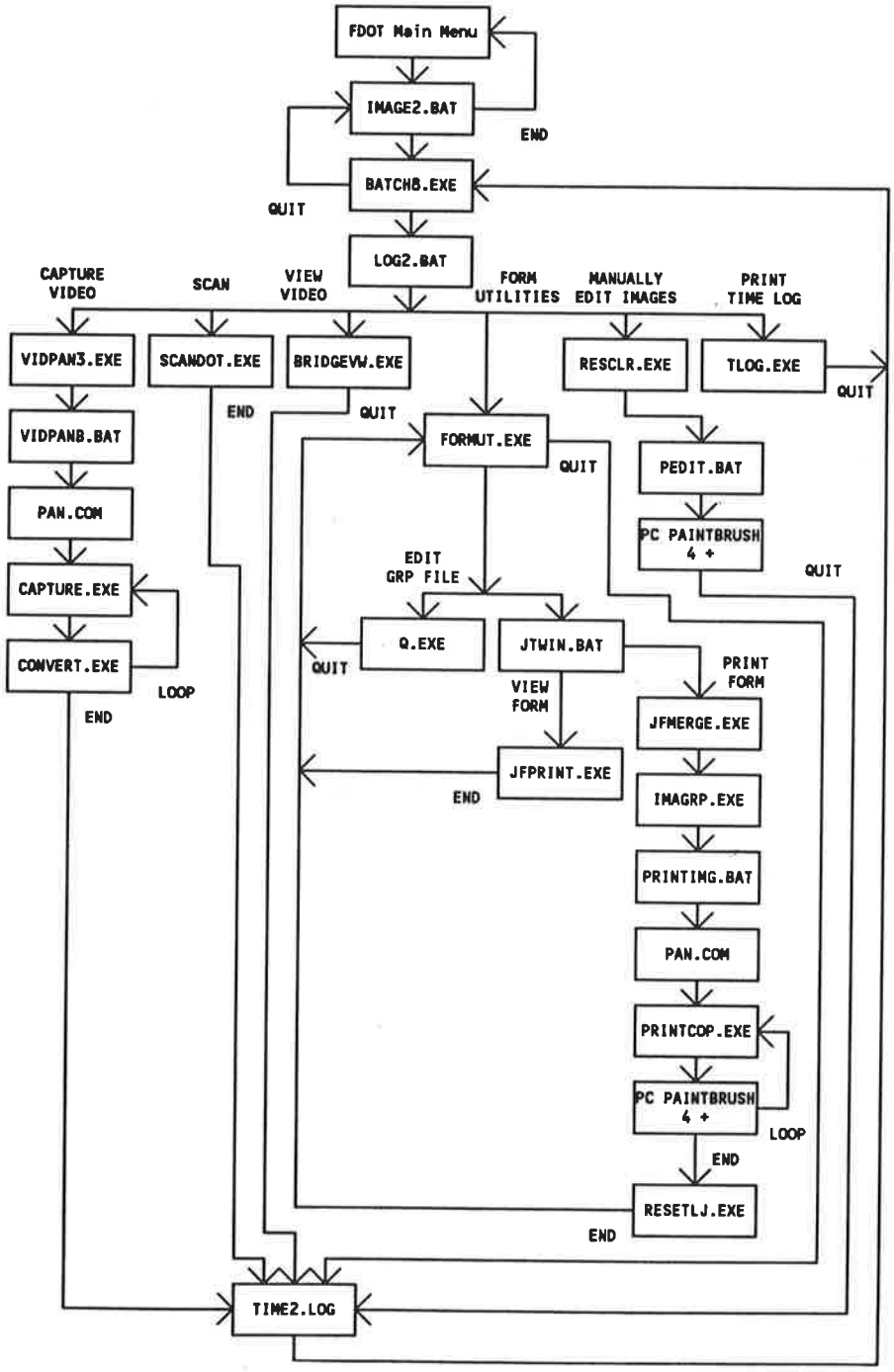


**FIGURE 10 Block diagram of image editing menu program interaction.**

important benefits of the computer-automated bridge inspection system.

## RESULTS AND CONCLUSIONS

The computer-automated bridge inspection system was tested in FDOT Bridge Inspection District One for 8 weeks. Field data collection time averaged 56 min. This time is 26 min more than the 30 min estimated average of the current method. However, two of the five bridge inspections required less than 30 min for data collection. It is estimated that once inspectors became thoroughly familiar with the automated data collection system, they would require no more time than with the conventional method.

Report preparation averaged 24 min, a 21-min savings over the conventional report preparation method. Reports are completed by inspectors without the aid of typists. A list of other benefits from this system follows.

- Data are organized and handled efficiently by computer software.

**TABLE 1 Inspection Times for Computer-Automated Bridge Inspection System**

| BRIDGE # | 100238 | 100124 | 100216 | 100075 | 550064 |
|---|---|---|---|---|---|
| DATE | 05-02-90 | 05-09-90 | 06-04-90 | 06-05-90 | 06-14-90 |
| TYPE | PRE-STRESSED CONCRETE | PRE-STRESSED CONCRETE | PRE-STRESSED CONCRETE | STEEL | STEEL |
| SPANS/ LENGTH | 3/153' | 3/146' | 3/135' | 6/151' | 6/398' |
| SKETCHES | 2 | 0 | 2 | 11 | 1 |
| PHOTOS | 0 | 0 | 0 | 0 | 0 |
| VIDEO | 0 | 2 | 0 | 0 | 2 |
| SECTION B PAGES | 1 | 1 | 1 | 2 | 1 |
| FIELD TIME (MIN.) | 71 | 92 | 27 | 62 | 29 |
| OFFICE TIME (MIN.) | 8 | 38 | 9 | 42 | 23 |
| TOTAL TIME (MIN.) | 79 | 130 | 36 | 104 | 52 |

- Inspection reports have a consistent format.
- Inspection data are stored on computer disk.
- Transfer of bridge inspection reports between offices can be done electronically.
- Data are accessible through FDOT's bridge management system.
- Computer software ensures that data are complete before inspectors leave the bridge site.
- Consultant reports would more easily conform to FDOT specifications.

The following statement was made by Dewey Oliver, District One Structures and Facilities Engineer:

> It is my estimate that once this system is fully implemented, a savings in excess of $500,000 per year will be realized on inspection of state structures. If we require consultants to use the system, then we can double our savings.

Our current process allows 45 days from inspection until the report is finalized. We average 30 days in our current process. Using the automated process, this time frame could be reduced to under 5 days. In most cases we have tested so far, an inspection report preparation and report finalization have occurred in less than 5 hours.

**TABLE 2 Comparison of Average Completion Times for Typical Bridge**

| PROCEDURE | AUTOMATED INSPECTION METHOD | CONVENTIONAL INSPECTION METHOD |
|---|---|---|
| PREPARATION FOR INSPECTION (MIN.) | 15 | 15 |
| INSPECTION (MIN.) | 56 | 30 |
| PREPARING SKETCHES (MIN.) | 30 | 30 |
| REPORT COMPLETION (MIN.) | 24 | 45 |
| PROOFING (MIN.) | 5 | 5 |
| TOTAL TIME (MIN.) | 130 | 125 |

TYPICAL BRIDGE IS LESS THAN 600 FEET IN LENGTH.

## ACKNOWLEDGMENTS

The authors gratefully acknowledge FDOT for its sponsorship; they are particularly grateful to Larry Davis, Chief Maintenance Engineer, and Dewey Oliver, District Structures and Facilities Engineer, for their inputs and cooperation during the trial field-implementation period.

*Publication of this paper sponsored by Committee on Structures Maintenance and Management.*

# Simulation Approach to Prediction of Highway Structure Conditions

YI JIANG AND KUMARES C. SINHA

Various techniques, either statistical or stochastic, have been applied to predict highway structure conditions. Researchers found the stochastic approach more appropriate than the statistical approach in highway project selections using dynamic optimization techniques. However, it was also found that condition predictions using the Markov chain could be biased, depending on the values of transition probabilities. In an attempt to minimize the bias in Markov chain predictions, the Monte Carlo simulation technique was applied in the present study in combination with transition probabilities obtained from Markov chain approaches. This study showed that the simulation method could produce more realistic predictions than the analytical Markov chain approach. The Monte Carlo simulation method is described and compared with the analytical Markov chain method. An application example is presented to show the mechanism of the Monte Carlo simulation method and to compare the results of the simulation and Markov chain predictions.

Stochastic processes, such as the Markov chain, have been successfully applied to predict pavement and bridge conditions (*1,2*). Advantages of the stochastic approach over the statistical approach were exhibited in highway project selections using dynamic optimization techniques (*3*). However, as with any other prediction techniques, uncertainty, randomness, and unrealistic assumptions are also involved in the stochastic techniques. It was found in this study that condition predictions using the Markov chain could be biased, depending on the values of transition probabilities. In an attempt to minimize bias in the Markov chain predictions, the Monte Carlo simulation technique was applied in combination with the transition probabilities obtained from Markov chain approaches. The Monte Carlo simulation method generates random numbers and compares these random numbers with transition probabilities of the Markov chain to determine the future condition of highway structures. The present study showed that the simulation method could produce more realistic predictions than the Markov chain approach. The simulation method is described here and is compared with the analytical Markov chain method. Although this prediction technique can be used for estimating conditions of any highway structures, bridge condition predictions are made in this paper for demonstration purpose. The Markov chain prediction model developed earlier for the Indiana Bridge Management System (*2*) is therefore briefly described to introduce the Markov chain transition probabilities and to compare the results of the two approaches.

Y. Jiang, Indiana Department of Transportation, Division of Research, 1205 Montgomery Street, Box 2279, West Lafayette, Ind. 47906. K. C. Sinha, School of Civil Engineering, Purdue University, West Lafayette, Ind. 47907.

## MARKOV TRANSITION PROBABILITIES

The Markov chain as applied to bridge performance prediction is based on the concept of defining states in terms of bridge condition ratings and obtaining the probabilities of bridge condition changing from one state to another (*2*). These probabilities are represented in a matrix form that is called the transition probability matrix, or transition matrix, of the Markov chain. Knowing the present state of bridges, or the initial state, the future conditions can be predicted through multiplications of initial state vector and the transition probability matrix.

According to the FHWA bridge rating system, bridge inspectors rate each inspected bridge with a number between 0 and 9, with 9 being the maximum rating number for the condition of a new bridge (*4*). The condition ratings below 3 need not be included in the Markov chain transition matrixes because the lowest rating number before a bridge is repaired or replaced is generally taken to be 3. Seven bridge condition ratings can be defined as seven states with each condition rating corresponding to one of the states. For example, condition Rating 9 is defined as State 1, Rating 8 as State 2, and so on. Without repair or rehabilitation, the bridge condition rating decreases as the bridge age increases. Therefore, there is a probability of condition changing from one state, say $i$, to another state, $j$, during a given period of time, which is denoted by $p_{i,j}$

Let the transition probability matrix of the Markov chain be $P$, given by

$$p = \begin{vmatrix} P_{1,1} & P_{1,2} & \cdot & \cdot & \cdot & P_{1,7} \\ \cdot & \cdot & \cdot & \cdot & \cdot & \cdot \\ \cdot & \cdot & \cdot & \cdot & \cdot & \cdot \\ \cdot & \cdot & \cdot & \cdot & \cdot & \cdot \\ P_{7,1} & P_{7,2} & \cdot & \cdot & \cdot & P_{7,7} \end{vmatrix} \quad (1)$$

The state vector for any time $T$, $Q_{(T)}$, can be obtained by the multiplication of initial state vector $Q_{(0)}$ and the $T$th power of the transition probability matrix $P$:

$$Q_{(T)} = Q_{(0)} * P * P * \ldots * P = Q_{(0)} * P^T \quad (2)$$

where $Q_{(0)}$ and $Q_{(T)}$ are the vector expressions of condition ratings at time 0 and $T$, respectively, and can be converted to condition rating values (*2*). Because the present condition $[Q_{(0)}]$ is known, the future condition at any given time $T$ can be predicted as long as the transition matrix $P$ is given.

The inspection of bridges includes ratings of individual components, such as deck, superstructure, and substructure, as well as of the overall bridge condition. Unless rehabilitation or repair is applied, bridge structures gradually deteriorate, so that the bridge condition ratings are either unchanged or changed to a lower number during a given time period. That is, a bridge condition rating should decrease or remain the same as the bridge ages. Therefore, the probability $p_{i,j}$ is null for $i > j$, where $i$ and $j$ represent the states in the Markov chain.

Because the rate of deterioration of bridge condition is different at different bridge ages, the transition process of bridge conditions is not homogeneous with respect to bridge age. However, a Markov process requires a presumption of homogeneity (*5*). Therefore, if only one transition matrix were used throughout a bridge's life span, the inaccuracy of condition estimation would occur as a result of nonhomogeneity of the condition transition process. To avoid overestimating or underestimating the bridge condition, an approach called zoning technique (*1*) was used to obtain the transition matrix.

A 1-year transition period was used in developing Markov chain transition matrixes. In other words, $p_{i,j}$ was the transition probability from State $i$ to State $j$ during 1 year. Bridge age was divided into groups, and within each age group the Markov chain was assumed to be homogeneous. A 6-year group was found appropriate for the data base as well as for solving equations of unknown probabilities. A separate transition matrix was developed for each group.

To make the computations simple, an assumption was made that the bridge condition rating would not drop by more than one state in a single year. Thus, the bridge condition would either stay in its current state or fall to the next lower state in 1 year. Therefore, the transition matrix of condition ratings has the following form:

$$P = \begin{vmatrix} p(1) & q(1) & 0 & 0 & 0 & 0 & 0 \\ 0 & p(2) & q(2) & 0 & 0 & 0 & 0 \\ 0 & 0 & p(3) & q(3) & 0 & 0 & 0 \\ 0 & 0 & 0 & p(4) & q(4) & 0 & 0 \\ 0 & 0 & 0 & 0 & p(5) & q(5) & 0 \\ 0 & 0 & 0 & 0 & 0 & p(6) & q(6) \\ 0 & 0 & 0 & 0 & 0 & 0 & 1 \end{vmatrix} \quad (3)$$

where $q(i) = 1 - p(i)$. $p(i)$ is corresponded to $p_{i,i}$ and $q(i)$ to $p_{i,i+1}$ in Equation 1. Therefore, $p(1)$ is the transition probability from Rating 9 (State 1) to Rating 9, and $q(1)$, from Rating 9 to Rating 8, and so on.

Because the lowest rating number before a bridge is repaired or replaced is 3, the corresponding transition probability $p(7)$ equals 1. For each age group the transition probabilities were obtained by minimizing the absolute distance between the average bridge condition rating at a certain age and the predicted bridge condition for the corresponding age generated by the Markov chain (*2*). With the obtained transition matrixes, the future condition can be predicted by using Equation 2.

To show the process of Markov chain prediction, a simple example is presented as follows. Suppose a concrete bridge on an Interstate highway is 35 years old now and has a deck condition rating of 6. It is desired to predict the deck condition in the next year. The transition matrix for the deck of this type of bridges of 31 to 36 years old was obtained (*2*):

$$P = \begin{vmatrix} 0.44 & 0.56 & 0 & 0 & 0 & 0 & 0 \\ 0 & 0.50 & 0.50 & 0 & 0 & 0 & 0 \\ 0 & 0 & 0.40 & 0.60 & 0 & 0 & 0 \\ 0 & 0 & 0 & 0.40 & 0.60 & 0 & 0 \\ 0 & 0 & 0 & 0 & 0.25 & 0.75 & 0 \\ 0 & 0 & 0 & 0 & 0 & 0.20 & 0.80 \\ 0 & 0 & 0 & 0 & 0 & 0 & 1.0 \end{vmatrix} \quad (4)$$

The deck condition rating is 6, and the initial state vector $Q_{(0)}$ of the bridge deck is [0 0 0 1 0 0 0], where the numbers are the probabilities of the condition ratings being 9, 8, 7, . . . , and 3, respectively. Because it is known that the current condition rating is 6, the number corresponding to Rating 6 in $Q_{(0)}$ is 1, and others are 0. Thus, $Q_{(1)}$ can be predicted using Equation 2:

$$Q_{(1)} = Q_{(0)} \times P$$

$$= [0001000] \begin{vmatrix} 0.44 & 0.56 & 0 & 0 & 0 & 0 & 0 \\ 0 & 0.50 & 0.50 & 0 & 0 & 0 & 0 \\ 0 & 0 & 0.40 & 0.60 & 0 & 0 & 0 \\ 0 & 0 & 0 & 0.40 & 0.60 & 0 & 0 \\ 0 & 0 & 0 & 0 & 0.25 & 0.75 & 0 \\ 0 & 0 & 0 & 0 & 0 & 0.20 & 0.80 \\ 0 & 0 & 0 & 0 & 0 & 0 & 1.0 \end{vmatrix} \quad (5)$$

or

$$Q_{(1)} = [0\ 0\ 0\ 0.40\ 0.60\ 0\ 0]$$

$Q_{(1)}$ can then be converted to a rating number, $r_1$, by multiplying a vector of condition ratings $R$:

$$r_1 = Q_{(1)} \times R$$

$$= [0\ 0\ 0\ 0.40\ 0.60\ 0\ 0] \begin{vmatrix} 9 \\ 8 \\ 7 \\ 6 \\ 5 \\ 4 \\ 3 \end{vmatrix} = 5.4 \approx 5 \quad (6)$$

Therefore, the deck condition rating in the next year is predicted as 5. It should be noted that the predicted value was rounded to its nearest integer number because the rating system uses only integers as rating numbers.

An examination of matrixes $Q_{(0)}$ and $P$ reveals that $Q_{(0)}$ has only one nonzero element, and each row, except the last row, in $P$ has only two nonzero elements. This indicates that the Markov chain prediction of the next year's condition rating $r_1$ is affected by only the transition probabilities corresponding to the current condition rating $r_0$, or $p(i)$ and $q(i) = 1 - p(i)$, where $i$ is the condition state of $r_0$ as defined in Equation 3. Therefore, the previous computations can be simplified as follows:

$$r_1 = r_0 \times p(i) + (r_0 - 1) \times q(i) \quad (7)$$

where $i$ is the condition state corresponding to the given condition rating. Thus, the prediction of the deck condition rating can be made in one step:

$$r_1 = 6 \times 0.4 + 5 \times 0.6 = 5.4 \approx 5. \quad (8)$$

## SIMULATION APPROACH

Simulation techniques are widely used by engineers and researchers to analyze the behavior of real systems using computers. The Monte Carlo method (*6*) is one of the most commonly used simulation techniques for engineering modeling. Through the Monte Carlo method, a decision is made by comparing a random number generated by computer to a known probability value of the given problem.

Bridge condition deterioration is a probabilistic process and not a deterministic one. Therefore, the Monte Carlo method is suitable for predicting bridge conditions as long as the probabilities of condition changes are determined. If the deck condition rating in the previous example is predicted by the Monte Carlo method, the following steps would be necessary.

1. Generate a random number from a uniform distribution in the interval [0.0, 1.0] using a computer or any other method (such as a random number table).
2. If the random number $\leq 0.40$, the predicted condition rating is 6. If the random number $>0.40$, the predicted condition rating is 5.

In this simulation, each of the uniform random numbers in the interval [0.0, 1.0] has an equal chance of occurring. Therefore, the probabilities of a random number falling into the interval [0.0, 0.40] and the interval [0.40 1.0] are 0.40 and 0.60, respectively, exactly the same as the given probabilities.

Transition probabilities for different types of bridges at different bridge ages were developed in an earlier study (*2*). The Monte Carlo technique was applied in bridge condition prediction using these probabilities. In this study, a simulation program in FORTRAN 77 was developed on a UNIX computer to predict bridge conditions. Random numbers can be generated by the program using a FORTRAN random number subroutine. Figure 1 shows a flow chart of the simulation prediction model. RNUN is an IMSL (*7*) subroutine which generates a uniformly distributed random number once it is called. This program can be used to predict the future conditions of a number of bridges. It can be modified to predict the conditions of highway structures other than bridges, such as pavements. To do so, a user needs to obtain the appropriate probabilities of condition deterioration of the structure, incorporate these probabilities into the program, and change the appropriate IF-THEN conditions.

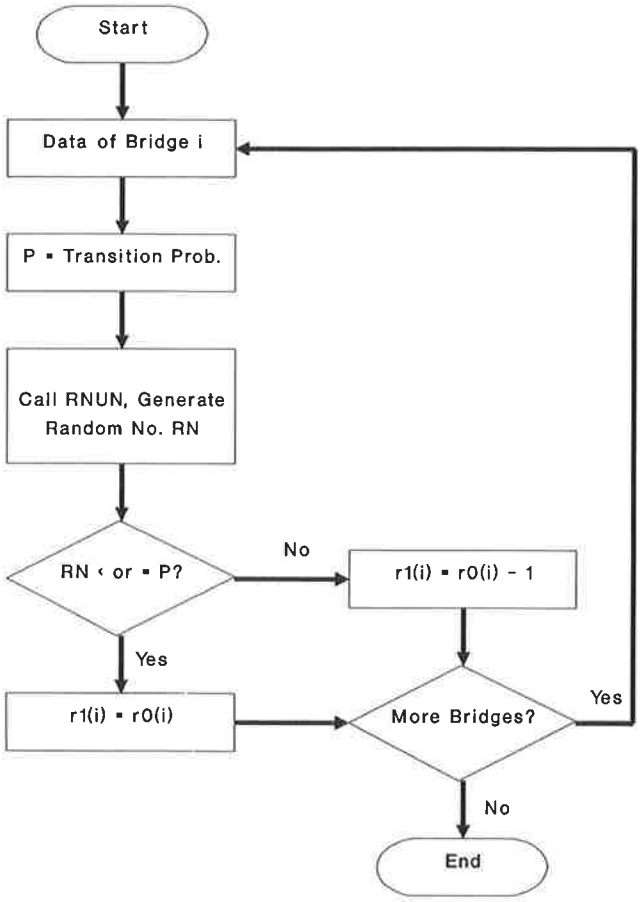


**FIGURE 1 Flowchart of simulation prediction program.**

## COMPARISON OF THE TWO APPROACHES

Both the Monte Carlo simulation and Markov chain analytical methods use transition probabilities to estimate bridge conditions. However, the results of the predictions are generally not the same because of the different mechanisms involved.

A random number generated in the Monte Carlo simulation has an equal chance of falling into any point in the interval [0.0, 1.0]. It is therefore expected that Monte Carlo estimation will closely reflect the given probability value when the number of bridges involved is reasonably large. For example, if there are 100 bridges with deck condition ratings of 6, the Monte Carlo simulation [$p(4) = 0.4$ from Equation 4] would yield a prediction that about 40 bridge decks will remain in Rating 6, and nearly 60 decks will deteriorate to Rating 5 in the next year.

On the other hand, as indicated by Equations 7 and 8, the Markov chain method predicts the deck condition ratings of all the 100 bridges as 5. The transition probability of $p(4) = 0.4$ means that for about 40 out of 100 bridges, or 40 percent, the deck condition rating would remain at 6 after 1 year. However, the future condition ratings of all the 100 bridge (100 percent) decks are predicted at 5 by the Markov chain method (Equation 8). The Markov chain method would, in this case, lead to an overestimation of bridge needs. As a result, the estimated budget and other resources needed for the coming year would be higher than what might be needed. Depending on the value of a transition probability, the Markov chain method can also underestimate the number of bridges that would deteriorate to a lower condition rating. This can be shown by writing Equation 7 as follows because $q(i) = 1 - p(i)$:

$$r_1 = r_0 + p(i) - 1 \tag{9}$$

Therefore, if $p(i) \geq 0.5$, $r_1$ is rounded to $r_0$, and if $p(i) < 0.5$, $r_1$ is rounded to $r_0 - 1$. In the former case [$p(i) \geq 0.5$], the number of bridges that would deteriorate to deck rating $r_0 - 1$ will be underestimated by the Markov chain method. In the latter case, the number will be overestimated.

To demonstrate the differences between the two prediction methods, 30 bridges were selected from the Indiana bridge

inventory file for estimation of deck conditions and repair costs if rehabilitation was found to be necessary. Table 1 presents the condition and cost information of these bridges and the prediction results of the Monte Carlo simulation and Markov chain methods. All the bridges had deck condition ratings of 6 and were 31 to 36 years old. The corresponding transition probabilities for these bridge decks were $p(4) = 0.4$ and $q(4) = 1 - p(4) = 0.6$. If a deck condition rating was equal to or less than 5, the bridge deck was considered a candidate for rehabilitation. To schedule the bridge rehabilitation activities for the next year, it was therefore necessary to estimate the number of bridge decks that would have a rating value of 5 the following year. The predictions of the condition ratings and the associated rehabilitation costs for the next year, made by both simulation and Markov chain methods, are also included in Table 1.

Using the Monte Carlo method, the deck condition of each bridge was predicted by generating a random number and comparing it with the transition probability 0.4. If the random number was less than or equal to 0.4, the predicted deck rating was 6; otherwise, the rating was 5. For the Markov chain method, Equation 7 was used to predict the future deck condition ratings. Because the decks with ratings of 6 would not be rehabilitated, their corresponding repair costs were estimated as $0 for the next year. However, if a deck rating was predicted to fall to 5, its estimated rehabilitation cost was included in the next year's total rehabilitation cost.

As shown in Table 1, the simulation method predicted that the rating of 13 bridge decks would remain at 6, and the ratings of 17 bridge decks would deteriorate 5 after one year. The predicted percentages of bridge decks remaining at Rating 6 and dropping to Rating 5 were 43 percent and 57 percent,

**TABLE 1 Results of Simulation and Markov Chain Predictions**

| Bridge No. | Current Deck Rating ($r_0$) | Rehab. Cost ($\$10^3$) | Simulation Prediction | | | Markov Prediction | |
|---|---|---|---|---|---|---|---|
| | | | Random No. | $r_1$ | Cost ($\$10^3$) | $r_1$ | Cost ($\$10^3$) |
| 1 | 6 | 235 | 0.2682 | 6 | 0 | 5 | 235 |
| 2 | 6 | 276 | 0.4435 | 5 | 276 | 5 | 276 |
| 3 | 6 | 387 | 0.9589 | 5 | 387 | 5 | 387 |
| 4 | 6 | 281 | 0.0986 | 6 | 0 | 5 | 281 |
| 5 | 6 | 107 | 0.5558 | 5 | 107 | 5 | 107 |
| 6 | 6 | 121 | 0.2997 | 6 | 0 | 5 | 121 |
| 7 | 6 | 210 | 0.1469 | 6 | 0 | 5 | 210 |
| 8 | 6 | 400 | 0.9883 | 5 | 400 | 5 | 400 |
| 9 | 6 | 257 | 0.6276 | 5 | 257 | 5 | 257 |
| 10 | 6 | 330 | 0.4300 | 5 | 330 | 5 | 330 |
| 11 | 6 | 270 | 0.2014 | 6 | 0 | 5 | 270 |
| 12 | 6 | 201 | 0.9986 | 5 | 201 | 5 | 201 |
| 13 | 6 | 205 | 0.0605 | 6 | 0 | 5 | 205 |
| 14 | 6 | 476 | 0.0528 | 6 | 0 | 5 | 476 |
| 15 | 6 | 102 | 0.1994 | 6 | 0 | 5 | 102 |
| 16 | 6 | 154 | 0.8356 | 5 | 154 | 5 | 154 |
| 17 | 6 | 621 | 0.1956 | 6 | 0 | 5 | 621 |
| 18 | 6 | 176 | 0.6856 | 5 | 176 | 5 | 176 |
| 19 | 6 | 124 | 0.1284 | 6 | 0 | 5 | 124 |
| 20 | 6 | 159 | 0.2720 | 6 | 0 | 5 | 159 |
| 21 | 6 | 247 | 0.1352 | 6 | 0 | 5 | 247 |
| 22 | 6 | 169 | 0.8433 | 5 | 169 | 5 | 169 |
| 23 | 6 | 93 | 0.4900 | 5 | 93 | 5 | 93 |
| 24 | 6 | 800 | 0.7173 | 5 | 800 | 5 | 800 |
| 25 | 6 | 500 | 0.6396 | 5 | 500 | 5 | 500 |
| 26 | 6 | 635 | 0.2340 | 6 | 0 | 5 | 635 |
| 27 | 6 | 545 | 0.8986 | 5 | 545 | 5 | 545 |
| 28 | 6 | 385 | 0.8000 | 5 | 385 | 5 | 385 |
| 29 | 6 | 193 | 0.9178 | 5 | 193 | 5 | 193 |
| 30 | 6 | 288 | 0.4251 | 5 | 288 | 5 | 288 |
| Total | | 8,947 | | | 5,261 | | 8,947 |

respectively. They were close to the given transition probabilities of 0.4 (or 40 percent) and 0.6 (or 60 percent). However, results from the Markov chain method predicted that the ratings of all 30 bridge decks (or 100 percent) would decrease from 6 to 5 in the next year (Equation 8).

The total cost of repairing all 30 bridges was \$8,947,000. The total expected cost for the next year can be computed using the transition probabilities (0.4 and 0.6) and estimated costs (\$0 for $r_1 = 6$; $c_i$ for $r_1 = 5$) of individual bridges:

$$\text{Total expected cost} = \sum_{i+1}^{30} (0.4 \times \$0 + 0.6 \times C_i)$$

$$= \$5{,}368{,}200 \qquad (10)$$

where $c_i$ is the estimated rehabilitation cost of Bridge $i$. Compared with the total expected cost (\$5,368,200), the total cost predicted by the simulation method (\$5,261,000) is apparently a more reasonable estimation than the total cost predicted by the Markov chain method (\$8,947,000).

The results of the predictions indicate that the simulation approach has advantages over the Markov chain approach in estimating the rehabilitation costs as well as the number of bridges to be repaired. Because a Monte Carlo simulation prediction is based on generated random numbers, the result varies with each different operation of the computer program. However, it is also generally true that for each of the runs of the computer program the percentage of bridges selected for rehabilitation will be close to the given transition probability, and the total cost predicted will also be close to the total expected cost. This is because the chances that the uniformly distributed random numbers fall into any subinterval of [0.0, 1.0] are proportional to the length of the subinterval.

To compare the results of different operations of the simulation program, the program was run 20 times. The results of the 20 predictions are shown in Figures 2 and 3. Figure 2

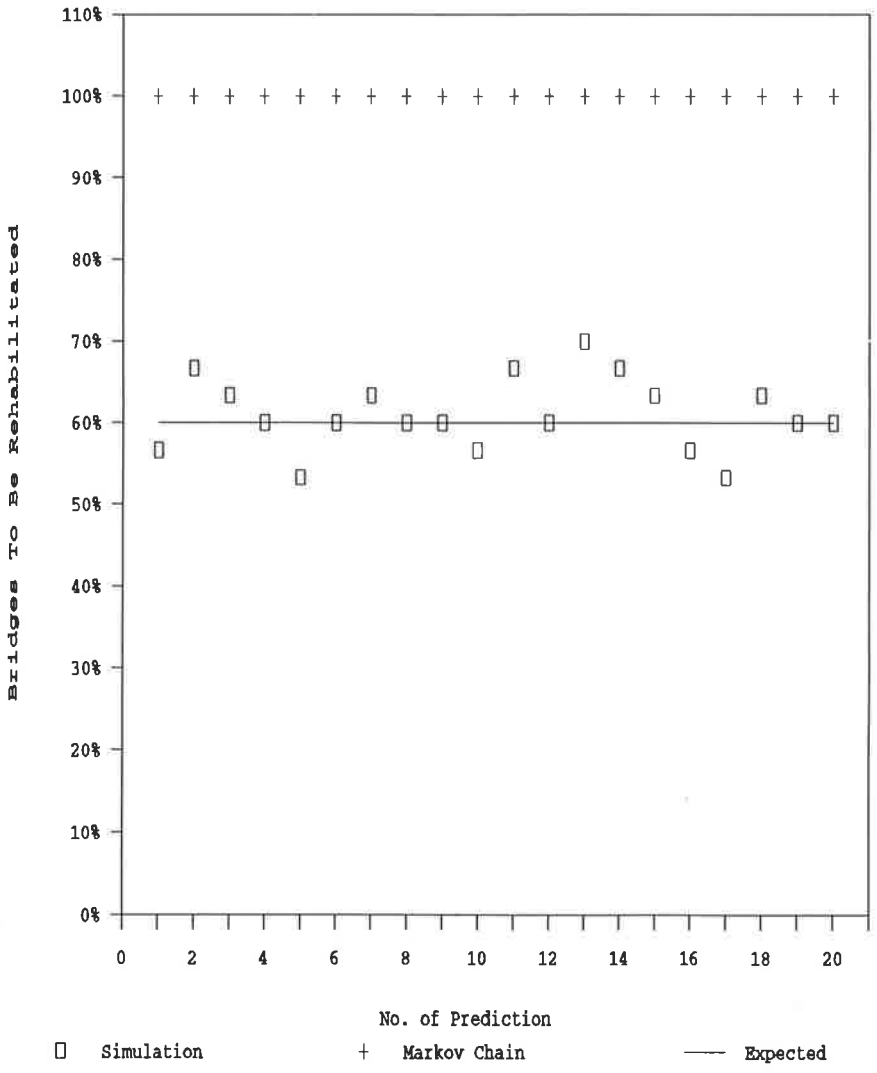


**FIGURE 2 Predictions of bridges to be rehabilitated by simulation and Markov chain methods.**

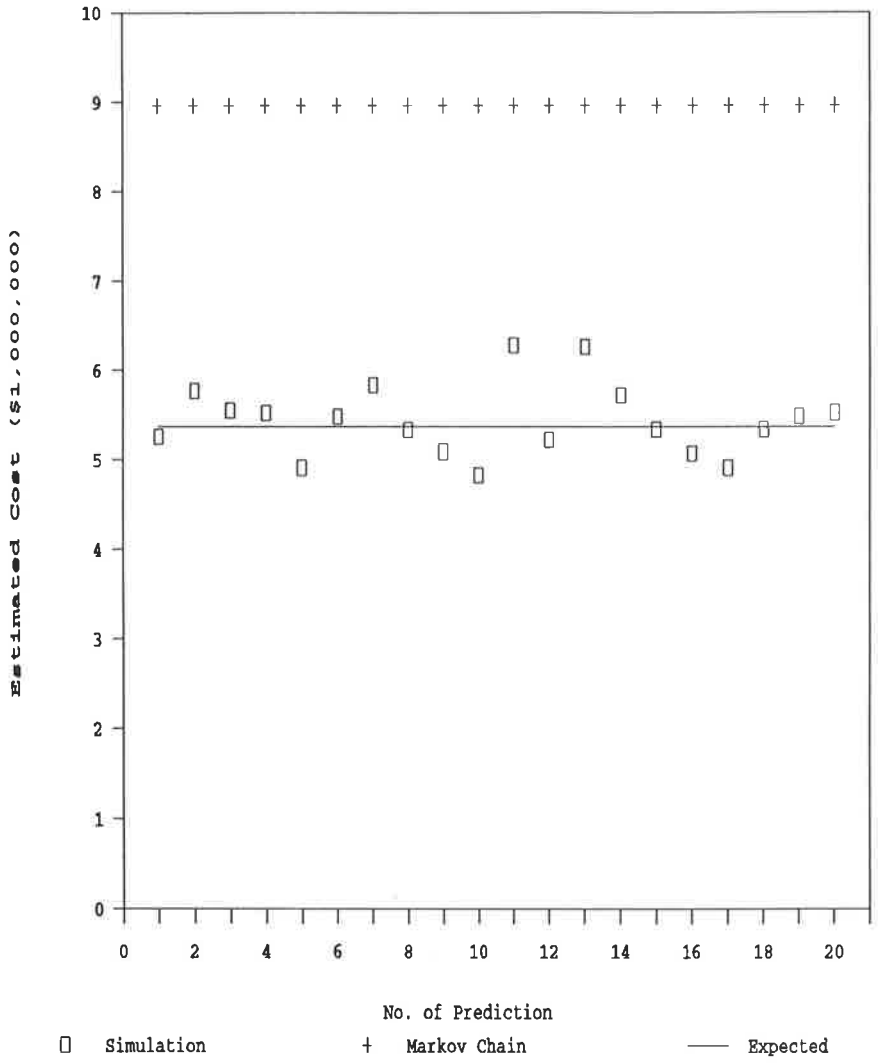


**FIGURE 3 Predictions of rehabilitation costs by simulation and Markov chain methods.**

expresses the predicted number of bridges to be rehabilitated (the ones with deck Rating 5 in the next year) as the percentage of the total bridges. The total estimated rehabilitation cost for these predictions is plotted in Figure 3. The results of the Markov chain predictions and the expected percentage (60 percent) and average cost ($5,368,200) are also included in the figures for comparison. The two figures illustrate that the simulation predictions of both the percentages and the total rehabilitation costs were in the close neighborhood of the expected values, whereas the Markov chain predictions were consistently higher than the expected values.

The previous example showed that the simulation predictions were reasonably close to the given transition probabilities. The simulation predictions will reflect transition probabilities more closely if a large number of highway structures is involved. For pavement or bridge management, the number of projects is usually sufficiently large. Therefore, the simulation method will be an appropriate approach for predicting facility conditions of these management systems. This method would be especially useful in updating conditions of highway structures if dynamic optimization techniques are applied for project selections (*3*).

## CONCLUSION

A highway structure condition prediction method using the Monte Carlo simulation technique was presented here. This method is suitable for pavement and bridge management. Results of the study showed that the Monte Carlo simulation method could provide more accurate predictions than the Markov chain method. The simulation prediction model can be incorporated into a dynamic optimization program to update structural conditions at each stage of the optimization computation. It can also be used separately to program rehabilitation activities of highway structures. The simulation predictions of number of projects, budget, and other resources needed for a given program period would be close to reality as long as the transition probabilities are reasonable.

## REFERENCES

1. A. A. Butt, K. J. Feighan, and M. Y. Shahin. Pavement Performance Prediction Model Using the Markov Process. In *Transportation Research Record 1123*, TRB, National Research Council, Washington, D.C., 1987.
2. Yi Jiang and K. C. Sinha. *The Development of Optimal Strategies for Maintenance, Rehabilitation and Replacement of Highway Bridges, Final Report Vol 6: Performance Analysis and Optimization*. FHWA/IN/JHRP-89/13. Purdue University, West Lafayette, Ind., 1990.
3. Yi Jiang and K. C. Sinha. Dynamic Optimization Model for Bridge Management Systems. In *Transportation Research Record 1211*, TRB, National Research Council, Washington, D.C., 1989.
4. Federal Highway Administration. *Recording and Coding Guide for the Structure Inventory and Appraisal of the Nation's Bridges*. U.S. Department of Transportation, Washington, D.C., 1979.
5. U. N. Bhat. *Elements of Applied Stochastic Process*. John Wiley and Sons, Inc., New York, N.Y., 1972.
6. W. J. Gajda and W. E. Biles. *Engineering: Modeling and Computation*, Houghton Mifflin Company, Boston, Mass., 1978.
7. *International Mathematical and Statistical Libraries (IMSL)*. UNIX User's Manual. Purdue University ECN System, West Lafayette, Ind., 1991.

*Publication of this paper sponsored by Committee on Structures Maintenance and Management.*

# Assessment of Bridge Vulnerability to Hydraulic Failures

A. M. Shirolé and M. J. Loftus

A comprehensive Bridge Safety Assurance (BSA) program is being implemented in New York State. It provides a system to identify, assess, and evaluate the vulnerability of bridges to catastrophic failures and then implement actions to eliminate or mitigate such vulnerabilities. On the basis of a national survey of bridge failures, six failure modes were identified as being the most significant in terms of the potential damage they can cause to highway bridges in New York State: hydraulic, overload, steel structural details, collision, concrete structural details, and earthquake. The assessment phase of the overall BSA program as it relates to the hydraulic failure mode is described. Specific details of screening, classifying, and rating steps are described, and the current status of these assessment efforts in New York State is presented. Vulnerability-reduction actions that have been implemented as a result of the assessment process to ensure bridge safety against hydraulic failures are described as well.

The New York State Department of Transportation's (NYSDOT's) Bridge Safety Assurance (BSA) program provides a systematic method to reduce vulnerability of the state's bridges to all potentially significant modes of failure. The program has four phases:

- Identification of significant modes of failure,
- Assessment of vulnerability of bridges to failure modes,
- Evaluation of vulnerable bridges, and
- Implementation of recommendations to reduce vulnerability.

Planning aspects of these four phases have been described previously by Shirolé and Holt (*1*). The identification phase has been completed, and the following six failure modes were identified as the most significant in terms of the potential damage they can cause to highway bridges in New York State:

- Hydraulic,
- Overload,
- Steel structural details,
- Collision,
- Concrete structural details, and
- Earthquake.

The failure modes were identified on the basis of the results of a survey on bridge failures since 1950 compiled by NYSDOT.

The evaluation and implementation phases are basically similar for all the identified modes of failure. These phases are described elsewhere (*1*) and will not be discussed here.

New York State Department of Transportation, 1220 Washington Avenue, State Office Campus, Building 5, Albany, N.Y. 12232.

This paper is focused on the assessment phase of the BSA program as it relates to hydraulic vulnerability. Specific details of the assessment process and some vulnerability reduction actions that have been implemented to ensure bridge safety are described.

## PROCEDURES FOR HYDRAULIC ASSESSMENT

The objective of the hydraulic assessment phase of the BSA program is to rate the state's bridges according to their relative vulnerability to hydraulic failure. This objective is accomplished through a series of screening, classifying, and rating steps that review hydraulic characteristics of individual bridges to group them according to their relative susceptibility, and classify and rate them on a list for appropriate actions.

Figure 1 is a flowchart of the overall hydraulic vulnerability assessment phase. Key elements in the process are the screen, classify, and rate steps. Each is designed to provide an increasing understanding of the bridge's hydraulic vulnerability. They are intended to be progressed sequentially on a priority basis. Bridges with higher vulnerabilities are moved through the subsequent steps first to focus assessment and corrective activities on the most critical bridges in the shortest time. This results in a staggered progression of bridges through the assessment process.

Vulnerability reduction measures shown in Figure 1 consist of actions based on findings of the screening, classifying, and rating steps. They include establishing floodwatch and post-flood inspection lists, and identifying bridges requiring immediate or future scour-protection retrofit.

The procedures used in the screening and classifying phases of the assessment process are based in part on recommendations made by a special Bridge Safety Assurance Task Force (BSATF), appointed to study bridge safety assurance measures in New York State. It was made up of nationally recognized experts in a variety of fields, including hydraulics. Richardson and Huber (*2*) reported on BSATF recommendations relating to hydraulics. For implementation purposes, task force recommendations were modified to better fit conditions in New York. In general, the modifications did not affect specific vulnerability factors being used, but consisted of changes in the logic used in the screening or classifying processes or adjustments in the importance or weight assigned to vulnerability factors. For example, the classification step uses only the most critical substructure unit as the basis of final evaluation results, whereas the task force process used a combination of pier and abutment evaluations. In New York there is concern over hydraulic vulnerability of single-span

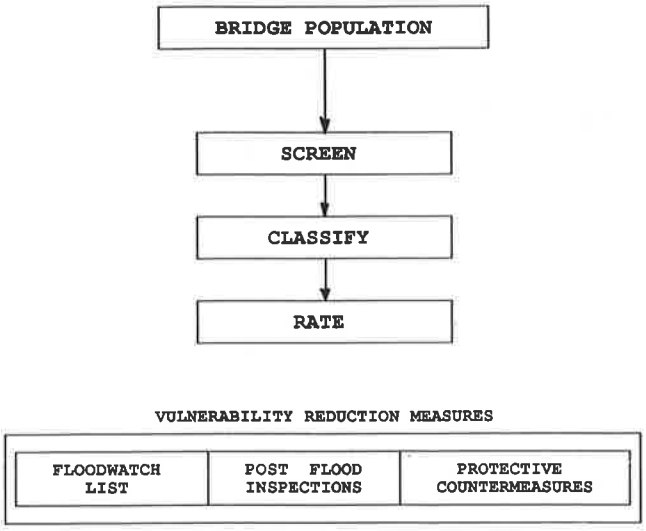


**FIGURE 1 Hydraulic vulnerability assessment process.**

bridges, and the task force procedures made it unlikely that a bridge without piers would be evaluated as highly vulnerable. Another example of an area that changed is the weights used for different types of pier and abutment foundation configurations. These weights were adjusted to provide a greater distinction between configurations of different vulnerabilities.

The assessment procedures described here are not being used to assess vulnerability of bridges on Long Island and in the New York City area. Bridges in those areas are subject to hydraulic forces (e.g., tidal) that differ from the forces in the other areas of the state. Consequently, different methods are required to assess vulnerability. Procedures to assess the vulnerability of bridges in those areas are being developed.

Descriptions of the different steps in the vulnerability assessment process follow.

## Screen

Figure 2 is a flowchart of the screening process. The primary goal of the screening step is to set priorities for progressing bridges to the classifying step. This goal is accomplished through a preliminary inventory data base screen and a more refined susceptibility screen. As a result of these screens, bridges are put into four susceptibility groups, which rank the order for progressing to the classifying step.

The inventory screen is designed to evaluate a large population of bridges, using information contained in Bridge Inventory and Inspection System (BIIS) data files. Structures not over water are identified and removed from the assessment process. No further actions are required for them. The remaining bridges are screened on the basis of key substructure, superstructure, and hydraulic information in the BIIS data base. This screening provides a relative assessment of hydraulic susceptibility of a bridge and is used to set the order for progressing bridges to the susceptibility screening step.

As seen in Figure 2, the susceptibility screening process is divided in two parts (*3*). This process uses a review of bridge plans, construction documents, inspection reports, and any other available information to place bridges in four susceptibility groups, which imply a relative susceptibility to damage from hydraulic forces and determine the order in which they are progressed to the classifying step.

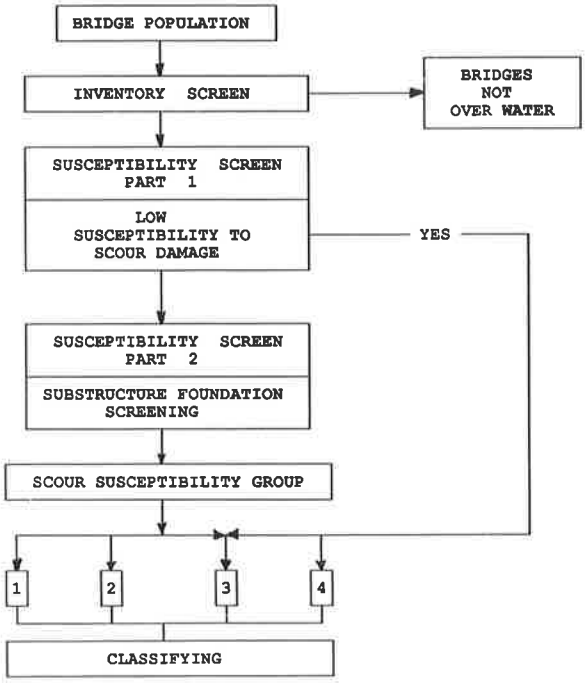


**FIGURE 2 Hydraulic vulnerability assessment screening process.**

In the first part of the susceptibility screening, structures having a low susceptibility to scour damage are identified on the basis of the following screening criteria:

- Piers and abutments out of floodplain,
- Slow stream velocity,
- Nonscourable foundation materials, and
- Culverts.

Structures meeting any one of these criteria are placed in the third or fourth susceptibility group. Bridges not meeting these criteria are progressed to the second part of the susceptibility screening step. The actual group selected depends on whether any indications of scour damage are noted in the inspection and condition reports. If scour damage is indicated, the structures are placed in the higher susceptibility group. For example, bridges with piers and abutments founded on sound nonscourable rock foundations are identified and placed in the fourth group, provided that there are no indications of scour damage. If there are, then the third group would be appropriate.

In the second part of screening, bridges are placed in the first, second, or third susceptibility group on the basis of pier and abutment foundation configurations and assessment of scour conditions. Figure 3 shows screening criteria and recommended susceptibility groupings. Again, as in the first part of the screen, if there is scour damage, a higher susceptibility group is recommended. For example, a bridge with vertical wall abutments on short piles goes into the second susceptibility group unless it shows scour damage, in which case the first group is recommended.

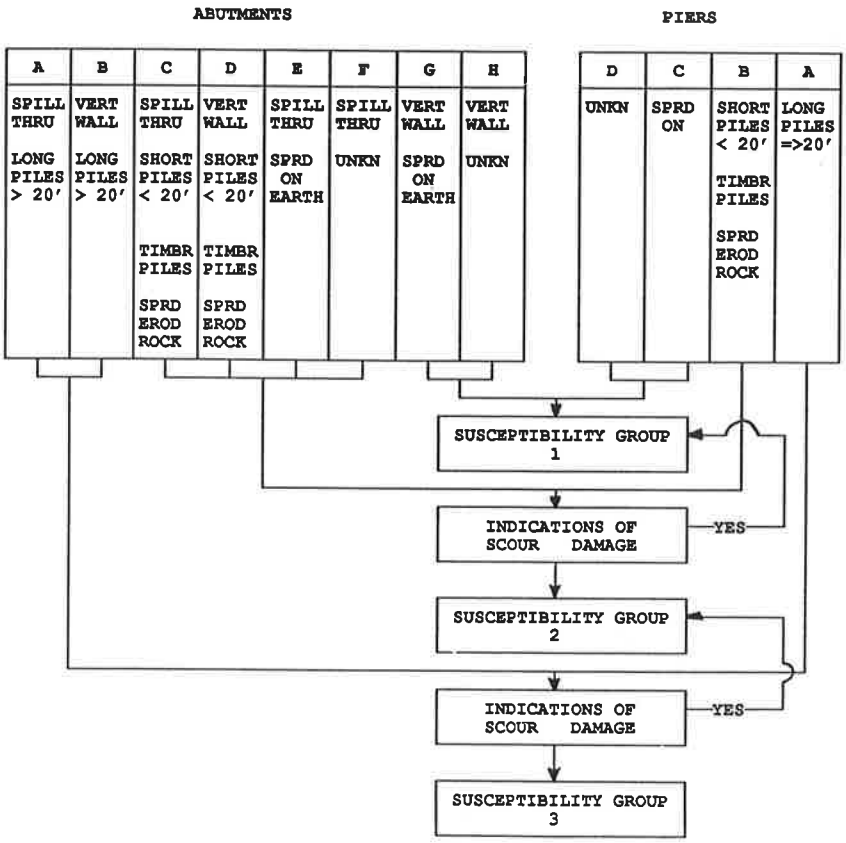


**FIGURE 3 Substructure foundation screening.**

After susceptibility screening, bridges in susceptibility Group 1 progress to the classifying step, followed by bridges in Groups 2, 3, and 4, respectively.

## Classifying

The purpose of the classifying step is to evaluate the vulnerability of a structure to scour damage on the basis of its geologic, hydraulic, and riverine conditions. The product of this step is a classification score that serves two purposes. First, it quantifies potential vulnerability of a structure to hydraulic damage relative to other bridges in the classification process. Second, it places a structure in a high, medium, or low hydraulic vulnerability class.

The vulnerability classes describe the potential of a structure for failure due to scour or other hydraulic forces relative to other bridges in the classifying process. The classes are used in determining vulnerability rating for a structure and also in deciding whether a structure should be placed on a floodwatch list (*4*) or a postflood inspection list.

Field evaluation of the bridge is essential to complete the classifying step. In addition, it is important that classification procedures are performed by an engineer specially trained in bridge hydraulic principles, as these require judgments to be made about hydraulic characteristics of a bridge and its stream.

The high, medium, and low hydraulic vulnerability classes are defined in the following paragraphs.

### *High Vulnerability Class*

For a structure to be placed in the high vulnerability class, conditions must exist on the structure or in the stream that create an unacceptable potential for failure due to scour or other hydraulic forces. "Unacceptable" implies a risk clearly greater than is consistent with design practice, and a single intermediate or large flood could result in a failure. These bridges would be candidates for scour retrofit on a priority basis or on a short-term programmed basis and would have highest priority for detailed hydraulic analysis. Until action is taken and the bridge can be placed in a lower vulnerability class, bridges should be on the floodwatch list. These bridges would also be considered for a postflood inspection list.

### *Medium Vulnerability Class*

For a structure to be placed in the medium vulnerability class, conditions must exist on the structure or in the stream creating a recognizable potential for failure due to flooding. Risk of failure due to a single design flood or a historic flood is slight, but repetitive floods of these magnitudes will probably result in failure. These structures would be candidates for scour-protection retrofit on a programmed basis. A detailed hydraulic analysis is required for these structures, and inclusion on the floodwatch list should be considered. Bridges in this category may also be candidates for a postflood inspection list.

*Low Vulnerability Class*

For a structure to be placed in the low vulnerability class, conditions must exist on the structure or in the stream presenting little potential for failure due to flooding. There is no risk of failure due to a single design or historical flood, and only a remote chance of failure due to an extreme flood. Scour-protection retrofit is not required for bridges in this category, but scour conditions should be checked as part of general bridge inspections and after major floods. These structures should receive the lowest priority for a hydraulic analysis and need not be placed on the floodwatch list. Inclusion on a postflood inspection list may be considered for some structures in this category.

Figure 4 outlines the classification process, which is composed of two sections: general hydraulic assessment and foundation assessment. The foundation assessment section includes separate evaluations for abutments and piers. Figure 4 also shows the classifying score ranges used to determine vulnerability class for a structure. The ranges are overlapped to allow the evaluating engineer some discretion in assigning a vulnerability class.

In each section of the classifying process, several parameters are examined and a specified value assigned that describes existing conditions, with more vulnerable conditions receiving higher values. Figure 5 shows criteria and classification scores which are used in the general hydraulic assessment process, and Figures 6 and 7 show the criteria and the scores for the abutment and pier foundation assessment processes, respectively. Specific instructions on applying these criteria are in the *NYSDOT Hydraulic Vulnerability Assessment Manual* (*3*).

In the foundation assessment section all abutments and piers on a structure are evaluated, but only the most critical substructure unit is used to determine the foundation assessment score.

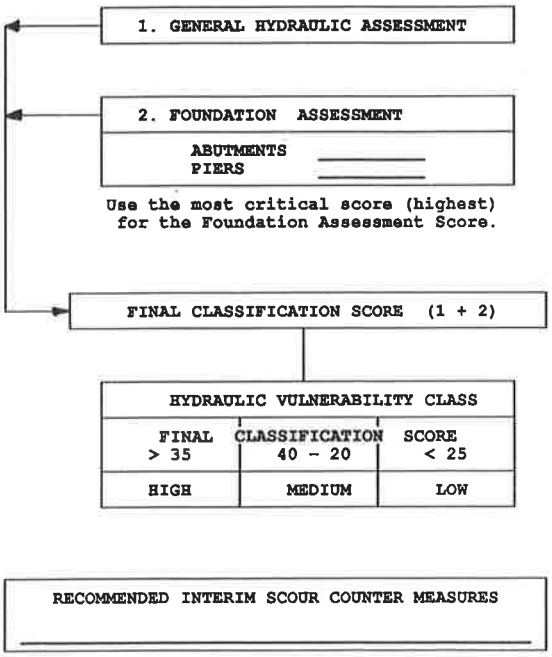


**FIGURE 4 Classification process.**

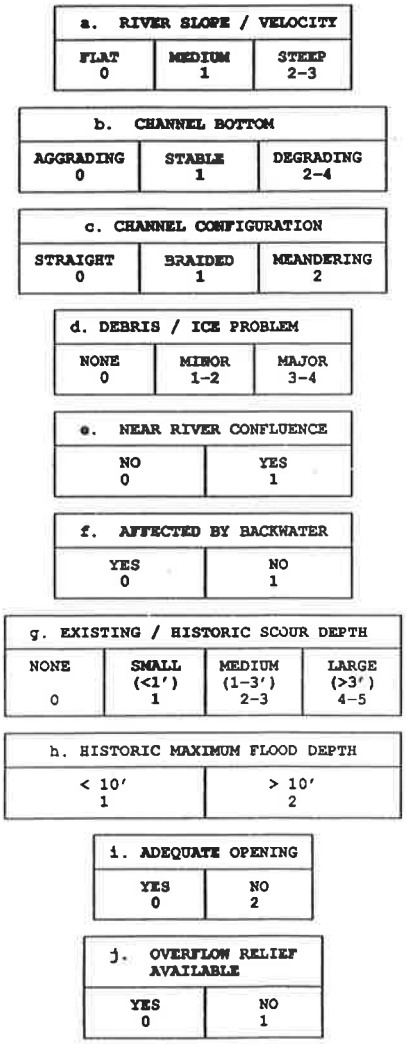


**FIGURE 5 General hydraulic assessment criteria.**

The final classification score for a structure is determined by adding scores from the general hydraulics assessment process and the foundation assessment process. The highest score represents the most vulnerable structure. Classification scores are then used to determine appropriate vulnerability classes based on the ranges shown in Figure 4.

Classification procedures are designed to ensure objectivity and provide a degree of uniformity in evaluations, yet allow for the judgment of a trained hydraulic engineer. The process allows for engineering judgment in assessing observed conditions and accounting for factors pertinent but possibly not covered in the detailed procedures. Evaluators have the option of increasing or decreasing scores, and can use some judgment in deciding the final vulnerability category for a structure.

An ancillary function of the classifying step is to identify any bridges exhibiting potentially catastrophic conditions that require immediate scour-protection countermeasures to safe-

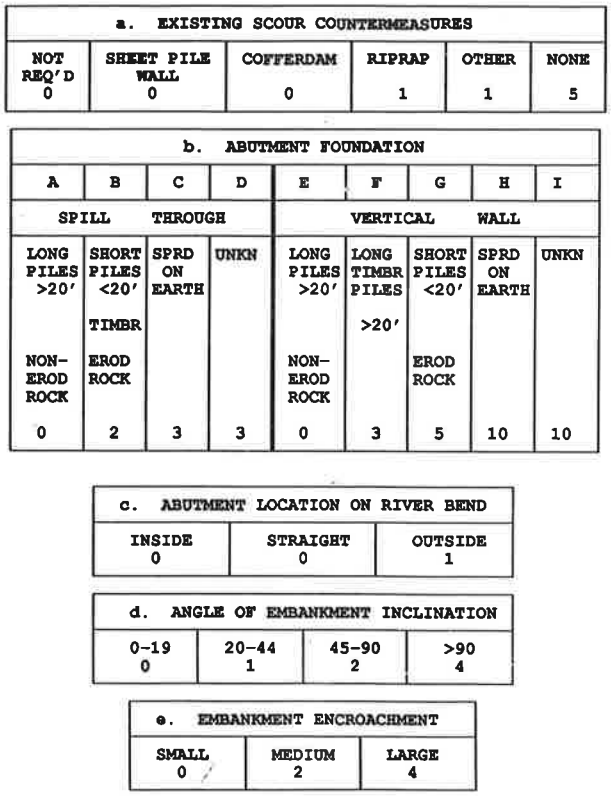

a. EXISTING SCOUR COUNTERMEASURES

| NOT REQ'D | SHEET PILE WALL | COFFERDAM | RIPRAP | OTHER | NONE |
|---|---|---|---|---|---|
| 0 | 0 | 0 | 1 | 1 | 5 |

b. ABUTMENT FOUNDATION

| A | B | C | D | E | F | G | H | I |
|---|---|---|---|---|---|---|---|---|
| SPILL THROUGH | | | | VERTICAL WALL | | | | |
| LONG PILES >20' NON-EROD ROCK | SHORT PILES <20' TIMBR EROD ROCK | SPRD ON EARTH | UNKN | LONG PILES >20' NON-EROD ROCK | LONG TIMBR PILES >20' | SHORT PILES <20' EROD ROCK | SPRD ON EARTH | UNKN |
| 0 | 2 | 3 | 3 | 0 | 3 | 5 | 10 | 10 |

c. ABUTMENT LOCATION ON RIVER BEND

| INSIDE | STRAIGHT | OUTSIDE |
|---|---|---|
| 0 | 0 | 1 |

d. ANGLE OF EMBANKMENT INCLINATION

| 0-19 | 20-44 | 45-90 | >90 |
|---|---|---|---|
| 0 | 1 | 2 | 4 |

e. EMBANKMENT ENCROACHMENT

| SMALL | MEDIUM | LARGE |
|---|---|---|
| 0 | 2 | 4 |

**FIGURE 6 Foundation assessment criteria (abutments).**

guard against failure. If potentially catastrophic conditions are observed, then interim fixes can be implemented until more permanent remedial measures can be designed and constructed. Typically, these interim fixes consist of heavy stone fill placed around abutments and piers.

## Rating

The purpose of the vulnerability rating step is to provide a uniform measure of a structure's vulnerability to failure on the basis of likelihood of occurrence and consequences of a failure. Six vulnerability rating categories have been established, common to all six BSA failure modes, allowing comparison among bridges vulnerable to different failure modes.

Definitions for the six vulnerability rating categories are presented in the following list. These categories specify the type of corrective actions needed and the urgency with which these actions should be implemented. They were developed to apply to the modes of failure listed previously.

1. Safety priority action. This rating designates vulnerability to failure resulting from loads or events that are likely to occur. Remedial work to reduce the vulnerability must be given immediate priority, and completion of work is desired within 18 months.
2. Safety program action. This rating designates vulnerability to failure resulting from loads or events that may occur. Remedial work to reduce the vulnerability is desired within 3 years.

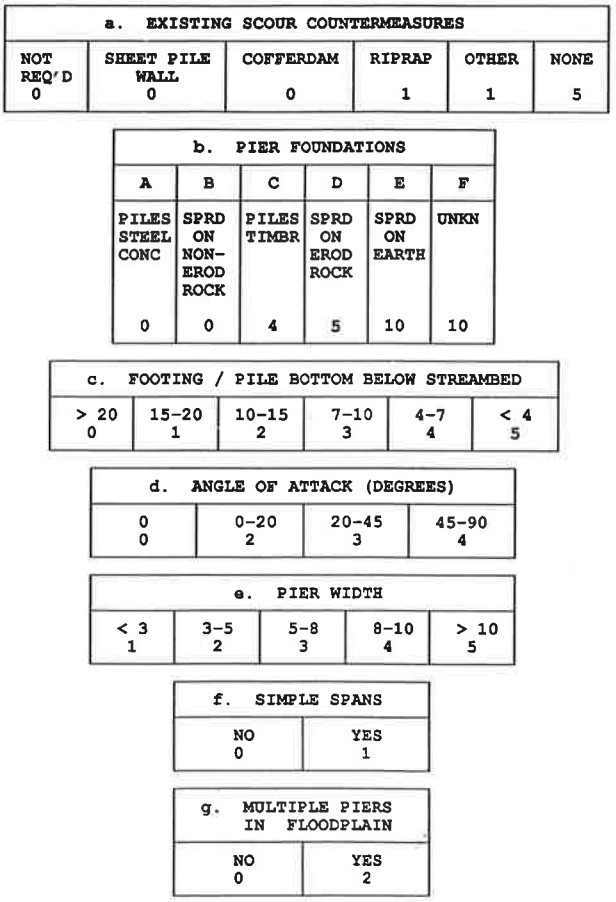

a. EXISTING SCOUR COUNTERMEASURES

| NOT REQ'D | SHEET PILE WALL | COFFERDAM | RIPRAP | OTHER | NONE |
|---|---|---|---|---|---|
| 0 | 0 | 0 | 1 | 1 | 5 |

b. PIER FOUNDATIONS

| A | B | C | D | E | F |
|---|---|---|---|---|---|
| PILES STEEL CONC | SPRD ON NON-EROD ROCK | PILES TIMBR | SPRD ON EROD ROCK | SPRD ON EARTH | UNKN |
| 0 | 0 | 4 | 5 | 10 | 10 |

c. FOOTING / PILE BOTTOM BELOW STREAMBED

| > 20 | 15-20 | 10-15 | 7-10 | 4-7 | < 4 |
|---|---|---|---|---|---|
| 0 | 1 | 2 | 3 | 4 | 5 |

d. ANGLE OF ATTACK (DEGREES)

| 0 | 0-20 | 20-45 | 45-90 |
|---|---|---|---|
| 0 | 2 | 3 | 4 |

e. PIER WIDTH

| < 3 | 3-5 | 5-8 | 8-10 | > 10 |
|---|---|---|---|---|
| 1 | 2 | 3 | 4 | 5 |

f. SIMPLE SPANS

| NO | YES |
|---|---|
| 0 | 1 |

g. MULTIPLE PIERS IN FLOODPLAIN

| NO | YES |
|---|---|
| 0 | 2 |

**FIGURE 7 Foundation assessment criteria (piers).**

3. Capital program action. This rating designates vulnerability to failure resulting from extreme loads or events that are possible but not likely. This risk can be tolerated until a normal capital construction project can be implemented. Remedial work to reduce the vulnerability is desired within 5 years.
4. Inspection program action. Possible but unlikely expectation of a failure that could cause traffic disruptions. Inspection monitoring desired to ensure adequate load resistance.
5. Not vulnerable. Adequate structural resistance to this type of vulnerability. Failure unlikely.
6. Not applicable. No exposure to this type of failure vulnerability.

A vulnerability rating for a bridge is determined in a manner similar to the classification process, where scores are assigned to evaluate parameters for the likelihood and consequences of a failure. These scores are combined and a range of values used to determine the appropriate vulnerability rating category.

The likelihood of a failure occurring is evaluated using results of the classification process and, when available, results of a detailed hydraulic analysis. This ensures that all known information about a structure's vulnerability and resistance to it are included in the rating process.

Consequences of failure are determined on the basis of the type of failure to which a structure is prone, and includes factors to account for the traffic volume and highway classification of the structure.

## STATUS OF THE ASSESSMENT PHASE

The hydraulic vulnerability assessment process is currently being implemented for state-owned bridges over water. Advice is being provided for locally owned structures. At this time, state-owned bridges on Long Island and in the New York City area also are not included, as was mentioned previously. The current program encompasses more than 95 percent of the entire state bridge population over water.

The status of the vulnerability assessment program as of July 1991 is presented in the following list. To date, more than 99 percent of bridges included in the program have been screened and more than 40 percent classified. Rating tasks have not yet begun. It is estimated that all state bridges over water will have been screened, classified, and rated by the end of 1993.

- Number of state-owned bridges: 6,625;
- Number of bridges over water: 3,919;
- Susceptibility screening
  - –Group 1: 1,163,
  - –Group 2: 684,
  - –Group 3: 1,022,
  - –Group 4: 1,003,
  - –Total screened: 3,872;
- Classifying
  - –High vulnerability: 141,
  - –Medium vulnerability: 675,
  - –Low vulnerability: 843,
  - –Total classified: 1,659.

In addition to vulnerability assessment steps, the hydraulic vulnerability assessment process also includes continuing strategies to provide protection against hydraulic failures. These strategies include a floodwatch program and postflood inspection program to provide monitoring of vulnerable bridges during and after floods.

### Floodwatch Program

The floodwatch program was established with issuance of the *NYSDOT Bridge Flood Warning Action Plan* (*4*). Its purpose is to ensure that bridges with a high susceptibility to damage or failure from hydraulic forces are monitored during periods of flooding for as long as they remain vulnerable. It calls for continual or periodic monitoring of bridges during periods of flood warning as issued by the National Weather Service (NWS). Personnel are placed at a bridge site for the duration of the flood warning event. If any movement, damage, or potentially dangerous conditions are observed, appropriate action, such as bridge closure, can be taken.

Continuous monitoring is provided for bridges having a potential for sudden and catastrophic collapse due to the force of flood waters or other hydraulic forces. These are placed in a high-risk floodwatch category. Bridges less prone to sudden collapse but to more gradual settlement or sagging failure receive intermittent monitoring during a flood. These are placed in a non-high-risk floodwatch category. Both the superstructure type and foundation type are considered in judging potential for collapse.

Criteria for selecting the bridges to be placed on the floodwatch list are based on results of the vulnerability assessment procedures, with more precise criteria applying after each step in the assessment process.

Currently, 703 bridges are included in the New York State floodwatch program.

### Postflood Inspection Program

The purpose of this program is to monitor performance of vulnerable bridges after major floods. Bridges over water having a pier or abutment protected with riprap, stone fill, or paving blocks are included on the postflood inspection list. Bridges in the floodwatch program are also placed on the list.

Inspections are conducted following issuance of a flood warning by the NWS, after flood waters have receded enough to allow substructures to be inspected. Only the structures in areas included in the flood warning need to be inspected.

The inspection consists of visual inspection of substructures and protective countermeasures on the bridge. If any movement, loss of material, or any type of damage is observed, the conditions are documented and appropriate corrective actions implemented.

## CONCLUSION

The hydraulic vulnerability assessment process described here provides a systematic method for determining hydraulic vulnerability of a large population of bridges. Through a series of screening, classifying, and rating steps, the hydraulic characteristics of bridges are examined, and prioritized lists are developed for corrective action. Concepts included in the assessment process have been developed with substantial input from numerous expert sources, and implementation of these procedures as part of the overall BSA program will significantly lower the vulnerability of New York's bridges to hydraulic failures.

Currently, only state-owned bridges over water are being addressed through the hydraulic assessment procedures. To date, more than 99 percent of these bridges have been screened and more than 40 percent classified. It is estimated that all screening, classifying, and rating efforts for state bridges will be completed by the end of 1993.

## REFERENCES

1. A. M. Shirolé and R. C. Holt. Planning For A Comprehensive Bridge Safety Assurance Program. In *Transportation Research Record 1290,* Vol. 1, TRB, National Research Council, Washington, D.C., 1991, pp. 39–50.
2. E. V. Richardson and F. W. Huber. Evaluation of Bridge Vulnerability to Hydraulic Forces, Stream Instability, and Scour. In *Transportation Research Record 1290,* Vol. 1, TRB, National Research Council, Washington, D.C., 1991, pp. 25–39.
3. *NYSDOT Hydraulic Vulnerability Assessment Manual.* Structures Design and Construction Division, New York State Department of Transportation, Albany, Dec. 1991.
4. *NYSDOT Bridge Flood Warning Action Plan For State Bridges.* Structures Design and Construction Division, New York State Department of Transportation, May 1989.

*Publication of this paper sponsored by Committee on Structures Maintenance and Management.*

*Abridgment*

# Network Bridge Deck Surveys Using High-Speed Radar: Case Studies of 44 Decks

KENNETH R. MASER AND ALAN RAWSON

The DECAR radar system was evaluated for highway-speed bridge deck condition assessment by the New Hampshire Department of Transportation on three survey networks comprising 44 decks. DECAR (DEck Condition Assessment using Radar) incorporates van-mounted radar equipment, computer-based digital data acquisition equipment operating in the van, a set of procedures for organizing and conducting surveys, and software for collecting and processing the data. It was shown in each of the three surveys that groups of bridge decks could be successively surveyed at highway speeds up to 55 mph during a continuous round trip over the survey route. At this speed, production rates of 10 to 20 decks per day can be easily expected. Of the 44 decks surveyed, 19 were evaluated during replacement or repair to determine deck condition, and an additional 8 were new decks. The radar deterioration predictions using DECAR were compared with these known conditions, with a correlation ($R$-squared) of 0.81, and a standard error of $\pm 4.4$ percent of the total deck area. When the radar data were used to classify the decks into one of four categories, the radar results were accurate 93 percent of the time. The DECAR results were shown to be repeatable when repeat surveys were conducted at different times by different personnel. It was concluded that the DECAR system could be effectively and economically used to set up a bridge deck condition data base for bridge management and to monitor deck performance over time.

A major problem with bridge deck deterioration is the difficulty in assessing its severity and extent. The mechanisms of deterioration occur below the surface, and their manifestations are not readily seen in visual inspections. This is particularly true for overlaid decks, where both delamination and freeze/thaw damage can occur without visual manifestations. Many decks built during the Interstate construction period fall into this category, with degrees of deterioration from 0 to 50 percent. Agencies are forced to program, rank, and budget the repair and replacement of many structures whose conditions are virtually unknown.

Recent research has led to the development and verification of ground penetrating radar (GPR) for bridge deck condition assessment (*1*). The work described here focuses on a network survey application of GPR to support the implementation of a bridge management system (BMS). In a network level survey a radar van travels continuously at normal highway speed logging data for every bridge deck that it crosses. For a given round trip the van makes one pass on each lane. Multiple round trips are required to obtain complete transverse coverage of the deck. This survey method yields production rates of 20 to 30 decks in a day, a rate that would allow for complete coverage of a typical state bridge inventory in 50 to 300 working days. Additionally, the automated nature of the radar processing allows efficient analysis of the large quantity of data generated in these surveys. At this high production rate, a BMS data base of the condition of all decks in the network can be established during a 2- to 3-year period and updated periodically. These updates would yield deterioration rates and would be helpful in implementing a preventive maintenance program.

The objective of the reported work was to implement, test, and evaluate a pilot high-speed system for network-level bridge deck evaluations. A description of the DECAR (DEck Condition Assessment using Radar) system, developed and evaluated by INFRASENSE and delivered to the New Hampshire Department of Transportation (NHDOT), is presented here. Also described are the field surveys that were carried out with the DECAR system, including descriptions of the decks and the survey methods, the results of the analysis of the radar data collected during these surveys, and the comparison of these results to other available information (*2*).

## DESCRIPTION OF RADAR DECK SURVEY SYSTEM

The DECAR system for highway-speed bridge deck surveys consists of the following elements (*2*):

- Radar equipment, fifth wheel, and van (Figure 1). The equipment used in this project was developed for FHWA by various vendors and loaned to NHDOT for this project (*3*).
- An on-board computer, with an analog/digital (A/D) conversion and data storage system.
- User interface and data analysis software.

The user interface software organizes a four step network survey methodology as follows:

- Layout of the survey route: Data on the decks to be covered are found in the bridge inventory and entered into the bridge description table of the program.

K. R. Maser, INFRASENSE, Inc., 765 Concord Avenue, Cambridge, Mass. 02138-1044. A. Rawson, Bureau of Materials and Research, New Hampshire Department of Transportation, P.O. Box 483, Stickney Avenue, Concord, N.H. 03302-0483.

- Detailed design of the survey: The surveyor estimates the number of passes required for each bridge from the width data and for the sequence of decks from maps. A network survey of a typical 2-lane Interstate deck would consist of 6 passes, one in each wheelpath of each lane, and two on the 10-ft shoulder.
- Conduct of the field survey: As each pass of each deck is about to be surveyed, the surveyor moves the cursor to the appropriate cell of the survey matrix and presses a key to initiate data collection. After the deck is crossed, data collection is terminated by pressing a key, and the data are automatically filed under a name that identifies the name of the bridge and the transverse location of the pass. Normally the radar vehicle will stay in the same wheelpath for a particular round trip. A complete survey is carried out by successive round trips of the survey vehicle, during which all passes of each deck are successively covered. The method was tested during this program and was found to work effectively at speeds up to 55 mph.
- Analysis of the radar data: The DECAR software is designed for quantity analysis of the network radar data. This analysis distinguishes the bridge deck data from the adjacent pavement sections; sets up a batch file that includes the names of the raw data files for each deck, the beginning footage of each deck pass, and the known bridge length; and runs the batch file for each deck, analyzing the data for each pass of the deck and computing the total deck deterioration.

## FIELD SURVEYS AND RESULTS

### Description of Decks and Deterioration Analysis

Three networks representing 44 Interstate bridge decks were surveyed during the course of this project. The surveys were designed to include decks scheduled for rehabilitation in the near future. A summary of the types and ages of decks included in these surveys is presented in Table 1.

FIGURE 1 Radar equipment.

TABLE 1 Types and Ages of Decks in Surveys

| No. of decks | Type | Age (years) |
|---|---|---|
| 27 | IB-C, DPG | 25–32 |
| 8 | IB-C | <5 |
| 5 | IB-C, CRF | 18–19 |
| 4 | CRF | 25–32 |

NOTE: IB-C = concrete deck on I-beam girders, CRF = concrete rigid frame, and DPG = concrete deck on plate girders.

### Data Analysis

The data collected during these surveys were analyzed with the DECAR data analysis system. The product of this analysis is a percentage deterioration for each deck surveyed. For decks whose conditions were known (because they were new) or subsequently determined during rehabilitation, the predicted percentages were compared with the known ones.

The prediction method used in this study was identical to that developed during previous research (*1,4,5*). The percent deterioration was determined by first computing the dielectric constant of the concrete from the amplitude of the asphalt/concrete reflection. For each pass, the percent of the pass that exceeded the mean plus a threshold was computed; this percent was averaged for all passes. This computation is shown graphically in Figure 2. The percent computed was then fit to the known deterioration conditions to develop a formula for computing the deck deterioration from the radar-based percentage. The formula for deterioration is based on the 20 percent threshold:

$$\text{Percent deterioration} = K1 + K2*(R20) \quad (1)$$

where $R20$ is the percentage of the dielectric constants exceeding the mean plus 20 percent, computed as described previously. The constants $K1$ and $K2$ were reevaluated during this project to take into account differences in the data acquisition equipment and level of detail in the radar survey from what was done previously.

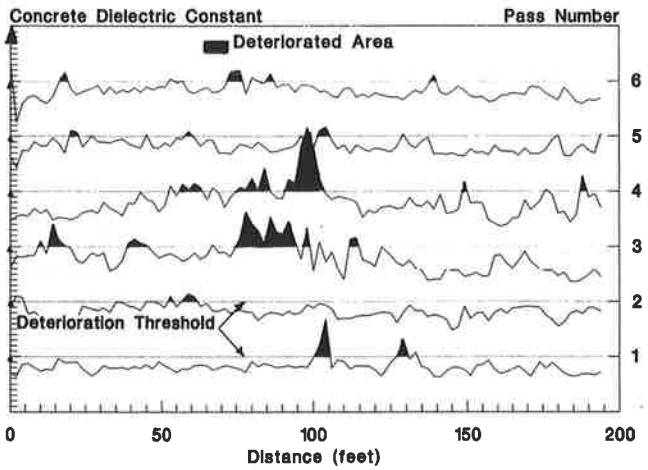


FIGURE 2 Concrete dielectric constant versus distance along deck.

For new decks the actual deterioration was assumed to be zero. For older decks the actual deck deterioration was determined during deck reconstruction after removal of the asphalt by visual observation and chain drag of the exposed concrete.

Table 2 presents a detailed analysis of the match between the radar predictions and known levels of deterioration. The analysis considers two factors: the accuracy in categorizing the condition of the deck for ranking purposes and the closeness of the match between the predicted versus known percent deterioration. The radar predictions are based on a regression fit between *R*20 values and the measured surface conditions for 26 of the 27 decks. One was eliminated from the regression because of the poor match between the radar value and the measured condition.

The radar predictions were used to place the decks into four categories, as shown in Table 2 and Figure 3. These radar-based categorizations were then compared with the categorization based on the observed deck surface conditions. Based on this comparison, the radar-based deck categorization is accurate 93 percent of the time and only two of the 27 decks are incorrectly categorized.

The closeness of match between the radar predictions and the surface-measured conditions are described by the *R*-squared and standard error. For the data in Table 2, the *R*-squared is 0.81, indicating a reasonably good fit between the radar predictions and the directly measured conditions. The standard error, which is the standard deviation between the predicted and actual values, is 4.42 percent of the deck area. An examination of the table shows that radar predictions for 21 of the 27 decks are within 5 percent of direct observations, and 25 of the 27 are within 7 percent. Only 2 decks show significant deviations: 116/109 at 11 percent and 207/041 at 25 percent. The 25 percent discrepancy for 207/041 was a result of the presence of large areas of deteriorated concrete, which were not covered by the survey passes.

**TABLE 2 Summary of Actual Versus Predicted Conditions**

| BRIDGE ID# | DETERIORATION RADAR | DETERIORATION KNOWN | CATEGORY * Radar | CATEGORY * Measured | |
|---|---|---|---|---|---|
| NEW HAMPTON - ASHLAND | | | | | |
| 148/081 | 15 | 18 | 2/3 | 3 | |
| 186/118 | 15 | 8 | 2/3 | 2 | |
| 089/050 | 30 | 25 | 3 | 3 | |
| 089/057 | 19 | 24 | 3 | 3 | |
| 086/119 | 23 | 25 | 3 | 3 | |
| 147/082 | 11 | 10 | 2 | 2 | |
| 148/081 | 4 | 0 | 1 | 1 | |
| 186/118 | 0 | 0 | 1 | 1 | |
| 089/050 | 3 | 0 | 1 | 1 | |
| 089/057 | 3 | 0 | 1 | 1 | |
| FRANCONIA - LITTLETON | | | | | |
| 132/086 | 0 | 0 | 1 | 1 | |
| 132/095 | 2 | 0 | 1 | 1 | |
| 069/122 | 4 | 1 | 1 | 1 | |
| 148/060 | 7 | 2 | 2 | 1 | |
| 219/040 | 16 | 10 | 2/3 | 2 | |
| 211/040 | 13 | 15 | 2 | 2/3 | |
| 208/042 | 13 | 7 | 2 | 2 | |
| 207/041 | 5 | 30 | 1/2 | 3 | ** |
| 211/039 | 0 | 5 | 1 | 1/2 | |
| 100/050 | 18 | 25 | 3 | 3 | |
| 147/060 | 5 | 10 | 1/2 | 2 | |
| 053/122 | 1 | 3 | 1 | 1 | |
| 068/121 | 0 | 2 | 1 | 1 | |
| 077/115 | 29 | 25 | 3 | 3 | |
| 116/109 | 19 | 30 | 3 | 3/4 | |
| 131/095 | 1 | 0 | 1 | 1 | |
| 132/086 | 1 | 0 | 1 | 1 | |

* CATEGORIES
1= 0-5
2= 6-15
3= 16-30
4= >30

** Result not included in prediction model

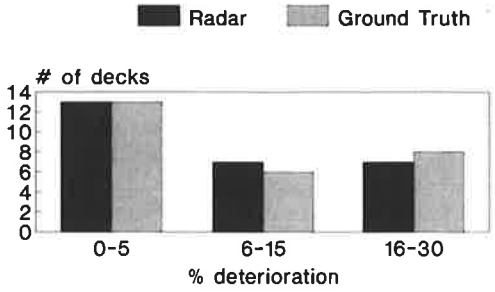


**FIGURE 3 Radar versus ground truth, bridge deck categories.**

### Influence of Survey Speed

Survey speed influences the longitudinal spacing of the radar data. A study was conducted to investigate the influence of survey speed on the radar predictions for deck deterioration. For eight bridge decks, the deck deterioration was then calculated in two ways: (a) using data at 2-ft spacing and (b) using data at 1-ft spacing. The average difference between these two analyses was 0.64 percent, the maximum difference 1.8 percent. These differences are minimal, and, consequently, survey speed does not appear to significantly affect the results of the radar survey.

### Repeatability Study

Factors affecting repeatability include (a) small differences in locating the beginning and end of the deck in the data from each pass, (b) deviations in the position of the antenna from survey to survey, (c) differences in deck conditions and environmental conditions, and (d) variations in the characteristics of the radar signal from survey to survey. To investigate repeatability, three repeat surveys were conducted: the first by INFRASENSE staff on May 2, one day after rain; the second by NHDOT personnel under INFRASENSE supervision on June 7, 2 days after rain; and the third by NHDOT personnel alone on August 14, 4 days after rain.

Figure 4 shows the comparisons of the results of the three surveys for each of the 8 bridges of the network. The figure shows that the radar analysis is highly repeatable. The average difference between the three sets of analyses is 1.5 percent, the maximum difference 3.1 percent.

## CONCLUSION

The project has demonstrated that radar can be used to accurately survey bridge decks on a network basis. The data collection and analysis procedures have been automated and

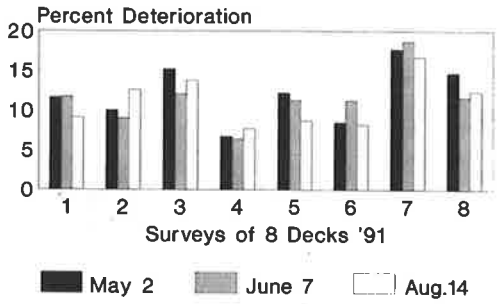


**FIGURE 4 Repeatability study.**

organized so that they can be carried out by state transportation department personnel with minimum training. The survey results are independent of survey speed and are objective and repeatable. The information from these surveys can be entered into a bridge deck condition data base, which can be used as an integral part of a BMS. Repeat surveys on the same decks can be carried out to monitor the progressive development of problem conditions.

## ACKNOWLEDGMENT

The work described here was carried out under an FHWA HPR study [HPR-PR-PL-1(28)] by the NHDOT Bureau of Materials and Research and INFRASENSE, Inc. The authors wish to acknowledge the cooperation and support of FHWA and NHDOT and the contributions of Michael Juranty and Paul Matthews of NHDOT and Arash Sotoodehnia and Virginia Games of INFRASENSE, Inc.

## REFERENCES

1. K. R. Maser. *New Technology for Bridge Deck Assessment.* Report FHWA-NETC-90-01. New England Transportation Consortium, Center for Construction Research and Education, Department of Civil Engineering, Massachusetts Institute of Technology; FHWA, U.S. Department of Transportation, May 1990.
2. K. R. Maser. *Bridge Deck Evaluation Utilizing High Speed Radar.* New Hampshire Department of Transportation, Bureau of Materials and Research, Nov. 15, 1991.
3. C. G. Neill, Jr. *Evaluation of Ground-Probing Radar for Rapid Delamination Detection.* Report FHWA/RD-86-190. FHWA, U.S. Department of Transportation, 1986.
4. T. Chung and C. R. Carter. *Radar Signal Enhancement for DART.* Report MAT-89-05. Research and Development Branch, Ontario Ministry of Transportation, Downsview, Ontario, Canada, June 1989.
5. K. R. Maser. Bridge Deck Condition Surveys Using Radar: Case Studies of 28 New England Decks. In *Transportation Research Record 1304,* TRB, National Research Council, Washington, D.C., 1991.



*Publication of this paper sponsored by Committee on Structures Maintenance and Management.*

# Use of High Molecular Weight Methacrylate Monomers To Seal Cracks in Bridge Decks, Retard Alkali-Silica-Aggregate Reactions, and Prime Bridge Surfaces for Overlays

MICHAEL M. SPRINKEL

Presented are the results of a study undertaken to evaluate the performance of high molecular weight methacrylate (HMWM) monomers used to (a) treat the cracks and seal the surfaces of two tined bridge decks, (b) seal the surface of one untined bridge deck, (c) fill the cracks and seal the surface of a pavement to retard an alkali-silica-aggregate reaction, and (d) prime the surface of a bridge deck for a polyester styrene concrete overlay. For the two tined bridge decks, the evaluation was based on data collected during application, skid tests, permeability tests on cores removed from decks, petrographic examination of the cracks in the cores, and inspections of the decks for leaks. The evaluation indicated that no significant problems were associated with the application and that the treatments partially filled the top ½ in. of the cracks. However, because of traffic- and temperature-induced strains across the cracks, the polymer in many of the treated cracks was cracked after 1 year in service. Even so, the treatments significantly reduced the permeability to chloride ions of the top 2 in. of both the cracked and uncracked sections of the decks. The permeability of cores taken from treated cracked and uncracked areas after 1 year was 59 and 43 percent, respectively, of the permeability of the untreated bases. After 3 years, the permeability was 64 and 42 percent, respectively. Study results indicate that applying HMWM monomers is a practical way to reduce the infiltration of chloride ions into concrete surfaces with cracks that are wider than 0.15 mm because of the low cost and ease with which the treatment can be applied as compared with a pressure injection of epoxy. Results also indicate that HMWM monomers can be applied as a prime coat to improve the bond strength of polyester styrene concrete overlays.

Cracks in concrete can provide water and salt easy access to reinforcement, which can cause premature corrosion. The use of an injection of epoxy to seal cracks is costly and time-consuming; therefore, a more economical method of sealing cracks is needed. High molecular weight methacrylate (HMWM) monomers can be applied to the surface of a bridge deck to seal the concrete and fill and seal the cracks (*1*–*7*). The application is a simple process that does not require specialized pressure-injection equipment. Typically, a promoter and an initiator are mixed with the monomer, and the monomer is applied to the cracked surface with a broom or squeegee. Aggregate is usually broadcast onto the monomer to provide for adequate skid resistance. When cracks are not closely spaced, the monomer can be applied only to the cracks, without covering the entire deck surface.

The California Department of Transportation applied HMWM monomers to seal cracked and deteriorated concrete in bridge decks, retard alkali-aggregate reactivity, and prime surfaces before placing a premixed polyester overlay (*1,7*). HMWM monomers have been used to seal cracks in a bridge in Texas (*1*), a bridge in Iowa (*2*), and a bridge in Florida (*3*), and to extend the life of a continuously reinforced concrete pavement in South Dakota that was spalling because of an alkali-silica-fine aggregate reaction (*4*).

The Virginia Department of Transportation (VDOT) has also used HMWM monomers on bridge decks (*6*). Tests for recracking strength and filling conducted on concrete specimens prepared in the laboratory indicated that HMWM monomers can be successfully used to seal cracks of variable widths (0.2 to 2.0 mm) and moisture content (*5*).

## BACKGROUND

A demonstration conducted in 1987 showed that a simple application of an HMWM monomer was as effective in sealing some cracks in the tined deck of a bridge on I-81 in Virginia as a vacuum injection of methacrylate and was more effective than a pressure injection of epoxy (*8*). Although none of the three treatments successfully filled the cracks (typically 0.1 to 0.2 mm wide), a low-modulus HMWM monomer (Rohm & Haas PCM 1680) filled approximately 50 percent of the volume of the cracks in the top 4 in. of the deck. It is believed that a factor in the relative success of using the HMWM monomer was the time of application—it was applied in the early morning when the cracks were open. Because of the time required to prepare cracks for injection, injections of the other materials were not performed until the afternoon, when the cracks were closed. The HMWM monomer was selected to treat the cracks in the deck because of the anticipated low cost: approximately $1/ft, compared with approximately $6/ft for routing and sealing with a low-modulus epoxy, $20/ft for a pressure injection of epoxy, and $40/ft for a vacuum injection of methacrylate (*6*). In addition, the entire deck

Virginia Transportation Research Council, Box 3817 University Station, Charlottesville, Va. 22903-0817.

surface could be sealed with the HMWM monomer for about $1/ft^2$.

A meeting was held by VDOT to obtain the input necessary from FHWA and industry representatives to draft a special provision for the treatment of the cracks in the decks of the bridges on I-81 (*6*). Because it had been noted during the demonstration that a small amount of the HMWM monomer had leaked through the cracks into the New River, the special provision required that the contractor protect traffic, waterways, and bridge components from the monomer. It is believed that the unit price for the treatment was high because of this requirement, which made it necessary for the contractor to work on the underside of the deck to seal the cracks or collect the drips.

At least five companies market an HMWM monomer for use in treating cracks. Four were noted elsewhere by Sprinkel (*6,8*), and the fifth, Transpo Industries, Inc. (New Rochelle, New York), supplied the T-70-M and T-70-X monomers that were used. Unfortunately, data on the physical properties of HMWM monomers and concrete are limited, and recommendations for applications differ as a result of the recent development of the monomers. Therefore, it was necessary to collect the data needed to revise the special provision to prescribe the physical properties of the monomers and the application requirements for future installations. The literature from the five manufacturers stated that each could provide an HMWM monomer with a viscosity of 8 to 25 cps (Brookfield Model LVT Viscometer, Spindle 1 at 60 rpm), specific gravity of 1.02 to 1.08 at 77°F, low odor, bulk cure in less than 3 hr at 73°F, surface cure in less than 8 hr at 73°F, and gel time of 20 to 50 min.

## PURPOSE AND SCOPE

The purposes of this paper are as follows:

1. Describe the application of two HMWM monomers on two tined bridge decks, the condition of the cracks immediately following the treatments and 1 and 3 years after installation, and data on the physical properties of the monomers (*6*). The evaluations were based on skid tests (ASTM E524), permeability tests on cores (AASHTO T277), petrographic examination of cores taken from cracks, and periodic on-site inspections of the underside of the decks for leaks.
2. Describe the results of using an HMWM monomer to seal an untined bridge deck.
3. Describe the results of using an HMWM monomer to fill cracks and seal the surface on a section of I-64 to retard an alkali-silica-aggregate reaction.
4. Describe the results of using an HMWM monomer as a primer for a polyester styrene concrete overlay for a bridge deck.

## RESULTS

### Tined Bridge Decks on I-81

#### *Description of Application*

The two bridges are continuous-span, steel-plate-girder bridges constructed with prestressed concrete subdeck panels and composite, site-cast concrete decks (*6*). Each bridge has five plate girders and 10 spans. The southbound travel lane (SBTL) was opened to traffic in September 1985 and the northbound travel lane (NBTL) in September 1986. Transverse cracks were observed in both decks in 1986 directly above the joints between the subdeck panels. Longitudinal cracks were observed above the girders.

Cracks in two spans treated with a high-modulus HMWM monomer (T-70-M) and cracks in two spans treated with a low-modulus HMWM monomer (T-70-X) were evaluated. The application of the two HMWM monomers was performed in accordance with the special provision (*6*) that required the contractor to protect traffic, waterways, and bridge components from the monomer. To satisfy this requirement, the contractor suspended polypropylene tarpaulins under the decks from the parapets on each side of the bridges. By using the tarpaulins to catch drippings, it was not necessary to caulk or seal the cracks on the underside of the decks. According to the contractor, no monomer dropped onto the tarpaulins.

The special provision also required that the concrete surface and the cracks be blasted with oil-free compressed air to remove dirt, dust, and other loose material before application of the monomer. Finally, the special provision required that the monomer be applied between 1 a.m. and 11 a.m. at a deck surface temperature between 55°F and 70°F. According to the inspector, the monomer was applied between sunrise and 11 a.m. at a deck surface temperature between 51°F and 70°F. On many days, the application was stopped before 11 a.m. because the deck temperature had reached 70°F (*6*).

Each monomer was mixed in 1- or 2-gal batches and poured into 2-gal spray cans that were used to apply it to the cracks. HMWM monomer gels rapidly when contained in large quantities, and therefore 1 gal or less of mixed monomer was placed in a spray can. The monomer was applied to the cracks at the rate of 200 ft/gal. According to the inspector, many spray cans became inoperable because the monomer gelled in the nozzle or in the line between the nozzle and the container. The special provision required three applications to each crack. However, because of the narrow width of many of the cracks and because the first application tended to seal the top of the cracks, only the wider cracks received more than one application. As can be seen in Figure 1, the deck surface within 3

**FIGURE 1 HMWM monomer applied to cracks in tined bridge. To maintain good skid number, excess resin in valleys must be broomed over deck surface before it gels.**

in. of a crack was usually treated with the resin. When too much resin was applied to a crack, the excess resin was brushed over the deck surface before it gelled so that the grooves were not filled.

Once the cracks were filled, the monomer was applied to the deck surface to seal the concrete and bring the color of the deck surface between the cracks close to the color of the surface in the vicinity of the cracks. The monomer used to seal the deck surface was mixed in 5-gal batches and applied with an airless sprayer (see Figure 2).

The monomers were supplied by Transpo Industries, Inc. and applied by Academe Paving, Inc. The application was initiated on May 10 and completed on June 2, 1988, with no significant problems. Only 13 workdays and 17 days of lane closure were required for the $271,496 contract. The cost was as follows:

- Traffic control: $39,538 (14.6 percent),
- Crack sealing: 15,000 ft @ $2.97/ft + 226 gal HMWM @ $85.20/gal = $63,805 (23.5 percent), and
- Deck treatment: 125,656 ft² @ $0.77/ft² + 838 gal @ $85.20/gal = $168,153 (61.9 percent).

### *Mechanical Properties of HMWM Polymer Specimens*

The mechanical properties of the HMWM polymer specimens are presented in Table 1. The 2-in. cube specimens of T-70-X and T-70-M were molded at the job site using an ASTM C33 concrete sand. The sand/monomer ratio was approximately 4.5 to 1 by weight. Some of the neat tensile specimens were molded at the job site, and some were molded in the laboratory of VDOT's Materials Division. Subsequent to the treatment of the decks on I-81, other HMWM monomers were evaluated. Data for specimens of RPM-1100-V polymer that were molded at the materials laboratory and at a pavement job site (I-64 in New Kent County) are also presented in Table 1.

The data for compressive strength and modulus of elasticity (ASTM C109) shown in Table 1 are typical for cubes of HMWM polymer and sand. The data for tensile strength, elongation at break, and modulus of elasticity (ASTM D638) are typical for very brittle polymers, such as T-70-M, and flexible polymers, such as RPM-1100-V. On-site inspections in June 1988 revealed many cracks in the T-70-M polymer in the deck cracks and few cracks in the T-70-X polymer in the deck cracks. However, it can be seen from the data that the T-70-X polymer lost most of its flexibility within 15 months, which may explain the large increase in the number of cracks in the polymer in the deck cracks after 1 year in service. The T-70-M specimens were too brittle to test after 15 months. Neat cubes of T-70-M made during the installation on I-64 shattered at compressive strengths of less than 3,000 psi when tested at 30 hr and 28 days. On the other hand, neat cubes of RPM-1100-V were compressed 1 in. without failure when tested at 28 days of age. More flexible polymers such as RPM-1100-V should do a better job of sealing cracks that move.

**FIGURE 2 Airless spray guns were used to apply HMWM resin to surface of tined bridge deck. Note that work crew is wearing rubber boots and gloves, impermeable coveralls, and canister breathing masks.**

### *Tests on Cores*

Cores 4 in. in diameter and approximately 5.5 in. in length were removed from the NBTL of Spans 6 and 7 (treated with T-70-X) and Spans 8 and 9 (treated with T-70-M). Twenty-eight cores were removed in June 1988, and 14 were removed in July 1989. The cores were taken through transverse cracks, longitudinal cracks, and concrete that did not appear to be cracked (see Table 2).

Two 2-in.-thick slices were cut from each core. One slice was cut from the top 2 in. of each core ("top" in Figure 3), and the second slice was cut at a depth of 2 1/8 in. to 4 1/8 in. from the top surface ("base" in Figure 3). In 1988, the cores were taken in pairs approximately 2 ft apart along cracks selected for evaluation. Two slices from one core in each pair were subjected to rapid permeability tests, and two slices from the other core were subjected to a tensile splitting test.

After the rapid permeability tests were conducted, a slice ¾ in. thick, 2 in. wide, and approximately 4 in. long was cut from each permeability specimen. The slice was cut in the vertical plane and perpendicular to the crack in the specimens with the cracks (see Figure 3). Both surfaces were polished and examined under the microscope so that the width of the crack could be measured as a function of depth and so that the percentage of the crack width that was filled with HMWM monomer could be recorded as a function of depth. Forty-eight cracked surfaces were examined in 1988; none were examined in 1989.

The two segments that were left after the center slice was cut from each permeability specimen were subjected to a flexural test. A total of 56 specimens were tested in flexure in 1988; none were tested in 1989.

After the permeability tests on cores taken in 1989, the specimens were subjected to a splitting tensile test, and, therefore, 14 cores did not have to be taken for splitting tensile tests in 1989. The intent of the tests on the cores was to obtain as much information as possible from as few cores as possible.

**Permeability to Chloride Ion** The results of the tests for the permeability to chloride ion (AASHTO T277) of slices of cores 2 in. thick taken in 1988 and 1989 are presented in Table 3. A value of 1,000 to 2,000 C is considered to represent low permeability; 2,000 to 4,000, moderate; and more than 4,000,

**TABLE 1 Mechanical Properties of Specimens of HMWM Polymer**

| Specimen Type | Age | Strength (psi) | | Elongation at Break (%) | | Young's Modulus of Elasticity[a] ($lb/in^2 \times 10^4$) | |
|---|---|---|---|---|---|---|---|
| | | $\bar{X}$ | $s$ | $\bar{X}$ | $s$ | $\bar{X}$ | $s$ |
| T-70-M mortar cubes | 2 mo | 6,420 | 660 | — | — | 24.0 | 5.5 |
| T-70-M mortar cubes | 15 mo | 6,500 | 330 | — | — | 25.5 | 2.4 |
| T-70-M mortar cubes | 3 yr | 6,440 | 12 | — | — | — | — |
| T-70-X mortar cubes | 2 mo | 8,000 | 160 | — | — | 20.3 | 2.7 |
| T-70-X mortar cubes | 15 mo | 8,540 | 590 | — | — | 25.5 | 6.3 |
| T-70-X mortar cubes | 3 yr | 8,680 | 176 | — | — | — | — |
| T-70-M neat tensile | 7 day | 215 | 106 | 0.5 | 0.3 | 4.40 | 0.37 |
| T-70-M neat tensile | 15 mo | — | — | — | — | — | — |
| T-70-X neat tensile | 7 day | 3,036 | 402 | 5.4 | 0.8 | 5.80 | 0.47 |
| T-70-X neat tensile | 15 mo | 881 | 397 | 1.3 | 0.4 | 6.77 | 1.05 |
| T-70-X neat tensile | 3 yr | 447 | 75 | 2.1 | 1.3 | 3.79 | 3.48 |
| RPM-1100-V neat cubes[b] | 28 day | 4,250 | 350 | — | — | — | — |
| RPM-1100-V mortar cubes | 28 day | 7,390 | 14 | — | — | — | — |
| RPM-1100-V neat tensile | 7 day | 2,900 | 230 | 20.2 | 5.0 | — | — |

[a]Measured at ≤0.004 in./in. for cubes and ≤0.05 in./in. for tensile specimens.
[b]At 1-in. deflection.

**TABLE 2 Tests Conducted on Tined Bridge Cores**

| Type Crack in Core | Number of Cores Taken | | Permeability Tests | | Petrographic Examinations | | Flexural Tests | | Tensile Splitting Tests | |
|---|---|---|---|---|---|---|---|---|---|---|
| | 1988 | 1989 | 1988 | 1989 | 1988 | 1989 | 1988 | 1989 | 1988 | 1989 |
| Transverse | 16 | 8 | 16 | 16 | 32 | 0 | 32 | 0 | 16 | 16 |
| Longitudinal | 8 | 4 | 8 | 8 | 16 | 0 | 16 | 0 | 8 | 8 |
| None | 4 | 2 | 4 | 4 | 0 | 0 | 8 | 0 | 4 | 4 |
| Total | 28 | 14 | 28 | 28 | 48 | 0 | 56 | 0 | 28 | 28 |

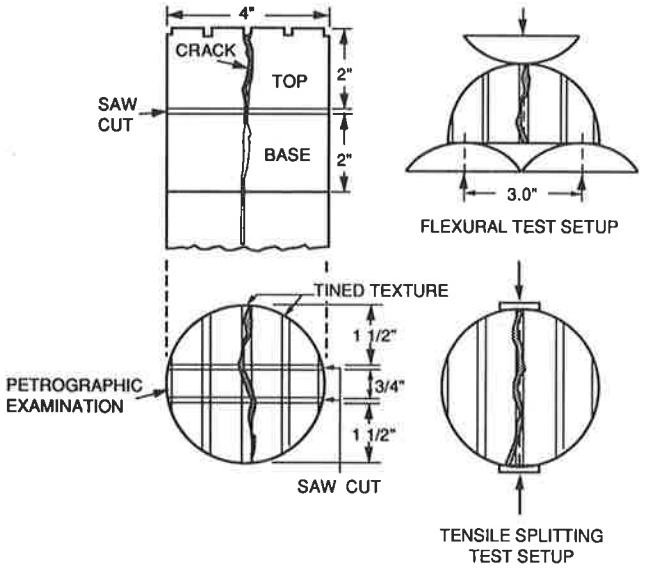


**FIGURE 3 Sketch of test specimens obtained from tined bridge cores.**

high. The data in Table 3 show that the average permeability of the top 2 in. of the cores taken in 1988 was 44 percent of that of the base concrete, and for cores taken in 1989, it was 52 percent of that of the base concrete. No tests were performed on base concretes in 1991, but the average permeability of the top 2 in. of the cores was 57 percent of the average of the bases tested in 1988 and 1989. The permeability increased after 1 and 3 years in service, probably as a result of traffic wearing away the HMWM coating and cracking the HMWM polymer in the cracks. However, the protection provided by the T-70-X polymer has not changed much in 3 years.

The data in Table 3 also suggest that after 1 and 3 years the permeability of the cracks treated with T-70-M had increased more than the permeability of the cracks treated with T-70-X, which was expected because the T-70-X is more flexible than the T-70-M. In addition, the permeability of the transverse cracks had increased more than that of the longitudinal cracks after 1 year, as was expected because the transverse cracks moved more than the longitudinal cracks. However, after 3 years, the permeability of the longitudinal cracks had also increased. It is not known why the average permeability for the base concrete without cracks was higher than

**TABLE 3 Permeability of Tined Bridge Cores to Chloride Ions (Coulombs)**

| Type Crack | HMWM Monomer | 1988 | | | 1989 | | | 1991 | | |
|---|---|---|---|---|---|---|---|---|---|---|
| | | Top 2 in. | Base | Top/ Base | Top 2 in. | Base | Top/ Base | Top 2 in. | Base | Top/ Base |
| Transverse | Both | 1,669 | 3,528 | .47 | 1,980 | 2,444 | .81 | 2,187 | 2,986 | .73 |
| Longitudinal | Both | 1,373 | 3,570 | .38 | 1,391 | 3,612 | .39 | 2,039 | 3,591 | .57 |
| Both | Both | 1,570 | 3,539 | .44 | 1,784 | 3,028 | .59 | 2,113 | 3,284 | .64 |
| None | Both | 1,297 | 3,850 | .34 | 1,908 | 4,404 | .43 | 1,718 | 4,127 | .42 |
| All specimens | T-70-X | 1,427 | 3,416 | .42 | 1,496 | 3,013 | .50 | 1,550 | 3,215 | .48 |
| All specimens | T-70-M | 1,635 | 3,571 | .46 | 2,107 | 3,960 | .53 | 2,412 | 3,766 | .64 |
| All specimens | Both | 1,531 | 3,497 | .44 | 1,801 | 3,487 | .52 | 1,981 | 3,492 | .57 |

the average for the concrete with cracks. The lower permeability of the cracked specimens cannot be attributed to the HMWM monomer because little monomer penetrated the cracks to a depth of 2 to 4 in.

**Petrographic Examinations** Figures 4 and 5 show the results of petrographic examinations of vertical, polished cracked surfaces obtained by cutting a slice ¾ in. wide from the top 2 in. and next 2 in. of each of 12 cores (see Figure 3). Both cut surfaces were polished and examined under the microscope, and, therefore, 48 surfaces were obtained from 12 cores taken through cracks in 1988. No petrographic examinations were performed in 1989.

Figures 4 and 5 show the average width of the cracks as a function of depth and the average width that is filled with HMWM monomer. The transverse cracks were typically wider than the longitudinal cracks. The following can be seen from Figures 4 and 5:

- Many of the cracks are much wider at the surface than throughout the top 4-in. depth of the deck.
- The cracks are very narrow (less than 0.2 mm), except on the surface.
- The HMWM monomer did not fill the cracks very well at depths greater than 0.5 in. from the surface.
- There is no difference in the performance of the monomers (T-70-X versus T-70-M) from the standpoint of percentage of crack width filled as a function of depth.

Laboratory work (*5*) indicated that the monomer worked well for cracks 0.2 to 2.0 mm wide. It is unlikely that any currently available crack-filling technique would have led to the cracks being filled more because of the narrow width of most of the cracks. Fortunately, the American Concrete Institute (ACI) indicates that cracks up to 0.18 mm wide are tolerable in concretes that are exposed to deicing chemicals and therefore do not need to be sealed (*9*). Because of their low viscosity, penetrating sealers (such as silanes or siloxanes) may have done a better job of sealing the walls of the cracks.

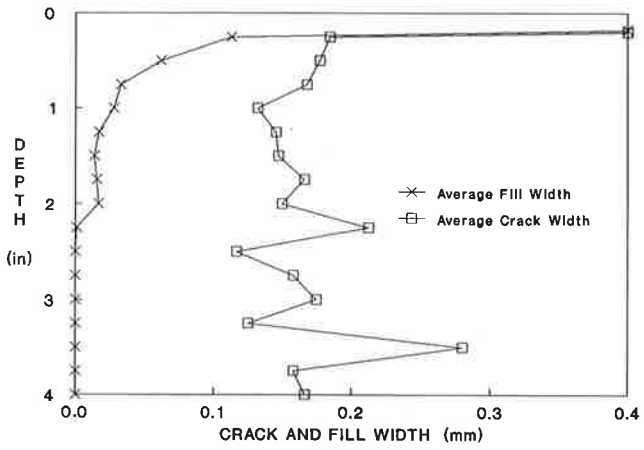


**FIGURE 4 Average crack width and crack width filled versus depth (tined bridge), all cracks, Spans 6 and 7 (T-70-X). At surface, average fill width = 1.09 mm and average crack width = 1.26 mm.**

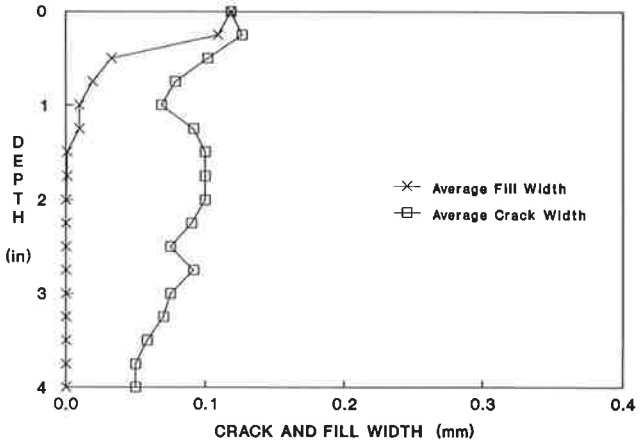


**FIGURE 5 Average crack width and crack width filled versus depth (tined bridge), all cracks, Spans 8 and 9 (T-70-M). At surface, average fill width = 0.12 mm and average crack width = 0.12 mm.**

To see the relationship of crack width and the percentage of crack width filled, cracks were grouped according to width for each of the depths from the surface for which measurements were made:

- At the surface, most cracks were 95 percent filled, regardless of width.
- At a depth of ¼ in. from the surface, cracks wider than 0.15 mm were 92 percent filled, but cracks 0.15 mm wide or narrower were 44 percent filled.
- At a depth of ½ in. from the surface, cracks wider than 0.15 mm were 57 percent filled, but cracks 0.15 mm wide or narrower were 35 percent filled.
- At depths of ½ in. or more from the surface, the data were too variable to draw conclusions, but most cracks were filled less than 20 percent, and no HMWM polymer was found at depths of more than 2¼ in. However, one crack as narrow as 0.05 mm was 100 percent filled at a depth of 1 in.

**Flexural Tests** As shown in Figure 3, the portions of the cores that were left after a slice was cut for petrographic examination were subjected to a three-point flexural test to determine the degree to which the HMWM monomer treatment had bonded the sides of the cracks together and restored the flexural strength of the concrete. A modulus of rupture was computed for each specimen using the ASTM C293 formula as follows:

$$R = 1.5\ Pl/bd^2$$

where

$R$ = modulus of rupture,
$P$ = maximum applied load,
$l$ = 3 in.,
$b$ = 2 in., and
$d$ = depth of specimen at point of fracture.

The treatment did not restore the flexural strength of the concrete. The average modulus of rupture was 110 psi for the

cracked specimens, compared with 990 psi for the uncracked specimens taken from the top 2 in. of the cores in 1988. The results were expected, considering that the HMWM monomer did not completely fill the cracks (*6*).

The surfaces of the failed specimens were examined to determine the location of the failure. For the cracked specimens, no failures occurred in the concrete, and all failures occurred through the cracks. On the average, 40 percent of the failed surfaces from the top 2 in. of the cores were coated with polymer and 60 percent were coated with dust, road dirt, and carbonation. Of the failed surfaces from the base slices, 100 percent were coated with dust, road dirt, and carbonation, and no polymer was observed. Because of the foreign material in a crack in a structure that is in service, it is unlikely that any crack-filling technique can bond the crack surfaces together unless a technique is developed to clean the surfaces of the crack before the filling operation. The restoration of flexural strength in laboratory specimens (*5*) can be attributed to the fact that the surfaces of the cracks were clean before the treatment because the specimens were fabricated, broken in flexure, put back in molds, treated with HMWM monomer, and broken in flexure a second time. No flexural tests were done on cores taken from the bridge deck in 1989.

### *Tensile Splitting Tests*

In 1988, slices 2 in. thick were cut from one core for each pair of cores taken along a crack and from one-half of the cores taken through uncracked concrete. The slices were subjected to a tensile splitting test as described in ASTM C496 and shown in Figure 3. The specimens were loaded at the rate of 2,000 lb/min, and the tensile splitting strength was computed as $2P/ld$, where $P$ is the applied load, $l$ is 2 in., and $d$ is 4 in. In 1989, tensile splitting tests were conducted on the specimens that had been subjected to the rapid permeability test because the specimens were not needed for petrographic examinations and flexural tests. Test specimens with an $l/d$ ratio of at least 1 as required by ASTM C 496 could not be tested because the HMWM did not fill the cracks at depths greater than 2.0 in.

Similar values in the range of 420 to 670 psi were found for the cracked and uncracked specimens in 1988 and 1989, which suggests that the HMWM monomer restored the tensile strength of the concrete across the crack. However, this result is not supported by the petrographic examinations or the flexural test results. Evidently, the test subjected the cracked surfaces to shear instead of tension, and there were enough irregularities between the surfaces that shear stresses were transferred as well as in the uncracked concrete. Approximately 30 percent of the failures in the cracked specimens occurred in the concrete in 1988 and 1989. The failures that occurred through the cracks provided surfaces that were coated with polymer, dust, road dirt, and carbonation.

### *Skid Resistance*

Skid tests were conducted at 40 mph using the bald tire (ASTM E524) and the treaded tire (ASTM E501). Tests were done with the bald tire in the summer of 1988, following the treatments, and with both tires in 1989. As can be seen from the data in Table 4, the treated surfaces have an acceptable skid resistance. The acceptable skid resistance (bald tire numbers greater than 20) can be attributed to the tined texture of the deck surface and the fact that the HMWM monomer did not fill the valleys in the texture. The application of sand (1 lb/yd$^2$) may have had a minor effect.

### *Visual Inspections*

The inspector made visual inspections of the underside of the bridges during periods of rain for 1 year following the treatments. According to the inspector, some leaks were noted on Spans 6–9 of the NBTL, but he attributed the leaks to the holes caused by taking cores from the deck. An inspection by the author in the spring of 1989 revealed efflorescence next to the joints between the subdeck panels on approximately 50 percent of the joints on the NBTL. Very little efflorescence was noted on the underside of the deck on the SBTL. The efflorescence was more prevalent in the negative moment areas, as was expected. There was not a clear difference between the quantity of efflorescence under Spans 6 and 7 as compared with Spans 8 and 9. The design of the continuous-span structure and the large amount of deflection under traffic likely accelerated the cracking of the polymer in the cracks.

## Untined Bridge Deck

Rohm & Haas PCM 1100 and 1500 monomers were applied to the eastbound lane of two spans of an untined bridge on Route 601 over Polecat Creek in June 1986. Approximately

**TABLE 4 Skid Numbers at 40 mph in Travel Lane**

| Structure | Spans | HMWM Treatment | Sand Application (lb/yd$^2$) | Skid Numbers | | | | |
|---|---|---|---|---|---|---|---|---|
| | | | | Treaded Tire | | Bald Tire | | |
| | | | | 1987 | 1989 | 1987 | 1988 | 1989 |
| I-81 Deck | 6 & 7 | T-70-X[a] | 1 | — | 48 | — | 36 | 36 |
| I-81 Deck | 8 & 9 | T-70-M[a] | 1 | — | 45 | — | 37 | 35 |
| I-64 Pavement | — | R & H 1540[b] | 0 | 7 | — | 7 | — | — |
| I-64 Pavement | — | R & H 1540[b] | 0.3 | 39 | — | 39 | — | — |
| I-64 Pavement | — | R & H 1540[b] | 1.0 | 55 | — | 47 | — | — |
| I-64 Pavement | — | R & H 1540[c] | Excess | 62 | — | 59 | — | — |
| I-64 Pavement | — | R & H 1540[d] | Excess | 61 | — | 59 | — | — |
| I-64 Pavement | — | None | 0 | 46 | — | 24 | — | — |

[a]150 ft$^2$/gal.
[b]126 ft$^2$/gal.
[c]58 ft$^2$/gal.
[d]38 ft$^2$/gal.

20 to 30 min after the deck was flooded with the HMWM monomers and before gelation of the monomers, the deck was covered with an excess of dry grade A silica sand (±No. 16 sieve size, Table II-19, VDOT *Road and Bridge Specifications*, July 1982) to provide a good skid number. Class I waterproofing (VDOT *Road and Bridge Specifications*, July 1982) was applied to all other areas of the deck. The sections with the HMWM monomers and the Class I waterproofing were opened to traffic at the end of each workday. The results of tests conducted on the overlays in July 1987 and November 1989 are presented in Table 5. The results are based on the average of three tests on each overlay. It can be seen from the data in Table 5 that the HMWM monomer treatment is performing almost as well as the Class I waterproofing (EP5-LV epoxy sand overlay). However, in 1989 the HMWM treatment had all been worn away in the wheel paths, whereas the epoxy overlay was in place. Therefore, epoxy overlays should be used when it is necessary to increase the skid resistance of a bridge deck.

### Pavement with Alkali-Silica-Aggregate Reaction

Test sections were placed in June 1986 and August 1987 on the untined westbound travel lane of I-64 in Louisa County near Route 616 and in October 1989 on the tined eastbound and westbound travel lanes of I-64 in New Kent County. Monomer was also applied with a squeeze bottle to individual cracks in June 1986.

The applications placed in June 1986 were removed the following year when the concrete was replaced. Cores taken through the cracks following the treatments indicated that the monomer partially filled the top 1 in. of the cracks.

The 50-ft sections placed in August 1987 were tested for skid resistance in September 1987. The relationship between the skid number and the sand application rate can be seen in Table 4. Sections placed with 0 and 0.3 lb/yd$^2$ of sand were removed before the opening of the pavement to traffic. Most of the sand placed on the other sections was in place in 1991.

The twenty 100-ft test sections placed in October 1989 are currently under evaluation. Monomers applied to these sections included Revolan RPM-1100-V, Transpo T-70-M, and Sika Pronto 19.

### Bridge with Polyester Styrene Concrete Overlay

A multiple-layer polyester concrete overlay was placed on a 33-span bridge on Route 33 in September and October 1988 (*6*). Approximately 1 hr before the placement of the first layer of the overlay on the westbound lane, a primer was placed on each of 6 spans.

The following materials were used in the installation:

- Primer, Span 7: a general purpose, one-component polyurethane primer called Deco-Rez Type I supplied by General Polymers;
- Primer, Span 8: a three-component high-modulus HMWM primer called T-70-P supplied by Transpo Industries;
- Primer, Span 9: a three-component low-modulus HMWM primer called T-70-X supplied by Transpo Industries;
- Primer, Span 10: a three-component low-modulus HMWM primer called RPM-1100-V supplied by Revolan Systems;
- Primer, Span 11: a three-component HMWM high-modulus HMWM primer called RPM-2000 supplied by Revolan Systems (routinely used as a primer for polyester overlays in California);
- Primer, Span 12: a three-component medium-modulus HMWM primer called RPM-2000XT supplied by Revolan Systems;
- Polyester resin: a one-component, general purpose, unsaturated polyester resin called 32-044 supplied by Reichhold Chemical; and
- Aggregate: a No. 8 to No. 20 graded, dry, angular-grained silica sand.

Tensile adhesion tests (ACI 503R) were conducted on each of 9 spans of the bridge: 3 spans with no primer and 6 spans with primer at the ages of 27 days, 1 yr, and 3 yr. The tests showed that the average tensile rupture strength at 27 days, 1 yr, and 3 yr was significantly greater for the spans that received the primer (see Table 6). On the basis of the test results, it is recommended that a primer be used for all multiple-layer polyester concrete overlays. A special provision for a multiple-layer polyester/methacrylate overlay system that consists of a first course of HMWM monomer and two courses of polyester was prepared (*6*).

**TABLE 5 Test Results for Untined Bridge**

| | Average Tensile Rupture Strength (psi) | | Failure at Bond Interface (%) | | Permeability of Top 2 in. (C) | | Permeability of Base Concrete (C) | |
|---|---|---|---|---|---|---|---|---|
| Overlay | 1987 | 1989 | 1987 | 1989 | 1987 | 1989 | 1987 | 1989 |
| HMWM | 294 | 453 | 20 | 83 | 1,301 | 1,529 | 7,189 | 5,640 |
| EP5-LV | 175 | 342 | 63 | 47 | 1,087 | 1,187 | — | 6,447 |

**TABLE 6 Tensile Rupture Strengths of Bridge Spans with Overlay**

| Span | Primer | Average Strength (psi) | | |
|---|---|---|---|---|
| | | 1988 | 1989 | 1991 |
| 7 | Polyurethane | 361 | 355 | 199 |
| 8 | T-70-P | 351 | 360 | 204 |
| 9 | T-70-X | 268 | 284 | 242 |
| 10 | RPM-1100-V | 363 | 181 | 179 |
| 11 | RPM-2000 | 338 | 298 | 194 |
| 12 | RPM-2000-XT | 365 | 307 | 183 |
| 6, 13, 14 | None | 186 | 229 | 103 |
| 7–12 | All | 341 | 298 | 200 |

## CONCLUSIONS

1. On the basis of inspections of cores, it is estimated that, on average, the HMWM monomer filled 95 percent of the crack width at the surface. Cracks wider than 0.15 mm were 92 percent filled at a depth of ¾ in., 57 percent filled at a depth of ½ in., and less at greater depths. Cracks 0.15 mm or less in width were 44 percent filled at ¾ in., 35 percent filled at ½ in., and less at greater depths. HMWM monomer was observed at depths up to 2¾ in. and in cracks as narrow as 0.05 mm.
2. The HMWM monomer probably did not penetrate and fill the cracks more completely because of the narrow width of the cracks, less than 0.2 mm on average. Cracks that are wider than 0.2 mm are better candidates for the HMWM monomer treatment.
3. The HMWM monomer treatment did not restore load transfer across the cracks because the monomer only partially filled the cracks and because of the dust, road dirt, and efflorescence on the cracked surfaces. Because of contaminants on the walls of cracks in structures in service, it is unlikely that crack treatments of any type can bond the sides of cracks together.
4. The HMWM monomer treatment reduced the permeability of the cracked and uncracked concrete to chloride ion. The reductions were greater for the longitudinal cracks than for the transverse cracks, particularly after 1 year in service. After 3 years, the protection provided by the T-70-M polymer had decreased, but that provided by the T-70-X polymer had not changed much.
5. Acceptable skid numbers were obtained when the HMWM monomer was applied to a tined texture and when an excess of sand was applied to the HMWM monomer applied on untined surfaces.
6. HMWM monomer can be applied as a prime coat to improve the bond strength of polyester styrene concrete overlays.

## RECOMMENDATIONS

1. The application of HMWM monomers such as T-70-X should be considered when it is necessary to reduce the infiltration of chloride ions into cracked concrete surfaces, with cracks having a width of 0.15 mm or more.
2. HMWM monomers should be used as a prime coat to improve the bond strength of polyester styrene overlays.

## ACKNOWLEDGMENTS

This study was sponsored by the Virginia Transportation Research Council and FHWA.

## REFERENCES

1. Minutes of the First Technical Advisory Committee Meeting for Demonstration Project No. 948, Polymers for Highway Construction and Maintenance. FHWA, Falls Church, Va., Nov. 6–7, 1985.
2. V. J. Marks. *High Molecular Weight Methacrylate Sealing of a Bridge Deck.* Iowa Department of Transportation, Ames, May 1987.
3. FlaDOT's Seven-Mile Bridge Is Sealed, Healed, and Protected with a Spread of Sika Pronto 19. *Sika News,* Vol. 4, No. 2, Spring 1990, pp. 13–17.
4. G. Crawford. Summary of Demonstration Projects in South Dakota Using High Molecular Weight Methacrylate. Memorandum to Ted Ferragut, Demonstration Projects Division, FHWA, Washington, D.C., July 29, 1988.
5. W. D. Mangum et al. *Repairing Cracks in Portland Cement Concrete Using Polymers.* Research Report 385-27. University of Texas at Austin, Nov. 1986.
6. M. M. Sprinkel. *Evaluation of the Use of High Molecular Weight Methacrylate Monomers to Seal Cracks in Decks on I-81 Over the New River.* VTRC 91-R19. Virginia Transportation Research Council, Charlottesville, April 1991.
7. P. D. Krauss and L. Ferroni. *New Bridge Deck Rehabilitation Techniques Being Implemented in California Utilizing Polymers.* California Department of Transportation, Sacramento, Spring 1985 (revised April 1986).
8. M. M. Sprinkel. Evaluation of Crack Repairs on I-81 NBL Over New River. Memo to D. V. Cranford, VTRC, Charlottesville, Va., July 15, 1987.
9. Control of Cracking. *Manual of Concrete Practice,* Section 224R-19, Part 3, American Concrete Institute, Detroit, Mich., 1987.

---

*The opinions, findings, and conclusions expressed in this report are those of the author and not necessarily those of the sponsoring agencies. Product names were included in the paper because the author did not have sufficient information to describe them generically. Their inclusion in no way constitutes an endorsement.*

*Publication of this paper sponsored by Committee on Adhesives, Bonding Agents and Their Uses.*

# Inclusion of Rebar Corrosion Rate Measurements in Condition Surveys of Concrete Bridge Decks

GERARDO G. CLEMEÑA, DONALD R. JACKSON, AND GARY C. CRAWFORD

The benefits derived from measuring rebar corrosion rates in existing concrete bridge decks as part of condition surveys were examined using data collected from several bridge decks by traditional inspection methods. Rebar corrosion rates correlated reasonably well with metal losses observed in rebar specimens. Further, it appeared that a metal loss of 3 percent to 6 percent by weight may be the threshold metal loss necessary to initiate delamination in reinforced concrete decks. However, because rebar corrosion rates also vary with location in a deck and with temporal fluctuating conditions in the concrete, their use in estimating the remaining service life for concrete decks will be questionable until an appropriate methodology for determining the representative rebar corrosion rate for a deck and relating such to service life has been developed.

Corrosion of embedded rebars is the primary cause of premature concrete deterioration in concrete bridge decks. Therefore, a combination of inspection methods, such as visual inspection for concrete cracks and spalls, sounding for delamination by chain drags or other techniques (*1–4*), measurement of half-cell potentials (ASTM C876), chemical analysis of concrete samples for chloride contents (*5,6*), and use of a pachometer for measurement of concrete cover, are used in condition surveys of bridge decks. Together, the first three inspection methods provide reasonably thorough information on the extent of the concrete deterioration already existing in a deck. The information provided by the remaining methods allows the bridge maintenance engineers only to guess what may happen to the rest of the deck in the near future. To eliminate such guessing by allowing the engineers to predict, with reasonable certainty, the amount of possible future corrosion damage to the rebars and the concrete would require a method for measuring the existing rate of rebar corrosion, which governs the rate of concrete deterioration. Such a method can also be useful in assessing the effectiveness of the various deck repair or treatment procedures in controlling rebar corrosion.

Responding to this need, FHWA sponsored a study at the former National Bureau of Standards that led to the development of a prototype portable device for measuring the corrosion rate of rebars in concrete in the field (*7*). Through adaptation of the three-electrode linear polarization (3LP) resistance technique, this device measures potentiostatically the DC polarization resistance of a rebar, from which the rate of corrosion of the rebar is calculated by using the Stern-Geary (*8*) equation:

$$I_{corr} = \frac{B_a B_c}{2.3(B_a + B_c)} \frac{dI}{dE} = k\frac{dI}{dE} \quad (1)$$

where

$I_{corr}$ = corrosion current (mA),
$(dI/dE)$ = slope of polarization plot (mA/mV),
$B_a$ = anodic Tafel coefficient,
$B_c$ = cathodic Tafel coefficient, and
$k$ = formula constant.

To facilitate its routine use in the field, this prototype 3LP device was modified and made available commercially by Clear (*9*).

The electrical resistance measured by this polarization technique includes the resistance of the concrete itself, which could contribute to considerable error in the calculated corrosion rate if not corrected for. The powerful AC impedance technique, which uses AC signals of varied frequencies to polarize the rebar, overcomes this problem by allowing separate measurement of the resistance of the concrete and, in addition, provides insight into the mechanism of the corrosion reactions (*10*). However, the technique requires complex data interpretation, which makes transfer of this technique from the laboratory to the field less practical than the DC polarization technique. For this reason, only the 3LP device was used in this study to measure rebar corrosion rate.

To predict future damage, the ability to measure the rebar corrosion rate in bridge decks alone is not adequate because, similar to half-cell potentials, the corrosion rate can be expected to vary with both location and time. Because of nonhomogeneity in concrete, rebars at different locations are exposed to varied corrosive conditions and, therefore, undergo corrosion at different rates.

The corrosion rate of rebars at any location, in turn, changes with time—reflecting the seasonal fluctuations of variables such as moisture and oxygen content in the concrete and temperature. It is also possible for an increase of chloride concentration in the concrete with time to influence the corrosion rate. Therefore, a measured corrosion rate is valid for only the time during which the measurement was made. It is, therefore, necessary to take into consideration these possible

G. G. Clemeña, Virginia Transportation Research Council, Box 3817 University Station, Charlottesville, Va. 22903-0817. D. R. Jackson, Federal Highway Administration, 6300 Georgetown Pike, McLean, Va. 22101. G. C. Crawford, Federal Highway Administration, 400 7th Street, S.W., Washington, D.C. 20590.

fluctuations of rebar corrosion rates in bridge decks when attempting to estimate future corrosion damage in terms of projected metal loss in the rebars and its resulting damage to the surrounding concrete.

To facilitate the understanding of the manner in which the rebar corrosion rate may fluctuate with location in a deck, the authors collected and analyzed data from several concrete decks using the 3LP method and various other traditional inspection methods. This paper describes the collection and analysis of these data. It also discusses data obtained from semicontinuous monitoring for more than a year of the corrosion rates of rebars in three fabricated concrete slabs that contained a high concentration of chloride. These data were intended to shed light on the manner with which the rebar corrosion rate may fluctuate seasonally.

## EXPERIMENTAL PROCEDURES

### Deck Surveys

In conjunction with another study that involved a half-cell potential survey of bridge decks, five concrete bridge decks were used in this study. During the survey on each deck, a preliminary sounding was conducted to allow selection of a survey area that included numerous delaminated areas. A square survey grid of 2.5-ft spacing was then marked on the selected area for detailed inspection through the use of various traditional inspection methods.

#### *Traditional Inspection Methods*

The traditional inspection methods used included visual inspection, sounding with chain drags and a hammer, and measurement of half-cell potentials. Visible concrete distresses such as cracks (especially those above the transverse rebars) and spalls were recorded and carefully mapped to within 2 in. Chain drags and a hammer were used to detect concrete delaminations, which were similarly mapped to within 2 in.

#### *Survey of Rebar Corrosion Rates*

The modified 3LP device was used to measure rebar corrosion rates in each deck. Because of the amount of time (at least 2 min) required to perform the measurement at each location, or grid point, a grid spacing of 5 ft was used.

To measure the corrosion rate of a rebar at each grid point, the location and depth of the nearest rebar were determined with a pachometer. A probe assembly, which consisted of a pen-sized $Cu/CuSO_4$ reference electrode and a surrounding counter electrode that was made of a sponge-encased copper mesh, was then placed directly above the rebar. The probe assembly was then connected to the rebar network in the deck and to the 3LP device, and procedures were conducted to measure the polarization resistance of the rebar. These procedures, described by Clear (*9*), essentially entailed incremental polarization of the rebar to achieve potential shifts of 4, 8, and 12 mV (in ascending order) and noting of the respective amounts of direct current needed to be applied through the counter electrode to effect these potential shifts. Using these data, the linear polarization resistance ($dE/dI$), which is the slope of the "best-fitting" line, was calculated. Assuming a formula constant of 41, as suggested by Clear (*9*), the corrosion current was calculated from Equation 1. To allow comparison, the calculated corrosion current (in milliamperes) was instead expressed in terms of corrosion current density ($I_d$) (i.e., current per unit area of rebar, which was under the influence of the counter electrode), by using the following formula:

$$I_d = \frac{I_{corr}}{A} = \frac{367\ I_{corr}}{BK} \tag{2}$$

where

$I_d$ = corrosion current density ($mA/ft^2$),
$A$ = surface area of rebar ($ft^2$),
$B$ = equivalent bar size (number of eighths of an inch), and
$K$ = rebar length beneath the counter electrode (in.).

The calculated corrosion current densities were then plotted in iso-contour lines for each deck.

After completion of each survey, the rebars at several selected locations were extracted by partial concrete coring for examination and determination of the thicknesses of concrete cover and accumulated metal or weight losses as a result of corrosion. The criterion used in the selection was that the measured corrosion rates of the rebars at these selected locations must closely represent the range of corrosion rates observed in the survey area.

The following procedures were used to determine the metal loss on each piece of extracted rebar:

1. The rebar was thoroughly cleaned by careful chipping with chisels and light sandblasting to remove corrosion products and the portion weakened by pittings.
2. The curved ends of the rebar were cut off to provide straight ends that facilitated measurement of the length ($L$) of the rebar, which was then made with a caliper to the nearest 0.01 in.
3. Using a top-loading balance, the weight of the rebar ($W$) was then measured to the nearest 0.01 g. The weight was divided by 453.6 to convert to pounds.
4. The metal loss of the rebar, in percentage by weight, was then estimated by using the following relationship:

$$ML = 100 \times [(W/L)_i] - [(W/L)_f]/(W/L)_i \tag{3}$$

where

$ML$ = metal loss,
$(W/L)_f$ = final weight per unit length (lb/in.), and
$(W/L)_i$ = estimated initial weight per unit length of the rebar (lb/in.).

The $(W/L)_i$ was assumed to be the same for all extracted rebars in each survey area and was the average weight per unit length of two extracted rebars from each survey area that had no visible sign of corrosion. The major sources of errors in each estimate of metal loss included the cleaning of the

rebar specimens (overcleaning or undercleaning) and the estimation of $(W/L)_i$ for each deck sampled. It was estimated that the combined error was at least 1.2 percent by weight.

## Monitoring Rebar Corrosion Rates in Concrete Slabs

### *Fabrication of the Concrete Slabs*

Three reinforced concrete slabs (3 ft × 3 ft), each with a different thickness of concrete cover (1, 2, or 3 in.) over the top-mat rebars, were fabricated according to the plan shown in Figure 1. The concrete mixture used was a Virginia Department of Transportation Class A4 concrete (*11*). To accelerate corrosion of the top-mat rebars, enough NaCl was added to the concrete mixture for the top 3-in. layer of each slab to yield a chloride ion concentration of 10 lb/yd$^3$ of concrete.

To allow measurement of the temperature and moisture content of the concrete, thermocouples and calibrated soil moisture probes were installed in each slab at two locations shown in Figure 1.

### *Monitoring of Slabs*

The slabs were allowed to cure outdoors for at least 60 days before the corrosion rate of the rebars, the concrete temperature, the moisture in each slab, and the outdoor air temperature were monitored. Measurements of the rebar corrosion rate in each slab were restricted to the two same rebars (see Figure 1) throughout the monitoring period, during which the slabs were exposed to the outdoor environment. The monitoring lasted for approximately 16 months—from December 1989 to April 1991.

## RESULTS AND DISCUSSION

The accuracy of the corrosion rates as determined by the commercial 3LP device was uncertain. This is due to uncertainty on the appropriateness of the suggested values of some parameters (*9*) used in the calculation of the corrosion rate, namely the Tafel constants ($B_a$ and $B_c$) and the surface area of the rebar that was actually under the influence of the counter electrode during each measurement. A recent comparison

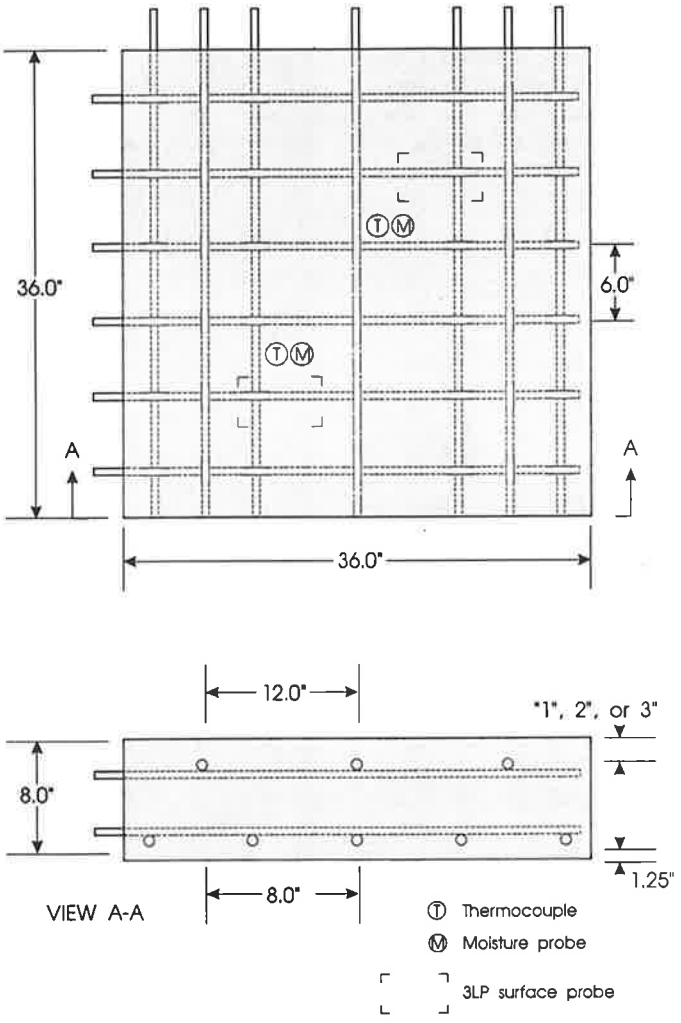


**FIGURE 1 Outdoor-exposed concrete slabs used to monitor variation of rebar corrosion rate with seasons.**

with other similar devices indicated that the corrosion rate values obtained with 3LP devices may be relatively high (*12*). Nevertheless, the calculated corrosion rates for each survey area were at least suitable for internal comparison.

### Variation of Rebar Corrosion Rate With Location

As expected, the corrosion rates of rebars across a concrete bridge deck varied. This variation is shown in Figure 2, which shows the contour map of the rebar corrosion rates observed in the survey area of Structure 09302. These corrosion rates ranged from 0.11 to 4.5 mA/ft², or 0.054 to 2.2 mil/year. (Higher corrosion rates have been observed in other decks.) This typical contour map shows the presence of several areas wherein rebars corroded at relatively high rates. The orientation of these active areas coincided with the orientation of the transverse top-mat rebars of the deck, which are typically the ones to corrode first. As Figure 2 shows, the concrete at many of these active areas was already deteriorated, as evidenced by the presence of transverse cracks and delaminations. That is not unexpected. The structure had been in service for approximately 20 years at the time of the survey, and the rebars may have been corroding for at least 10 years.

This variation in rebar corrosion rate with location has implications for how a survey of corrosion rates should be conducted for a bridge deck. Because the benefit of such a survey is to allow prediction of when the rebars will reach the threshold corrosion necessary to damage the concrete, it is obviously of no use to measure the corrosion rates in concrete that is already damaged. Therefore, if a deck does not yet show any sign of corrosion-related damage in the concrete, the survey of rebar corrosion rates should be conducted over the entire deck; otherwise, the survey should be limited to the portions of the deck that are still undamaged. A combination of sounding and a survey of half-cell potentials can be used to screen out the damaged areas before a survey of corrosion rates (see other paper in this Record by Clemeña et al.).

Once a survey has been completed, analysis of the observed corrosion rates would require use of appropriate statistical parameters. As shown in Figure 3, which shows the frequency distributions for the study areas in Structure 09302 and two other decks, the rebar corrosion rates in a bridge deck tend to assume a log-normal distribution instead of a normal distribution. Similarly, half-cell potentials in concrete bridge decks have been observed to assume log-normal distributions, with rare exceptions (see other paper in this Record by Clemeña et al.). Therefore, the use of statistical parameters appropriate to a log-normal distribution (such as a geometric rather than arithmetic mean) would avoid an erroneous estimation of the severity of the rebar corrosion rates in a bridge deck.

### Correlation Between Corrosion Rate and Metal Loss

The variation in rebar corrosion rate with location in a concrete deck, as shown in Figure 2, also raises an interesting question: Is there any possible relationship between the instantaneous corrosion rates that are obtained during a survey and the current physical condition of the rebars? To provide

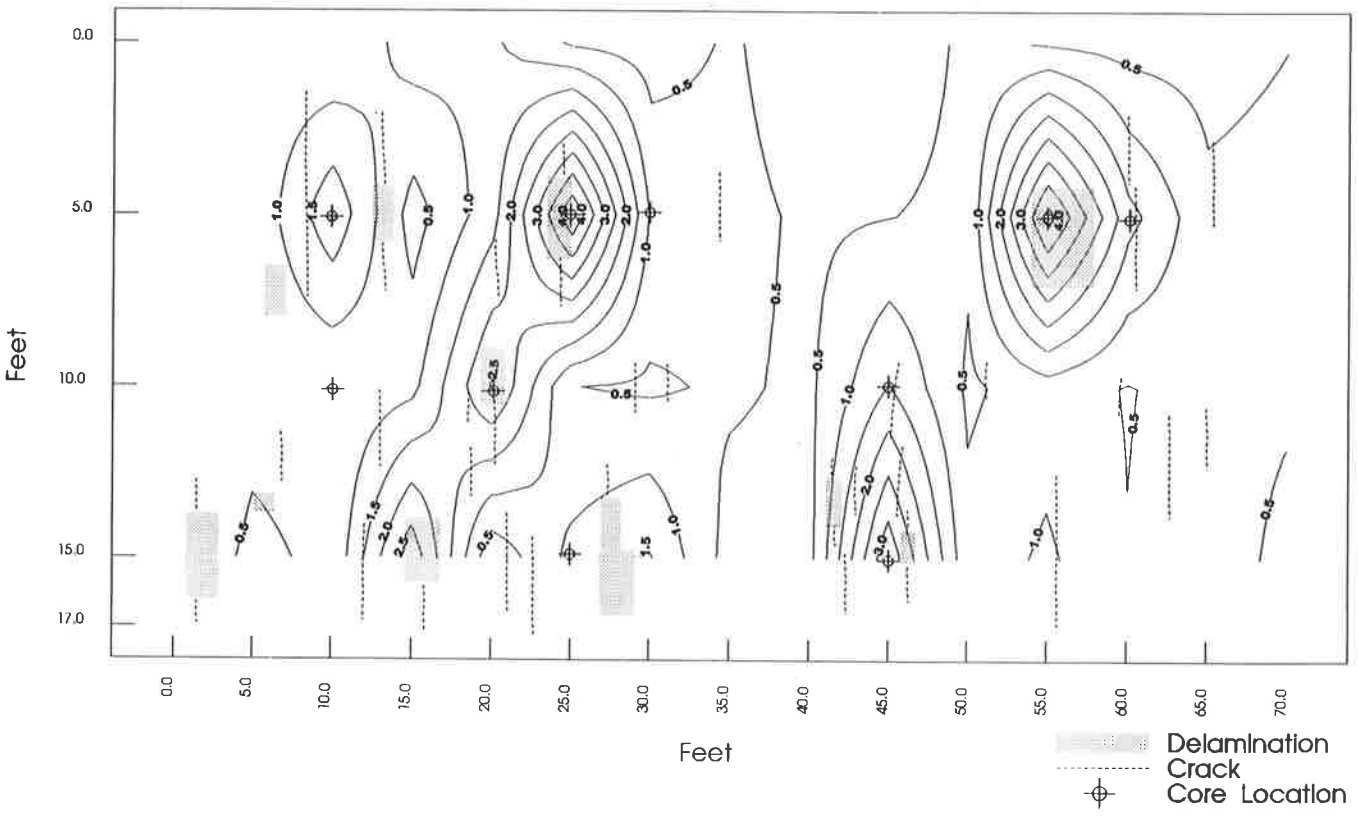


**FIGURE 2 Contour map of rebar corrosion rates (mA/ft²) observed in a section of Structure 09302.**

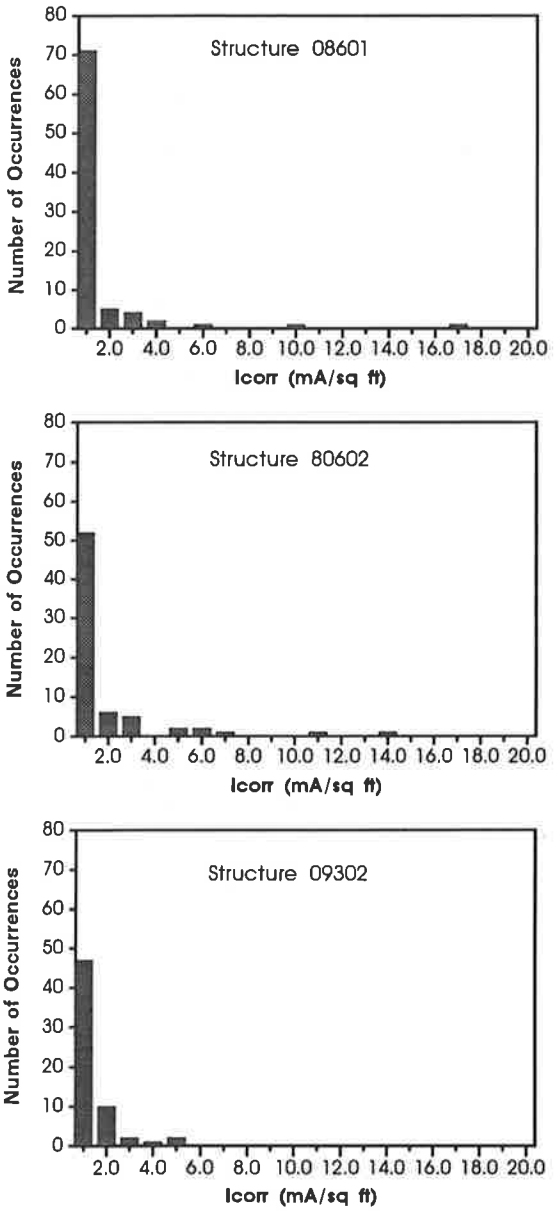


**FIGURE 3 Frequency distributions of rebar corrosion rates observed in three concrete bridge decks.**

an answer, it is necessary to examine the relationship between corrosion rate and severity of corrosion damage to a rebar or the extent of metal loss on the rebar. The metal loss (*ML*) on a rebar is, simply stated, an accumulated damage that is a direct function of the individual durations (*Ti*) of corrosion (e.g., in number of years) on the rebar and the corresponding individual average annual corrosion rates (*Ri*).

$$ML = \sum_i Ri \times Ti \tag{4}$$

If the annual corrosion rates were assumed to be practically uniform since the initiation of corrosion, then

$$ML = R \times \sum_i Ti = R \times Tt \tag{5}$$

where *Tt* is the total duration of corrosion experienced by the rebar. Equation 5 states that, if all the rebars in a deck started to corrode at different times and at different rates, the metal losses on the rebars at any time would not likely correlate with their corrosion rates alone.

However, correlations between metal losses and rebar corrosion rates alone appeared to exist for the bridge decks studied, at least for rebars from the same deck. For example, when the rebars at several selected grid points in the survey area in Structure 09302 were examined, it was observed that the severity of the damage on each rebar was visually directly related to the measured corrosion rate of the rebar (see Table 1). When the damage on the rebar was expressed quantitatively in terms of metal loss, it showed a significant degree of correlation (coefficient of 0.89) with the corrosion rate, as shown in Figure 4.

A similar correlation was found in the data for the other survey areas, although the degree of correlation appeared to vary from one deck to another (0.81 to 0.99). This implies that corrosion of at least the majority of the rebars in each deck studied started at about the same time. That is, *Tt* was practically the same for the majority of the rebars in a deck; therefore, any difference in the metal losses of the rebars at different locations in a deck was due mostly to differences in the (average) corrosion rates. This also indicates that it could be possible to predict future metal losses (and concrete damage) in statistical terms if the distribution of corrosion rates in a deck could be determined.

Incidentally, when the data from all the deck areas were combined, the resulting correlation between rebar metal loss and corrosion rate was reasonably good and had a correlation coefficient of 0.85 (see Figure 5). Although even less expected, such correlation was not impossible because the ages of these decks were similar (i.e., 19 to 23 years of service).

It is possible to equate metal loss and damage in a concrete, even in a very generalized manner, if a threshold metal loss at which concrete in bridge decks begins to fracture (due to the pressure of the corrosion products) is known. A range of typical threshold metal losses may have to be determined because the threshold is likely to vary among decks as a result of differences in the strength of the concrete and the thickness of the concrete cover over the rebars. Examination of the condition of the concrete and the rebars in the limited number (30) of concrete cores extracted in this study indicated that the threshold metal loss ranged from 3 percent to 6 percent (by weight) among the four decks surveyed, on which the average concrete cover was from 1.49 to 2.14 in. (No determination of the strength of the concrete involved was attempted.) As Table 2 shows, this threshold metal loss was considerably higher than the metal losses equivalent to the threshold depths of attack of 16 to 32 microns reported by Hladky et al. (*13*). However, it is in agreement with those equivalent to the threshold depths of attack reported earlier by the same researchers (*13*).

### Variation of Rebar Corrosion Rates with Time

As discussed earlier, the rebar corrosion rate measured for each location in a concrete deck represents only the instantaneous rate occurring during the survey. Therefore, to as-

**TABLE 1 Relationship Between Measured Corrosion Rate and Rebar Metal Loss in Structure 09302**

| Core Location | Rebar Condition | Corrosion Rate (mA/sq ft) | Rebar Length (in) | Final Weight* (lb) | Final Weight* (lb/in) | Metal Loss (lb/in) | Metal Loss (%) |
|---|---|---|---|---|---|---|---|
| (10, 10) | Very light corrosion in < 5% of surface | 0.56 | 3.373 | 0.2817 | 0.08353 | 0.00137 | 1.6 |
| (30, 5) | Very light corrosion in < 5% of surface | 0.91 | 3.810 | 0.3241 | 0.08506 | −0.00016 | −0.2 |
| (25, 15) | Light corrosion in 35 to 40% of surface | 1.12 | 3.661 | 0.3036 | 0.08292 | 0.00198 | 2.3 |
| (45, 10) | Light corrosion | 1.53 | 2.869 | 0.2432 | 0.08476 | 0.00014 | 0.2 |
| (60, 5) | Pitted in @ 40% of surface | 1.68 | 3.844 | 0.3150 | 0.08196 | 0.00294 | 3.5 |
| (10, 5) | Corrosion in @ 15% of surface | 1.87 | 3.834 | 0.3170 | 0.08269 | 0.00221 | 2.6 |
| (20, 10) | Pitted in @ 55% of surface | 2.55 | 3.312 | 0.2685 | 0.08107 | 0.00383 | 4.5 |
| (45, 15) | Severely pitted in > 50% of surface | 3.44 | 3.804 | 0.3003 | 0.07893 | 0.00597 | 7.0 |
| (55, 5) | Severely pitted in 80 to 90% of surface | 4.21 | 3.883 | 0.3049 | 0.07852 | 0.00638 | 7.5 |
| (25, 5) | Severely pitted in > 90% of surface | 4.47 | 3.834 | 0.3062 | 0.07987 | 0.00503 | 5.9 |

*The average initial weight of each rebar is estimated to be 0.08490 lb/in.

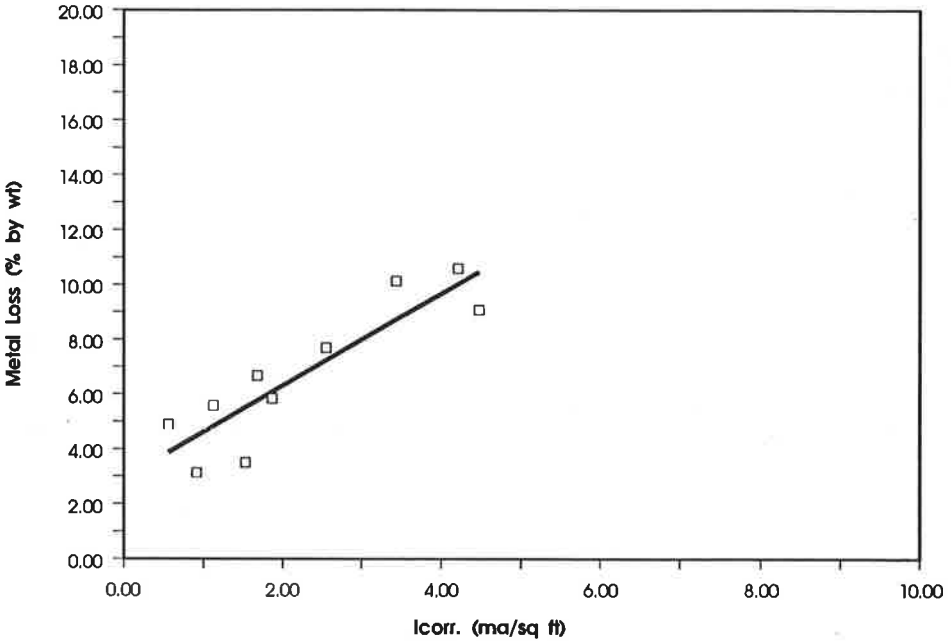


**FIGURE 4 Correlation between metal losses observed on rebar specimens in Structure 09302 and their corresponding corrosion rates.**

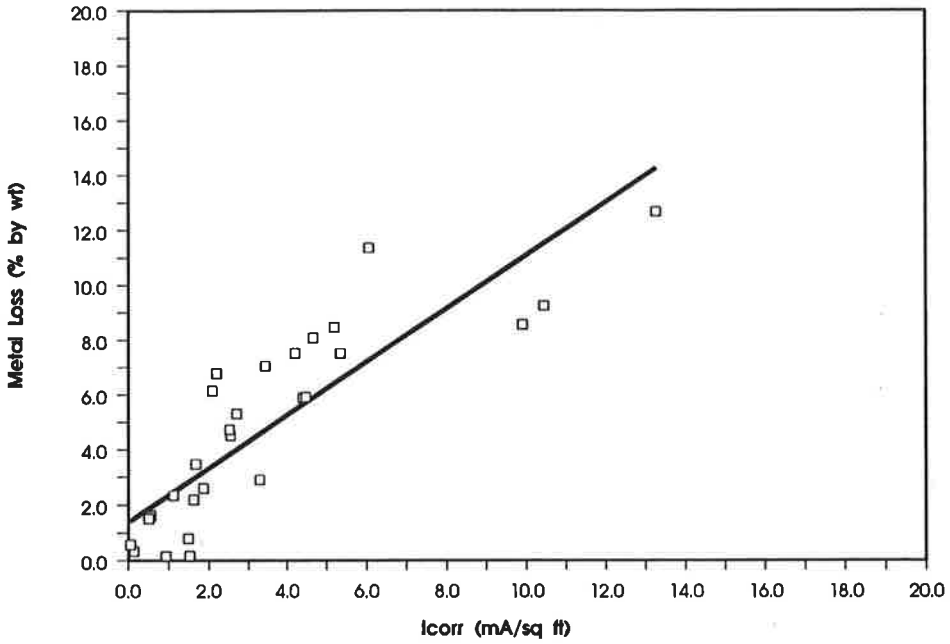


**FIGURE 5 Correlation between metal losses observed on all extracted rebar specimens and their corrosion rates.**

**TABLE 2 Estimated Threshold Depth Attack and Metal Loss on Rebars to Initiate Internal Concrete Cracking**

| Reference | Depth of Attack (μ) | Metal Loss (% by weight) |
|---|---|---|
| 14 | 150 to 300 | 1.9 to 3.8* |
| 14 | 16 to 32 | 0.20 to 0.40* |
| Present study | | 3 to 6 |

*Estimated from reported depths of attack and assuming that the nominal size of rebars was No. 5.

sume that the results of a single survey represent an entire year and the future would likely lead to either underestimation or overestimation of the remaining service life of a deck. To avoid such error, a practical methodology for determining the annual average rebar corrosion rate of a deck, without the time-consuming frequent repetition of the survey, must be developed. To facilitate the development of such a methodology, the influences of moisture and temperature on the corrosion rate of the rebars in three heavily salted concrete slabs were monitored for approximately 450 days, almost on a weekly basis.

As anticipated, the corrosion rates of rebars in the concrete slabs fluctuated considerably with seasons, as shown in Figure 6. The fluctuations were no doubt in response to the combined influences of, at the least, fluctuating moisture and temperature in the slabs, shown in Figure 7. There appeared to be more similarities between the profile for the rebar corrosion rates of the concrete slabs and the profile for the average moisture content in the slabs than with the profile for the average concrete temperature; this probably indicates that moisture has a greater influence on the corrosion rate of rebars than does temperature.

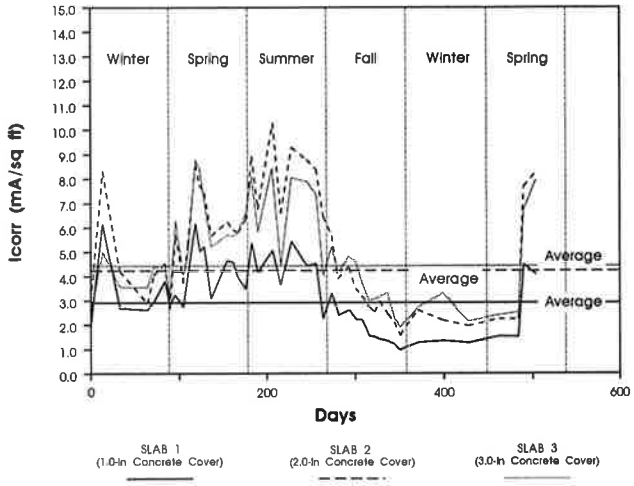


**FIGURE 6 Observed average rebar corrosion rates in test reinforced concrete slabs of varied concrete covers: (a) 1.0 in.; (b) 2.0 in.; and (3) 3.0 in.**

Separate regression analyses of the data for the three concrete slabs indicated that the best relationship between rebar corrosion rate ($I_d$), concrete moisture ($M$), and concrete temperature ($T$) was expressed by

$$I_d = me^{[a + \frac{b}{M} + \frac{c}{T}]} + n \quad (6)$$

where $a$, $b$, $c$, $m$, and $n$ are constants. However, the corresponding correlation coefficients varied considerably between the slabs: with 84 percent for Slab 1, 48 percent for Slab 2, and 66 percent for Slab 3 (see Figure 8).

It also appeared that the corrosion rates of the rebars observed during the monitoring period also tend to be distrib-

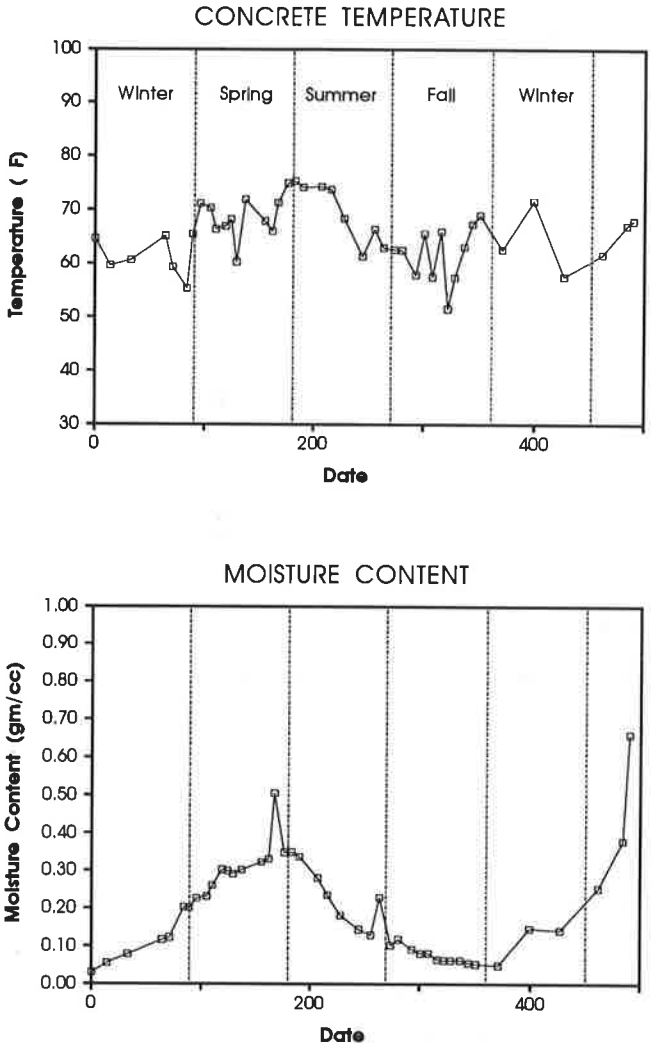


**FIGURE 7 Fluctuations of average temperature and moisture content in test concrete slabs.**

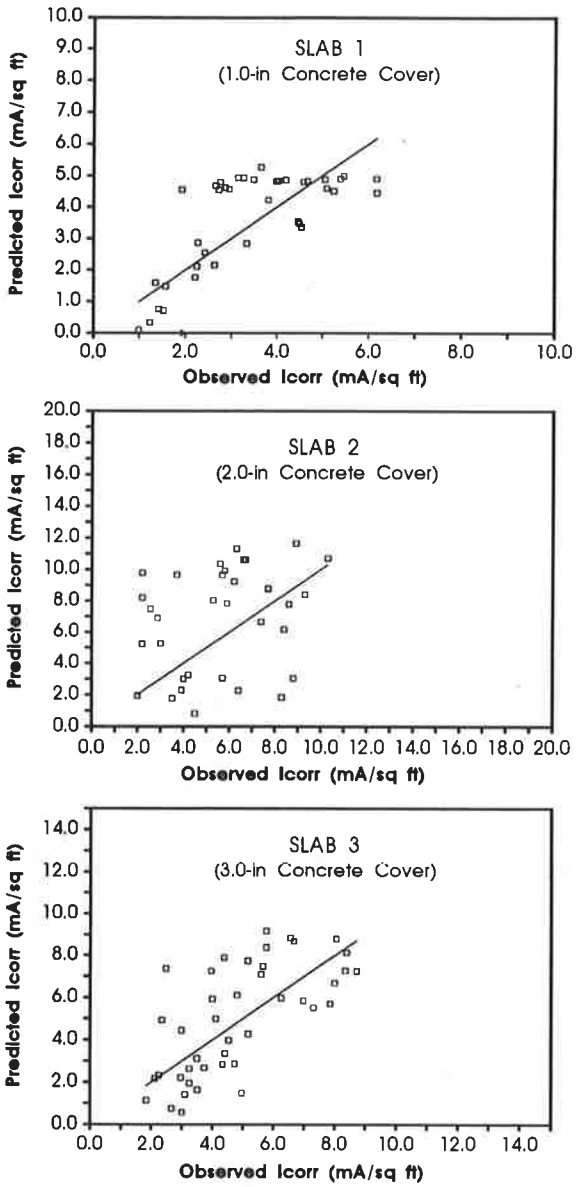


**FIGURE 8 Comparison between observed corrosion rates and those predicted based on concrete moisture and temperature.**

uted log normally (see Figure 9), just as corrosion rates for different locations in a deck were observed to assume. (This is not surprising because other weather-dependent physical variables, such as ambient concentrations of common air pollutants, also tend to assume log-normal distributions.) This is important because it indicates the appropriate statistical parameters to use when conducting a statistical analysis of data related to the spatial and temporal distributions of rebar corrosion rates for a deck.

In predicting the remaining service life of a concrete deck from the rebar corrosion rate, one can use (a) the average annual corrosion rate (at an average or the worst location in the deck), (b) the highest annual corrosion rate (for the worst case scenario), or (c) both the lowest and the highest annual corrosion rates (to estimate a range of possible remaining service life). Because the data presented confirmed that the corrosion rate of rebars in a concrete deck varies not only with location in the deck but also with time, determination of the average annual corrosion rate would require a proper statistical sampling procedure that takes into account both types of fluctuation, which undoubtedly would be time-consuming and costly.

The worst case scenario would be relatively less involved because it would require surveying a deck at a time when the rebar corrosion rate is likely to be at a maximum, which could be early summer or late spring, assuming that the patterns shown in Figure 6 are typical. A disadvantage associated with such worst case analysis is that the resulting estimate of remaining service life may be unrealistically low.

The third alternative could be relatively simple, too, because it probably requires just an additional survey—at a time when the rebar corrosion rate is typically at its lowest, which (according to Figure 6) could be midwinter. This analysis is, however, more practical than the other two alternatives because it yields a range for possible remaining service life. Although one approach may appear to be better in certain aspects than the others, it must be emphasized that the respective merits of these three alternative approaches to predicting the remaining service life of an existing bridge deck

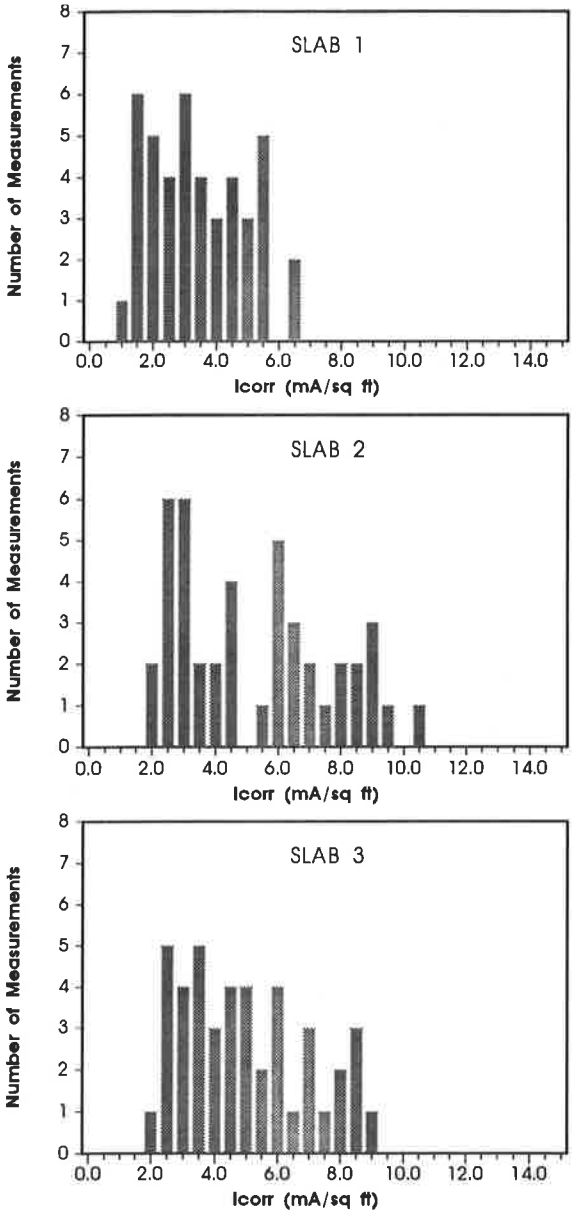


**FIGURE 9 Frequency histograms of rebar corrosion rates observed in test-reinforced concrete slabs.**

have not yet been studied; the data presented could serve as a starting point for such a study.

## CONCLUSIONS

1. Although its accuracy was not verified by another independent method, the 3LP device appeared to be a convenient tool for measuring the corrosion rate of rebars in field concrete. However, the time necessary to make each measurement (approximately 3 min) would make a complete survey of a bridge deck time-consuming.
2. Rebar corrosion rates appear to have a reasonable correlation with rebar metal losses. Based on the limited rebar samples involved in the study, the threshold metal loss that initiates delamination in concrete was estimated to be 3 percent to 6 percent, by weight.
3. Rebar corrosion rate varies not only with locations in a concrete deck but with other influencing factors in the concrete that appear to change with seasons. The frequency of corrosion rates, with respect to locations and time, appears to assume log-normal distributions.
4. In view of these fluctuations, a practical survey method for determining the representative rebar corrosion rate of a concrete deck and an analysis method for relating this rate to remaining service life still need to be developed. Until such methods are available, from the standpoint of bridge deck inspections, the benefits provided by field measurement of rebar corrosion rates would not be fully realized.

## ACKNOWLEDGMENT

This study was supported by highway planning and research funds administered through FHWA.

## REFERENCES

1. G. G. Clemeña and W. T. McKeel. Detection of Delaminations in Bridge Decks with Infrared Thermography. In *Transportation Research Record 664*, TRB, National Research Council, Washington, D.C., 1978, p. 180.
2. F. B. Holt and D. G. Manning. Detecting Delamination in Concrete Bridge Decks. *Concrete International,* No. 2, 1980, p. 34.
3. A. Alongi, T. Cantor, C. Kneeter, and A. Alongi, Jr. Concrete Evaluation by Radar—Theoretical Analysis. In *Transportation Research Record 853*, TRB, National Research Council, Washington, D.C., 1982, p. 31.
4. G. G. Clemeña. Nondestructive Inspection of Overlaid Bridge Decks with Ground-Penetrating Radar. In *Transportation Research Record 889*, TRB, National Research Council, Washington, D.C., 1983, p. 21.
5. H. A. Berman. *Determination of Chloride in Hardened Cement Paste, Mortar and Concrete*. Report FHWA-RD-72-12. FHWA, U.S. Department of Transportation, 1972.
6. G. G. Clemeña, J. W. Reynolds, and R. McCormick. *Comparative Study of Procedures for the Analysis of Chloride in Hardened Concrete*. Report FHWA-RD-77-84. FHWA, U.S. Department of Transportation, 1977.
7. E. Escalante, E. Whitenton, and F. Qui. *Measuring the Rate of Corrosion of Reinforcing Steel in Concrete—Final Report*. Report NBSIR-86-3456. National Bureau of Standards, Washington, D.C., 1986.
8. M. Stern and A. L. Geary. A Theoretical Analysis of the Shape of Polarization Curves. *Journal of the Electrochemical Society,* Vol. 104, p. 56, 1957.
9. K. C. Clear. Measuring Rate of Corrosion of Steel in Field Concrete Structures. In *Transportation Research Record 1211*, TRB, National Research Council, Washington, D.C., 1990, p. 28.
10. J. L. Dawson. Corrosion Monitoring of Steel in Concrete. In *Corrosion of Reinforcement in Concrete Construction* (A. P. Crane, ed.), Ellis Horwood, Chichester, England, 1983.
11. *Road and Bridge Specifications*. Virginia Department of Transportation, Richmond.
12. J. Flis, A. Sabol, P. D. Cady, H. W. Pickering, and K. Osseo-Asare. Evaluation of Corrosion Rates with Various Instruments. In *Assessment of Physical Condition of Concrete Bridge Components—Quarterly Report*, Pennsylvania Transportation Institute, University Park, July 1991.
13. K. Hladky, D. G. John, and J. L. Dawson. Development in Rate of Corrosion Measurements for Reinforced Concrete Structures. Presented at NACE/CORROSION 89, National Association of Corrosion Engineers, New Orleans, Louisiana, 1989.

*The opinions, findings, and conclusions expressed in this paper are those of the authors and not necessarily those of the sponsoring agencies.*

*Publication of this paper sponsored by Committee on Corrosion.*

# Benefits of Using Half-Cell Potential Measurements in Condition Surveys of Concrete Bridge Decks

GERARDO G. CLEMEÑA, DONALD R. JACKSON, AND GARY C. CRAWFORD

The benefits of using half-cell potential measurements in condition surveys of concrete bridge decks were examined using data collected from several decks by visual inspection, sounding with chain draggings, and measurement of half-cell potentials. Half-cell potentials on a deck were found to fluctuate from survey to survey, likely in response to seasonal fluctuations of temperature, oxygen, chloride, and moisture content in the concrete. Consequently, in contrast to ASTM interpretation guidelines (ASTM C-876), the numerical value of each measured half-cell potential by itself would be a poor indicator of the condition of rebars. Instead, the potential measured at each location should be considered relative to potentials measured in the surrounding concrete. When the potentials were plotted on an iso-potential contour map, the locations of active rebar corrosion and corrosion-induced damage in the concrete were associated with high negative potential gradients. Because of the localized nature of rebar corrosion, the recommended grid spacing of 4.0 ft (ASTM C-876) for surveys of bridge decks was found to be too large to allow location of existing active corrosion and the associated damage to concrete. It was determined that a grid spacing of no more than 2.0 ft should be used. If a half-cell potential survey is performed on a sufficiently small grid and the collected measurements are plotted on contour maps of iso-potential lines, the locations of existing active rebar corrosion and corrosion-induced damage in the concrete will be indicated with a high degree of accuracy by areas of relatively high potential gradients. When combined with the other inspection techniques, such a survey would be extremely useful in estimating necessary repair.

Because concrete deterioration resulting from corrosion of embedded rebars is the primary cause of premature deterioration of concrete bridge decks in many states (including Virginia), relevant deck conditions (such as cracking, spalling, delamination, chloride content in the concrete, condition of the rebars, and thickness of the concrete cover over the top-mat rebars) are given considerable attention in bridge deck surveys. Therefore, in addition to visual inspection, other inspection methods (such as sounding with chain dragging for delamination, use of a pachometer, measurement of half-cell potentials, and chemical analysis of extracted concrete samples for chloride contents) are routinely used in detailed condition surveys.

Because these inspection methods require many hours to complete, the adequacy and relevancy of each method must be reexamined whenever warranted. Different concerns are associated with the adequacy and relevancy of each of these inspection methods. Consequently, with the exception of half-cell potential surveys, various efforts have been made to either replace or improve existing methods.

Visual inspection is not quantitative and is tedious, time-consuming, and disruptive to traffic. Research efforts that may lead to its partial replacement have included the use of light-dependent resistors in measuring the width of cracks on concrete surfaces (*1*) and the development of image-processing algorithms for the analysis of the imagery of cracks in concrete surfaces (*2*).

Users have similar concerns with sounding to detect concrete delaminations. To replace it, the use of infrared thermography (*3,4*), short-pulse radar (*5,6*), and impact-echo (*7*) techniques have been reported.

The standard AASHTO method for chloride analysis (AASHTO T-260) is based on a potentiometric titration procedure developed by Berman (*8*) and improved by others (*9*). The method is destructive and expensive because the procedures involved are lengthy and require powdered samples from the deck. To reduce its cost by simplifying the analysis, shortcut procedures based on the same potentiometric approach have been attempted (*10,11*). Unfortunately, all of these procedures require reliance on a proper calibration curve because of adverse solution matrix effects on the potentiometric readings of the sample solutions. In addition, these procedures still require powdered samples from a deck.

The coexistence of corroding areas (or anodic half-cells) and noncorroding areas (or cathodic half-cells) on rebars is reflected in potential differences, or voltages, across the steel-concrete interfaces. These potentials can be measured relative to a constant reference potential provided by a suitable reference electrode. Accordingly, any change in the potential between the reference electrode and the steel-concrete interface can be attributed to, among other things, the corrosion activity at the surface of the steel.

The standard method for measurement of half-cell potentials in concrete (ASTM C-876) is based on a procedure developed by Stratful (*12*). In this method, the half-cell potential of the rebar in concrete is measured by a high-impedance voltmeter connected between the rebar network and a $Cu/CuSO_4$ reference electrode that is in contact with the surface of the concrete. To survey an entire structure, this measurement is repeated by moving the electrode to other locations or points following a grid pattern on the concrete surface. The standard procedure noted that a 4.0-ft grid spacing has

G. G. Clemeña, Virginia Transportation Research Council, Box 3817 University Station, Charlottesville, Va. 22903-0817. D. R. Jackson, Federal Highway Administration, 6300 Georgetown Pike, McLean, Va. 22101. G. C. Crawford, Federal Highway Administration, 400 7th Street, S.W., Washington, D.C. 20590.

been found to be generally satisfactory for bridge decks and that larger spacings increase the probability that localized corrosion areas will not be detected.

Based on data by Stratful et al. (*13*) obtained from surveying bridge decks and those from a laboratory study by Clear and Hay (*14*), the following guidelines are suggested for interpretation of data (ASTM C-876):

1. If potentials over an area are greater than −0.20 V, the probability that no steel corrosion is occurring in the area at the time of measurement is greater than 90 percent.
2. If potentials are in the range of −0.20 to −0.35 V, corrosion activity of the steel in the area is uncertain.
3. If potentials are less than −0.35 V, the probability that steel corrosion is occurring in the area at the time of measurement is greater than 90 percent.

This indicates that there is significant uncertainty in the relationship between half-cell potentials and the condition of rebars. This uncertainty has created doubts among bridge engineers concerning the benefits of using half-cell potential surveys to rank deck repairs and prepare repair plans where the ability to delineate and quantify the amount of needed repair, instead of predicting the probability of rebar corrosion occurring at each location, is desirable. The researchers believe that the uncertainty arose from the constant fluctuation of potential at any location with time, which has been reported recently (*15*), in response to the changing dynamics of the corrosion processes with seasonal fluctuations in the physical properties of concrete.

## PURPOSE AND SCOPE

Because the half-cell potential survey procedure is so simple, inexpensive, and nondestructive, the researchers believed it worthwhile to reexamine the relationship between half-cell potential and condition of the rebar and concrete and to determine if the uncertainty could be resolved so that potential surveys could be used to locate and quantify deteriorated rebars and concrete.

Another aspect that warranted reexamination was the adequateness of the 4.0-ft grid spacing suggested by ASTM (ASTM C-876). It is likely that this spacing is so large that a significant percentage of corrosion-affected concrete areas go undetected. This may have at least partially contributed to the reports of mixed success obtained from the results of using half-cell potential surveys.

To address these issues, the researchers collected data from several concrete bridge decks, using various inspection methods, and analyzed them. The collection and analysis of these data is discussed here.

## EXPERIMENTAL PROCEDURES

Five concrete bridge decks were surveyed in this study. During each survey, a preliminary sounding was conducted to allow selection of a survey area that included numerous delaminated areas. A square grid of either 1.0-ft or 2.5-ft spacing was then marked on the selected area for detailed inspection using various inspection methods.

Visible concrete distresses, such as cracks (especially those above the transverse rebars) and spalls, were recorded and carefully mapped to within 2 in. Sounding was used to detect concrete delaminations, which were similarly mapped to within 2 in.

The measurement of half-cell potentials was facilitated by use of a multiple half-cell array, which consisted of an array of four $Cu/CuSO_4$ electrodes. Depending on the grid spacing to be used in a survey, the electrodes were spaced 1.0 to 2.5 ft apart on a metal mounting bar, which was equipped with a wheel at each end to facilitate movement on the deck. A battery-powered portable data logger (Polycorder 700), which was preprogrammed to serve as a digital voltmeter (with a resolution of 1 mV), was used in conjunction with the half-cell array to store automatically, throughout each survey, all potential readings from the four electrodes. The stored data were then subsequently downloaded to a desktop computer for iso-potential contour mapping and statistical analysis using an appropriate graphic software.

## DISCUSSION OF RESULTS

### Half-Cell Potentials and Concrete Condition

The half-cell potentials obtained from all study areas were correlated with the condition of the concrete. To allow such correlation, it was necessary first to classify a concrete as either sound or deteriorated, on the basis of a criterion that the researchers believed reasonably conformed to the manner with which deteriorated concrete would be removed and repaired in a concrete deck. Accordingly, a concrete was classified as sound if there was no transverse crack, delamination, or spall within 6 in. of the point of measurement of half-cell potential; otherwise, the concrete was classified as deteriorated. Afterward, all the potential readings (approximately 2,000) were categorized into 50-mV increments (−151 to −200 mV, −201 to −250 mV, etc.).

This correlation showed that practically all of the concretes were in sound condition at potentials greater than or equal to −150 mV, and all the concretes were deteriorated at less than or equal to −450 mV (see Figure 1). However, this correlation was characterized by deviations of varied degrees between these extremes. For example, for concretes with potentials between −301 and −350 mV, only 28 to 85 percent were actually deteriorated; for concretes with potentials between −351 and −400 mV, only 70 to 100 percent were deteriorated. (It is believed that this correlation would still be generally valid even if a criterion other than 6 in. was used in classifying the condition of the concrete.) This observation agrees, in general, with the ASTM C-876 guidelines for interpretation of half-cell potentials, even though the guidelines attempted to relate potential only with probability for rebar corrosion.

It is clear that there was not a sufficiently well-defined relationship between concrete condition and the numerical values of individual half-cell potentials, with the exception of potentials at the extreme ends, that engineers can use to prepare repair plans with a reasonable degree of confidence. This also raises a concern about the appropriateness of replacing existing concrete simply because the potential is less than or

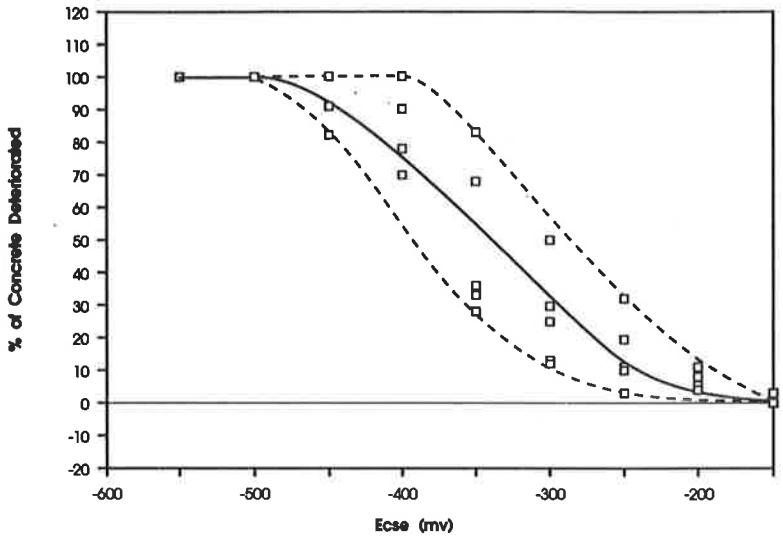


**FIGURE 1 Correlation between half-cell potentials and frequency of damaged concrete observed in all survey areas.**

equal to −350 mV, which is a common practice of many highway agencies.

As will be shown, the absence of such correlation is a result of fluctuation of half-cell potential at any location with time, which is likely in response to fluctuating temperature and moisture in the concrete.

### Potential Gradients and Concrete Condition

It was found that a convenient and effective way to locate active rebar corrosion and its associated damage to the concrete is to plot the results of a half-cell potential survey on an iso-potential contour map, on which the variation in potential gradient is reflected by the spacing between the contour lines, such as that shown in Figure 2 for one of the areas surveyed.

Because of the nonhomogeneity of concrete and, therefore, the distribution of chloride ions across the concrete, the corrosion found on rebars and the associated damage to the surrounding concrete are often localized in nature. Consequently, as the reference electrode is moved from one location on the concrete where the rebar underneath is not corroding to another nearby location where the rebar is actively corroding, the half-cell potential should become more negative. Further, the probability that localized rebar corrosion is occurring at the second location increases as the potential shifts toward a more negative value at a relatively high potential gradient (i.e., the contour lines are closely spaced). Conversely, if the potential shifts toward a more positive value, the probability of localized rebar corrosion occurring at the next location decreases.

Accordingly, the existence of numerous areas where active rebar corrosion was likely to be occurring is indicated in Fig-

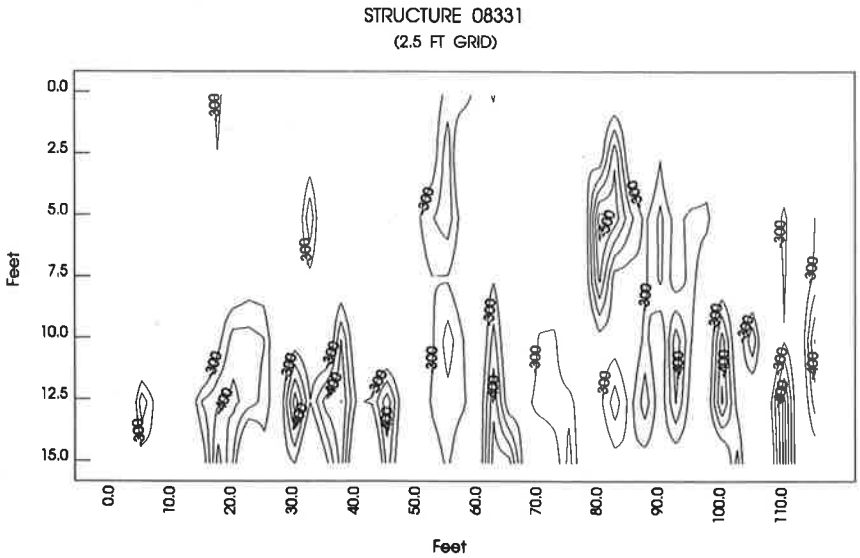


**FIGURE 2 Iso-potential contour map for a survey area. (Only E ≤ −300 mV are plotted in 50-mV increments.)**

ure 2. Over the surface of the concrete, the potential gradients corresponding to these areas ranged from approximately −72 to −172 mV/ft. It is worthwhile to note that the orientation of these areas coincided with the general alignment of the top transverse rebars of the deck, which are the rebars that are likely to corrode first.

Given sufficient time to corrode, the rebars would eventually accumulate a sufficient amount of oxidation products to initiate delamination in the surrounding concrete. Therefore, it is not unreasonable to expect that the concrete at some of the active areas indicated in Figure 2 would already be damaged, especially if the deck had been in service for 20 years. This was in fact the case. When the locations of all the transverse cracks and delaminations detected in the concrete were superimposed on the contour map in Figure 2 (as shown in Figure 3), it was evident that many of the deteriorated concrete areas matched the areas of high negative potential gradients.

A similar correlation between locations of high lateral potential gradients and locations of deteriorated concrete was found for the other survey areas involved in the study. In these areas, the potential gradients ranged from approximately −60 to −300 mV/ft.

It is estimated that at least 85 percent of the deteriorated concrete areas in the survey area depicted in Figure 3 were matched or accounted for by high potential gradients. The failure of this potential survey to account for or detect the remaining deteriorated concrete areas is attributed to the grid spacing of 2.5 ft used in the survey, which appeared to be too large. For example, consider the two narrow delaminated areas at around (61.0 ft, 2.5 ft) and (85.0 ft, 11.0 ft). The edges of both areas were located considerably far (at least 0.7 ft) from their nearest grid points for the effect of the localized corrosion on the rebars to be manifest on the potentials measured at those grid points.

**Optimum Grid Spacing for Half-Cell Potential Surveys**

To determine the optimum grid spacing, it was necessary to determine the maximum lateral distance from a corroding rebar at which the effect of corrosion on the half-cell potential was still discernible. Figure 4 shows a contour map that resulted from detailed measurements of half-cell potential, in an 0.5-ft spacing, around a typical small delaminated concrete area that was approximately 1.2 ft wide. The transverse rebar on which the corrosion that caused the delamination occurred was situated directly beneath the crack at the center; other transverse rebars were spaced 1 ft away. Again, the localized nature of rebar corrosion (and its resulting damage) was manifest in a large potential gradient, which was approximately −250 mV/ft in this case, as the potential shifted from −525 mV at the most active area (center top) to approximately −275 mV at 1 ft away on either side.

If the field of effect is defined as the maximum (lateral) distance from the edge of a delamination or crack to a point on the surface of the concrete where the half-cell potential has shifted sufficiently toward positive to indicate that the underlying rebar corrosion is almost indiscernible and if this potential is assumed to equal −300 mV, Figure 4 shows the field of effect to be less than 8 in. Therefore, if this delamination happened to fall in the middle of a 2.5-ft grid square, it would certainly not be detected. Because similar observations for the other decks indicated that the field of effect was typically no more than 8 to 10 in., it is quite clear that grid spacing of 2.5 ft—let alone the 4.0-ft spacing recommended by ASTM C-876 or the 5.0-ft spacing used by many highway agencies—would still be too large to provide a complete assessment of the condition of a concrete deck.

It appeared that the optimum grid spacing was approximately 1.0 ft. To ascertain this, a 1.0-ft grid spacing was used to conduct a half-cell potential survey on another concrete

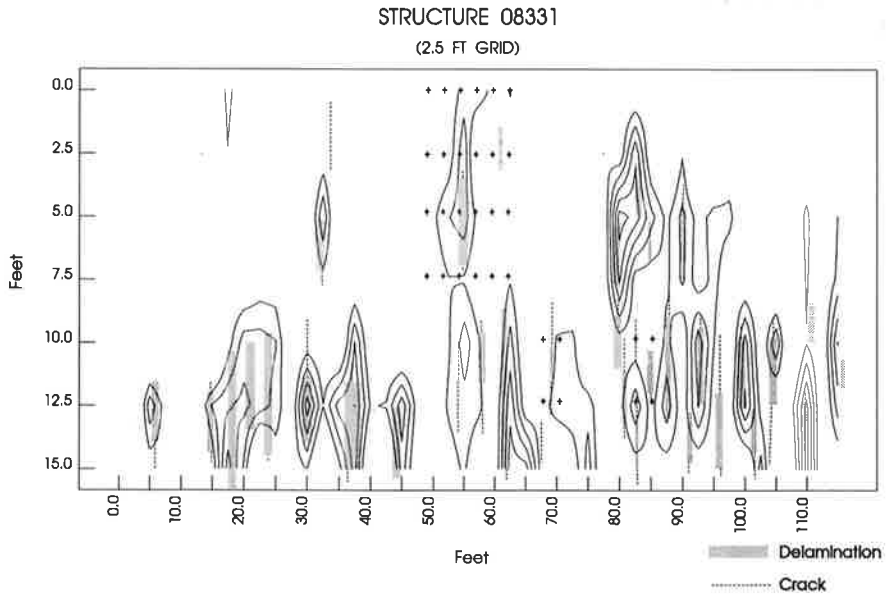


**FIGURE 3 Correlation of transverse cracks and delaminations with potential gradients (2.5-ft grid spacing).**

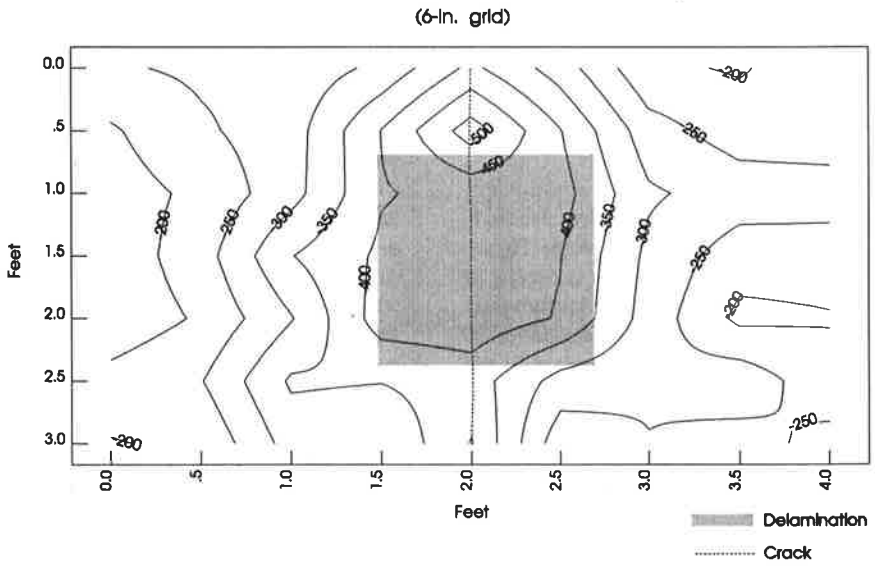


**FIGURE 4 Iso-potential contour lines surrounding a deteriorated concrete area.**

deck. Then, in addition to the usual analysis of the entire set of data, analyses to simulate the use of 2.0-ft and 4.0-ft spacings were also conducted by simply disregarding potentials measured at appropriate grid points during different simulations.

The iso-potential contour map that resulted from the use of 1.0-ft grid spacing (see Figure 5) clearly delineated the presence of numerous areas of high potential gradients, ranging from $-100$ to $-300$ mV/ft. These areas coincided with or accounted for all the delaminations and severe transverse cracks detected.

The contour map also showed several areas in which the potential gradients were high, indicating the presence of relatively active rebar corrosion, but the concrete was still reasonably sound (with the exception of the presence of some fine cracks) by the sounding inspection. In fact, the rebar corrosion rates in a few of these areas (A, B, and C) were measured by a 3LP device and found to be 2.87, 2.94, and 3.09 mA/ft$^2$, respectively; these rates were approximately 3 times higher than those found at grid points (13, 3) and (21, 1), which were 0.99 and 1.06 mA/ft$^2$, respectively.

Based on the generalized correlation between rebar corrosion rate and metal loss that was found to be true for several decks (with 19 to 23 years of service), the level of corrosion observed in areas A, B, and C may translate to a metal loss of approximately 2 percent to 6 percent by weight (see authors' other paper in this Record). Such metal loss is just below an estimated threshold at which concrete could begin to fracture, 3 to 6 percent by weight. This implies that if repair is contemplated a bridge engineer should include the small areas of A, B, C, and others in Figure 5 in the estimation of the quantity of necessary repair. This raises an issue that must be addressed in a future study—the determination of the extent of concrete in each area of high potential gradient that

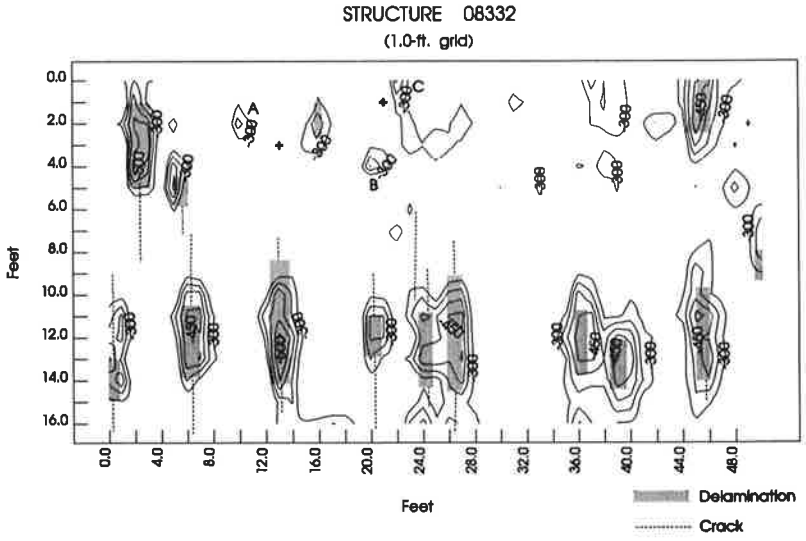


**FIGURE 5 Iso-potential contour map obtained with 1.0-ft grid spacing.**

must be included in the estimation of the quantity of necessary repair.

If a 2.0-ft grid spacing was used instead, as shown in Figure 6, the delamination at the vicinity of grid point (6, 5) became practically unaccounted for as a consequence of the incomplete data provided by this slightly larger grid spacing. Further, there were some losses of details and distortion of the configurations of some areas of high potential gradients. However, these errors were relatively small and probably negligible.

If an even larger, 4.0-ft grid spacing was used, the corresponding sampling of the same area would be so insufficient that approximately 50 percent of the deteriorated areas would be left undetected, and the areas of high potential gradients would be seriously distorted (Figure 7). The results would not represent the condition of the deck area surveyed with reasonable accuracy.

The failure rate in detecting areas of active rebar corrosion and concrete deterioration for a given grid spacing, with respect to the 1.0-ft grid spacing, was estimated based on two survey areas from which appropriate data were available (see Figure 8). Assuming that the failure rate for 1.0-ft grid spacing was 0 percent, the rate increased to 10 percent for 2.0-ft grid spacing and then abruptly to approximately 62 percent for 4.0-ft grid spacing. Although these failure rates may represent only the two particular survey areas, they nevertheless serve to illustrate that the reliability of a half-cell potential survey

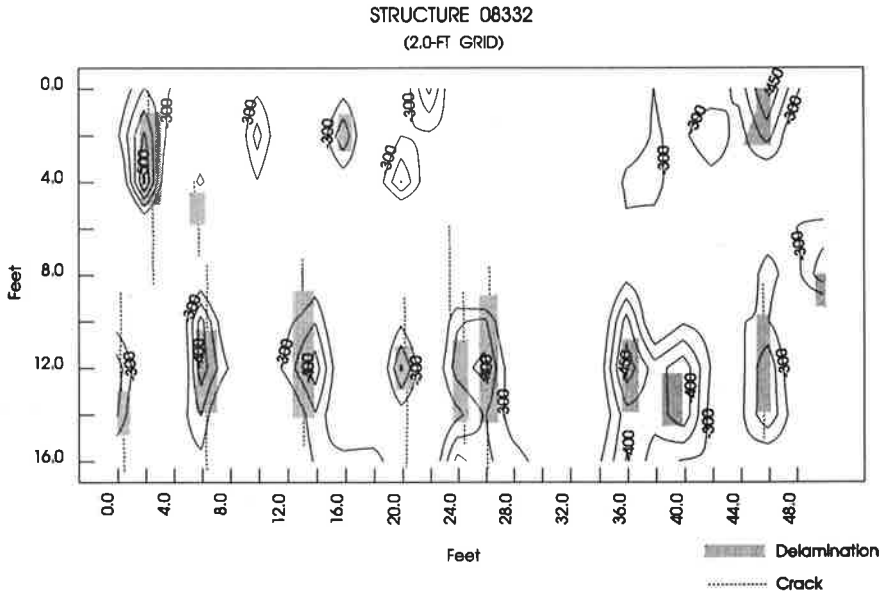


**FIGURE 6 Iso-potential contour map obtained with 2.0-ft grid spacing.**

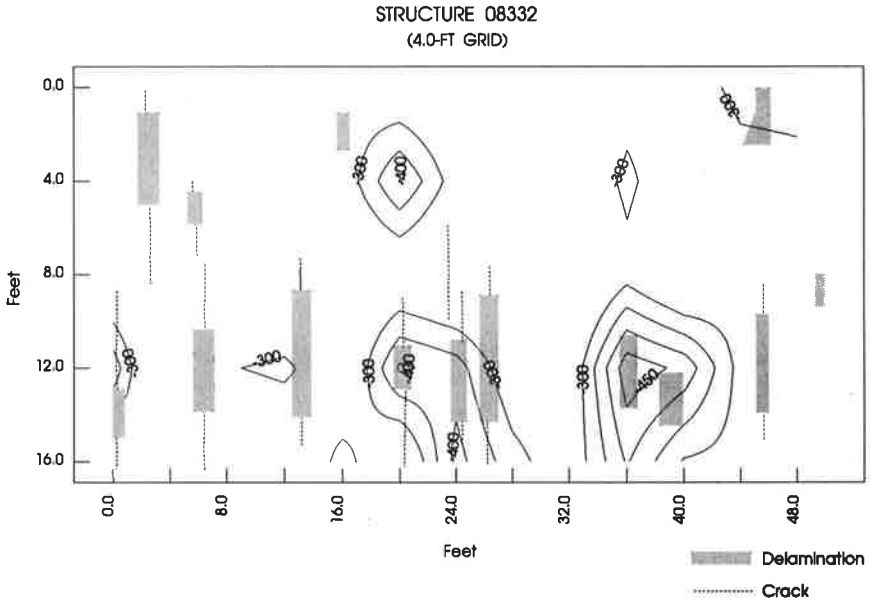


**FIGURE 7 Iso-potential contour map obtained with 4.0-ft grid spacing.**

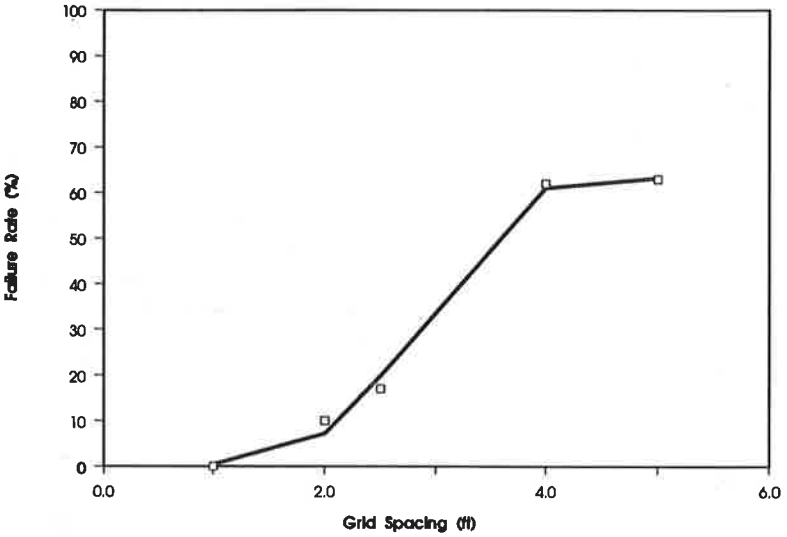


**FIGURE 8 Effect of survey grid spacing used in half-cell potential surveys on the estimated failure rate for locating corrosion-induced deterioration in concrete bridge decks.**

to provide a complete picture of the condition of a deck is considerably jeopardized when a large grid spacing, especially one larger than 2.0 ft, is used.

Of course, as the grid spacing is reduced, the required amount of sampling (or number of potential measurements) in a survey increases exponentially, as illustrated in Figure 9. If a 1.0-ft spacing were used, 1,084 individual potential readings would have to be recorded for 1,000 ft² of concrete deck area. The amount of sampling required decreases significantly by 73 percent or 87 percent when the spacing is increased to 2.0 or 3.0 ft, respectively. Beyond these grid spacings, the corresponding decrease in sample size required is comparatively less.

Selection of an optimum grid spacing should reflect a balance between reasonable accuracy (consistent with the purpose of the survey) and a reasonable sample size (with its associated survey time and cost). Consider the influence of a desired accuracy on the sample size required per unit percentage of accuracy, as shown in Figure 10. For the 100 percent accuracy provided by 1.0-ft spacing, the sample size required would be 10.8 measurements of potential per 1,000 ft² of concrete per percentage accuracy. In contrast, for the 90 percent accuracy provided by using a 2.0-ft grid spacing, the required sample size would be only 3.26 measurements per 1,000 ft² of concrete per percentage accuracy.

It must be emphasized that even though use of a small grid spacing would increase sample size exponentially, the concomitant survey and analysis time would increase only minimally by using an array of $Cu/CuSO_4$ electrodes and a portable microprocessor-based data recorder similar to those used in this study. However, if a compromise between accuracy and required sample size is necessary, the 2.0-ft spacing is

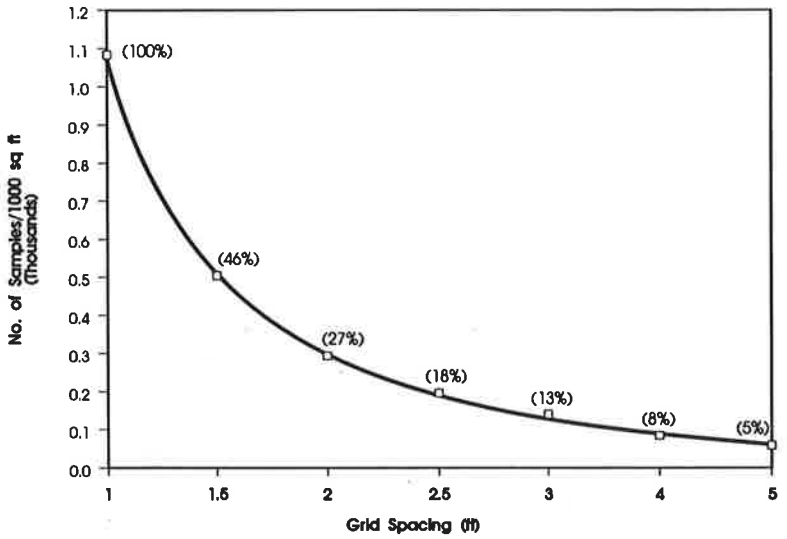


**FIGURE 9 Number of sample locations in survey grid used for half-cell potential survey as a function of square grid spacing.**

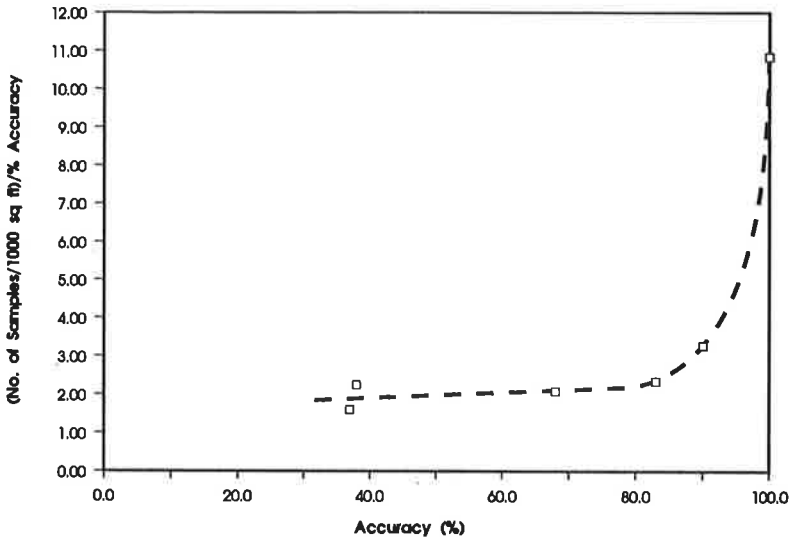


**FIGURE 10 Influence of desired accuracy on number of half-cell potential measurements required per 1,000 ft² of concrete deck per percentage of accuracy.**

undoubtedly a reasonable choice, especially considering that the field of effect on the potential from a corrosion site may be 8 to 10 in.

### Influence of Concrete Variables on Half-Cell Potentials

Half-cell potentials reflect not only the condition of the rebars and the concrete, as discussed previously, but also the electrical resistance of the layer of concrete between the rebars being measured and the $Cu/CuSO_4$ electrode. Because the resistance of the concrete at any location in a deck is determined to various degrees by the thickness of the concrete layer and the seasonally fluctuating variables of temperature and moisture content, half-cell potentials can fluctuate from survey to survey. The researchers believed that such fluctuation has contributed to uncertainty concerning the interpretation of half-cell potentials.

Because of this fluctuation, it is important to consider the potentials measured in any survey not in terms of their magnitude or numerical value (as recommended by the interpretation guidelines in ASTM C-876) but in terms of their relation to the magnitude of the potentials measured at the surrounding concrete.

This point can be demonstrated easily by superimposing contour maps from separate surveys of the same concrete deck area. Figure 11 shows the contour map in Figure 6 super-

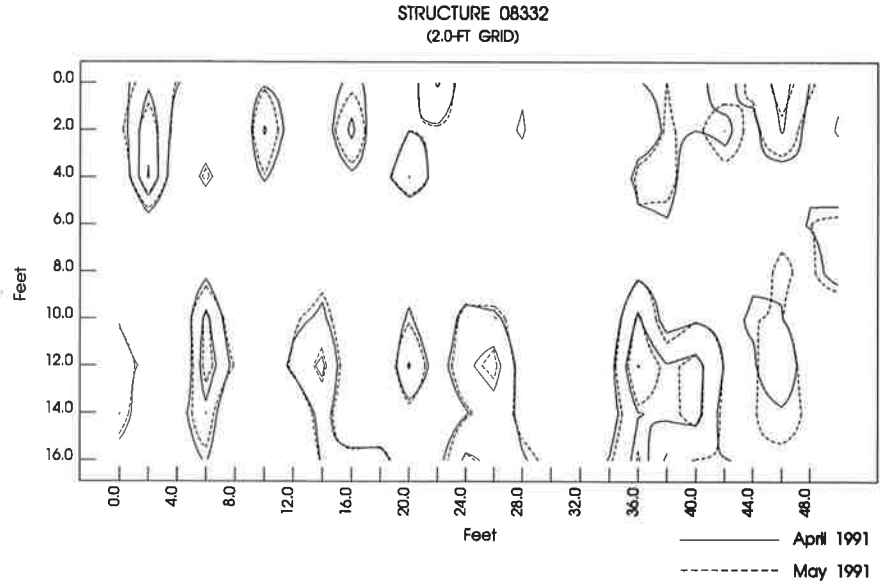


**FIGURE 11 Contour maps of half-cell potentials observed during two separate surveys of a section of a concrete deck. (Iso-potential lines in 100-mV increments, starting at −300 mV.)**

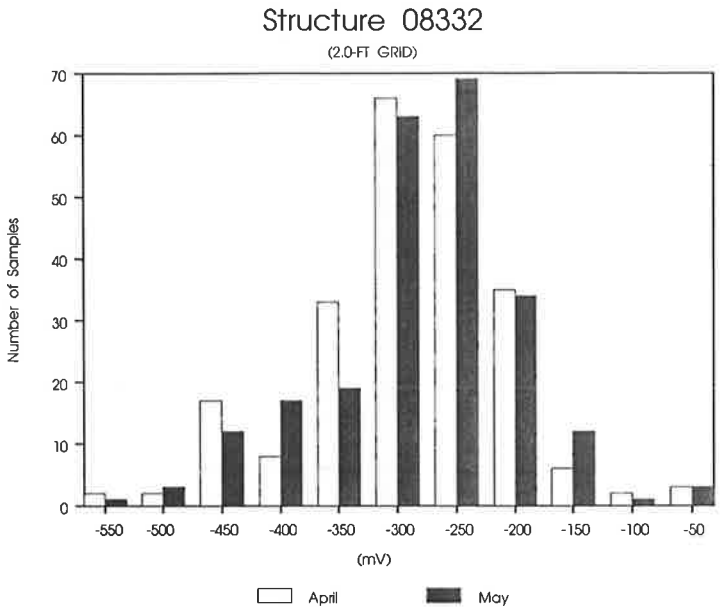


**FIGURE 12 Frequency histograms of half-cell potentials observed during two separate surveys of a section of a concrete bridge deck.**

imposed on another obtained a month earlier for the same concrete deck area. (The moisture content in the concrete deck may be relatively higher during the earlier survey because of rainfall in the area days before the survey.) With the exception of some minor differences, it is evident that the contour maps remained quite similar. More important, the general locations of the defective areas remained constant, despite some apparent differences in the histograms for the two sets of half-cell potentials (see Figure 12).

As the results show, as long as the overall condition of a concrete deck has not changed significantly between surveys, the resulting contour patterns should remain relatively unaltered, although the numerical values of the separate sets of half-cell potentials may vary. Therefore, the researchers argue that the numerical value of each measured potential by itself is a poor indicator of the condition of the rebars and the concrete; instead, a high potential gradient is a better indicator.

## CONCLUSIONS

1. The half-cell potentials in a concrete deck can vary from one survey to another, likely due to the influence of fluctuating temperature, moisture, and oxygen in the concrete. Therefore, the numerical value of each measured potential by itself is a poor indicator of the condition of the rebars or the concrete.

2. The localized nature of rebar corrosion (and the associated damage to the rebars and the concrete) leads to the manifestation of corrosion in large potential gradients on the surface of the concrete deck. Such potential gradients may range from $-60$ to $-300$ mV/ft. Consequently, a high potential gradient would be a better indicator of the locations of actively corroding rebars and damaged concrete than the numerical values of individual potentials.

3. Even the 4.0-ft grid spacing recommended in ASTM C-876 for half-cell potential surveys was found to be too large to allow location of all existing areas of corroded rebars and damaged concrete in bridge decks. This is likely a result of the localized nature of rebar corrosion and the resulting damage. Although a spacing of 1.0 ft is preferable, a spacing of no more than 2.0 ft would provide a reasonable balance between accuracy and required sample size.

4. A half-cell potential survey can be used to locate and reasonably quantify areas of active rebar corrosion and corrosion-induced damage to the concrete in a concrete bridge deck when conducted using a grid spacing of no more than 2.0 ft and plotting the recorded half-cell potentials on contour maps.

## ACKNOWLEDGMENT

This study was supported by Highway Planning and Research funds administered through FHWA.

## REFERENCES

1. A. S. El Din and J. M. Lovegrove. Measuring the Crack Width on Concrete Surfaces by Light-Dependent Resistor. *Magazine of Concrete Research,* Vol. 31, No. 106, 1979, p. 37.
2. *Research Products and Technical Progress.* Report SHRP-ID/UWP-91-511, Strategic Highway Research Program, National Research Council, Washington, D.C., 1991.
3. G. G. Clemeña and W. T. McKeel. Detection of Delaminations in Bridge Decks with Infrared Thermography. In *Transportation Research Record 664,* TRB, National Research Council, Washington, D.C., 1978, p. 180.
4. F. B. Holt and D. G. Manning. Detecting Delamination in Concrete Bridge Decks. *Concrete International,* No. 2, p. 34, 1980.
5. A. Alongi, T. Cantor, C. Kneeter, and A. Alongi, Jr. Concrete Evaluation by Radar-Theoretical Analysis. In *Transportation Research Record 853,* TRB, National Research Council, Washington, D.C., 1982, p. 31.

6. G. G. Clemeña. Nondestructive Inspection of Overlaid Bridge Decks with Ground-Penetrating Radar. In *Transportation Research Record 889,* TRB, National Research Council, Washington, D.C., 1983, p. 21.
7. M. Sansalome and N. J. Carino. *Impact-Echo: A Method for Flaw Detection in Concrete Using Transient Stress Waves.* NBSIR Report 86-3452. National Bureau of Standards, Gaithersburg, Md., 1986.
8. H. A. Berman. *Determination of Chloride in Hardened Cement Paste, Mortar and Concrete.* Report FHWA-RD-72-12. FHWA, U.S. Department of Transportation, 1972.
9. G. G. Clemeña, J. W. Reynolds, and R. McCormick. *Comparative Study of Procedures for the Analysis of Chloride in Hardened Concrete.* Report FHWA-RD-77-84, FHWA, U.S. Department of Transportation, 1977.
10. G. G. Clemeña. *Test of Chloride in Concrete Using a Rapid Test Kit.* Virginia Transportation Research Council, Charlottesville, 1990.
11. S. E. Herald, R. E. Weyers, and P. D. Cady. Measuring the Chloride Content of Concrete. Presented at the 70th Annual Meeting of the Transportation Research Board, Washington, D.C., 1991.
12. R. F. Stratful. Half Cell Potentials and the Corrosion of Steel in Concrete. *Highway Research Record 433,* HRB, National Research Council, Washington, D.C., 1973, pp. 12–21.
13. R. F. Stratful, W. J. Jurkovich, and D. L. Spellman. Corrosion Testing of Bridge Decks. In *Transportation Research Record 539,* TRB, National Research Council, Washington, D.C., 1975, pp. 50–59.
14. K. C. Clear and R. E. Hay. *Time-to-Corrosion of Reinforcing Steel in Concrete Slabs: Vol. 1, Effect of Mix Design and Construction Parameters.* Report FHWA-RD-73-32, FHWA, U.S. Department of Transportation, 1973.
15. C. C. Naish and R. F. A. Carney. Variability of Potentials Measured on Concrete Structures. *Materials Performance,* Vol. 27, No. 4, 1988, p. 45.

---

*The opinions, findings, and conclusions expressed in this report are those of the authors and not necessarily those of the sponsoring agencies.*

*Publication of this paper sponsored by Committee on Corrosion.*

# Improved Grouts for Bonded Tendons in Posttensioned Bridge Structures

NEIL G. THOMPSON, DAVID R. LANKARD, AND YASH P. VIRMANI

A serious problem in the United States and elsewhere is the deterioration of concrete bridges as a result of corrosion induced by chloride ($Cl^-$) intrusion into the concrete. Historically the problem has been associated with conventionally reinforced concrete bridge structures as opposed to prestressed or posttensioned structures. However, corrosion of steel tendons in prestressed concrete structures is of greater concern because the structural integrity of the bridge relies on the high tensile loading of the tendons. Any corrosion or corrosion-induced cracking of the tendon could lead to catastrophic failure of the structure. In bonded posttensioned construction, grout is the final line of defense against corrosion of the uncoated steel tendon. The purpose of this research was to develop and test new mixture designs for grouts, develop and perform accelerated corrosion test methods on the new grouts, and compare the corrosion performance of the new grouts with the standard grouts. A variety of modifiers and additives for grouts were examined, including high-range water reducers, fly ash, silica fume, latex polymer modifier, expansive agents, antibleed additives, and corrosion inhibitors. It was shown that these additives can favorably influence grout fluidity, open time, bleeding and segregation, $Cl^-$ permeability, mechanical properties, and the resistance to corrosion of steel tendons embedded in the grout. Several experimental grouts were designed that provided improved properties compared with the grouts used currently.

A detailed literature review was included in the research to determine the state-of-the-art of grouting materials and grouting technology for bonded posttensioned tendons. The results of this literature review are presented in FHWA Report FHWA-RD-90-102 (*1,2*).

In general, the performance of posttensioned concrete structures in the United States is good. Although several investigations have been performed, few examples of bonded posttensioned structures in which corrosion of the prestressed tendons has occurred are documented (*3–8*). Even in many of these instances, investigators of the structures speculated that corrosion might not have occurred if proper construction practices and designs had been followed. However, in one example (a Midwest parking garage), corrosion of imbedded strands in a posttensioned construction occurred when a large section of galvanized duct was breached due to corrosion as a result of chloride migration. The corrosion attack resulted in failure of at least one wire of the tendon.

It is inevitable that additional instances of corrosion-related problems will be observed as the average age of these structures continues to increase, deicing salts continue to be used, and the salts penetrate to greater depths within the concrete. The catastrophic nature of a serious failure within a bridge or parking garage makes it important for the industry to continue to improve its practices. Available technology could improve performance significantly if incorporated into standard practices.

One such area in which improvements are possible is the grouts used for filling the ducts containing the prestressed steel within the posttensioned structure. Because grouts provide the final defense against corrosion of the prestressing steel tendons that support the structure, it is imperative to provide a grout that incorporates state-of-the-art technology. Up to now, the majority of grouts used in bonded posttensioned concrete structures have been a simple mixture of portland cement and water with water/cement ratios typically specified to fall below 0.44 to 0.50 and with expansive and nonbleeding additives sometimes specified.

## EXPERIMENTAL

### Selection of Materials

Initially, screening trials were conducted to select admixtures and additives that were compatible with the portland cement used in the study. In most cases, each additive or admixture modifier category was represented by only one material. The following materials were selected for use in this study:

- Type II portland cement,
- Type F high-range water-reducing admixture (ASTM C494),
- Silica fume (also called microsilica),
- Class F fly ash (ASTM C618),
- A styrene-butadiene polymer modifier (supplied as a liquid with a solids content around 48 percent),
- Calcium nitrite corrosion inhibitor,
- Aluminum powder expansion agent,
- Polysaccharide gum antibleed agent,
- Celbex 209X commercial grout admixture (blend of superplasticizer, thickener, and controlled expansion agent), and
- Silica sand (maximum particle size 50 mesh).

### Grout Preparation Procedures

Grouts were prepared using a 0.5 HP, high-shear mixer with a propeller-type mixing blade (3 tines) typically operating at around 500 r/min. Dry batch weight of the grout ingredients

N. G. Thompson, Cortest Columbus Technologies, Inc., 2704 Sawbury Boulevard, Columbus, Ohio 43235. D. R. Lankard, Lankard Materials Laboratory, Inc., 400 Frank Road Columbus, Ohio 43207. Y. P. Virmani, Federal Highway Administration, 6300 Georgetown Pike, McLean, Va. 22101-2296.

ranged from 4.4 to 8.8 lb (2000 to 4000 gm). On a volume basis, this yielded around 91.5 to 183 $in^3$ (1500 to 3000 cc) of grout. In the majority of instances, the grout had the rheological characteristics of a thick liquid which could be poured from the mixing container. After mixing of the grout, specimens were prepared for measuring various physical and chemical properties.

## Grout Properties in the Fresh State

Two or more grout batches were required to prepare enough material for all of the measurements. In a number of instances, replicate batches were prepared to establish the precision of the tests.

### *Grout Unit Weight*

Unit weight is the density of the grout in the fresh state. Unit weight was measured by weighing a known volume of the fresh grout in a graduated cylinder.

### *Time of Set*

The time of initial and final set of the grouts was measured in accordance with the Standard Test Method For Time of Setting of Grouts For Preplaced Aggregate Concrete in the Laboratory (ASTM C953-87). This procedure uses the Vicat apparatus. Initial setting time is defined as the time when a needle penetration of 1 in. (25 mm) is obtained. Final set is defined as the time when the needle does not sink visibly into the sample.

### *Fluidity and Open-Time Measurements*

Most of the grouts behaved rheologically as liquids so it was possible to use the flow cone procedure to quantify fluidity. The procedure used here is defined by the Standard Test Method For Flow of Grout (Flow Cone Method) (ASTM C939-87). The time required for the 105.3 $in.^3$ (1725 cc) of grout to exit the cone is measured as the efflux time of the grout. Any grout that passes completely through the flow cone under the force of gravity alone, regardless of total efflux time, can be defined as a pourable grout.

A few of the grouts developed a thixotropic behavior immediately after mixing and would not pass through the flow cone. For other grouts, this thixotropic behavior developed at a much later time. In both of these instances, the fluidity of the grouts was then defined using the flow table procedure. The equipment and procedure for this test is defined in the Standard Specification For Flow Table For Use in Tests of Hydraulic Cement (ASTM C230-90). In this investigation, the initial fluidity of the grout was measured as the efflux time after a 1-min wait. Efflux times were then measured periodically (every 20 to 30 min) until the grout would no longer flow in a continuous stream through the cone. At that point, fluidity measurements were continued using the flow table. An open time for the grouts was defined as the sum of the total time the grout remained pourable (passed through the flow cone) plus the time during which the grout retained a flow value (from flow table) greater than 100 percent.

### *Expansion and Bleeding*

Expansion and bleeding of the fresh grouts was measured using the procedure of the Standard Test Method For Expansion and Bleeding of Freshly Mixed Grouts (ASTM C940-87). The expansion of the grout mixture and its bleeding are expressed as percentages of the initial volume of the grout.

### *Bleeding and Segregation Under Pressure*

Normally, bleeding occurs simply as a result of sedimentation of cement and aggregate particles with free water rising to the surface. Another form of bleeding has been described when grouts under pressure are in contact with strand tendons. In this instance, bleeding occurs because of the filtering action of the void spaces between the strands (*9*). Pressure from the grouting operation forces the grout against the strands where water passes through the interstices between the outer strand and the center wire, whereas solid particles in the grout do not. This filtering action is especially severe in strand tendons with a high vertical rise, and bleeding can amount to up to 20 percent of the height of the vertical rise. A test procedure is available to measure the relative bleeding characteristics of grouts that simulates the condition experienced in grouting vertical tendons (*9*). A small quantity of fluid grout, 42.7 $in.^3$ (about 700 cc), is placed in a pressure vessel having at one end a Gelman Type AE filter (Gelman Science, Inc., Ann Arbor, Michigan). Pressure is applied to the other end of the vessel with water forced from the grout through the filter, which retains 99.7 percent of all particles >.012 mils (>0.3 microns). The pressure at which water loss first occurs is measured as well as the amount of water lost at a given pressure up to 80 psi in 10 psi increments (552 kPa in 68.9 kPa increments).

## Grout Properties in the Hardened State

### *Compressive Strength*

Compressive strength measurements were made following the procedures of ASTM C942-86, the standard test method for compressive strength of grouts for preplaced aggregate concrete in the laboratory. Specimens for this test are 2 in (5.08 cm) cubes. In instances in which the grouts exhibit expansion before initial set, the test procedure provides for the placement of a plate over the cube mold to ensure that expansion is confined. In this investigation, compressive strength was measured at intervals of 1 day, 7 days, 28 days, and 90 days.

### *Permeability*

The permeability of the grouts was measured using the Rapid Determination of the Chloride Permeability of Concrete procedure (AASHTO T277-83). This test measures the total electrical charge passed through a specimen 2 in. (5.08 cm) thick

that contacts sodium chloride solution on one side and an alkali hydroxide solution on the other side.

Normally, the test is run at a voltage of 60 V DC for 6 hr. It was found that when grouts were used instead of concrete, a higher total charge was passed, which resulted in significant heating of the grout specimen. Subsequently, the test procedure, as applied to grouts, was conducted using an applied voltage of 30 V DC for 6 hr. This procedure accomplished the objective of minimizing the temperature rise in the specimen during the test.

### Accelerated Corrosion Test Method

The accelerated corrosion test method (ACTM) was designed based on the results of the preliminary experiments and consideration of several variables, including freeze-thaw cycles, wet-dry cycles, temperature, acceleration of $Cl^-$ migration, specimen loading, types of ducts, types of prestressing steel, grout cover, and grout curing. These variables are discussed elsewhere (*10*).

The focus of ACTM is on the grout and not the total post-tensioning system, which would include a detailed investigation of the entire system including tendon, grout, duct, and concrete cover.

Figure 1 shows the as-cast specimen and the specimen ready for testing. A primary focus of the as-cast specimen is the rigid, air-tight mold (PVC tube) used for casting and curing the specimen. After curing (minimum of 28 days), a gauge section of the PVC tube is removed to expose the grout specimen. This simulates a significant breach in the duct wall. The specimen is tested within 24 hr and is kept immersed in a saturated calcium hydroxide solution before testing. Maintaining moist conditions on the exposed gauge section is critical to prevent microcracking.

The following procedure is used to perform ACTM:

1. Set up the test cell arrangement as shown in Figure 2 with the grouted test specimen immersed in a 5 percent NaCl solution.
2. Use a potentiostat to polarize the grouted test specimen.
3. Set the potentiostat to apply +0.6 V (SCE).
4. Within 5 to 10 min of immersion, apply the +0.6 V (SCE) by switching the potentiostat from the "isolate" or "disable" mode to the "run" mode.
5. Record current and potential periodically during the test (every 10 to 30 min is sufficient).

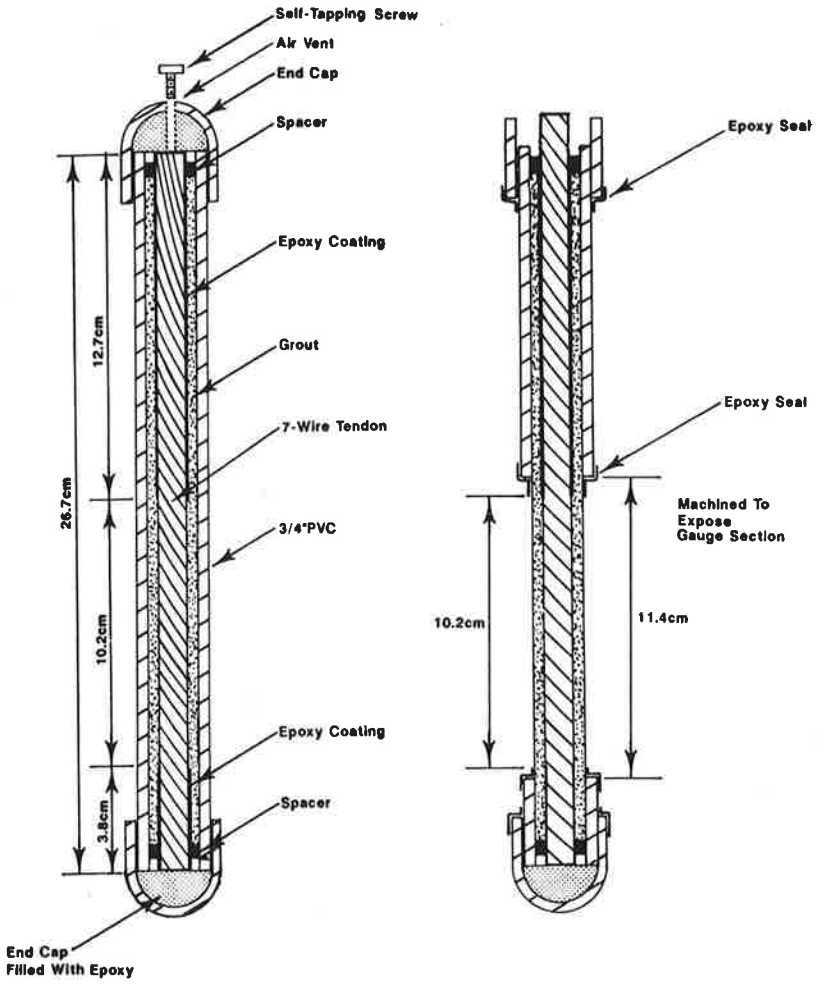


**FIGURE 1 Diagrams of grouted pipe specimen: before cutting gauge section (*left*) and ready for testing (*right*).**

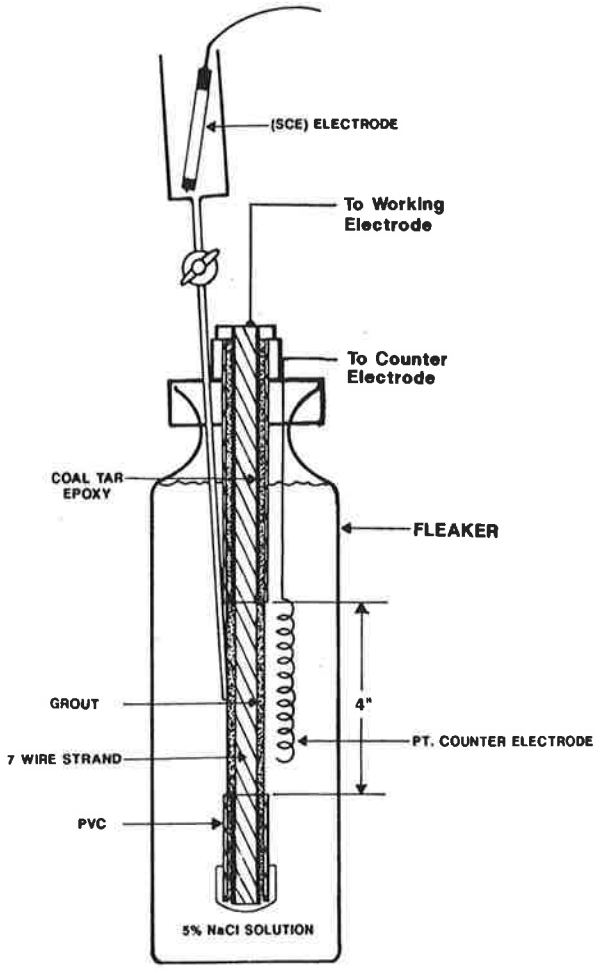


**FIGURE 2 Diagram of ACTM test cell arrangement.**

6. Plot current versus time until a rapid current increase. This signifies the initiation of corrosion.
7. Allow tests to continue for 48 hr after initiation of corrosion.

## RESULTS AND DISCUSSION

### Physical and Mechanical Properties

Nine different grout series were evaluated in this program. The distinction between the various series was made on the basis of grout additives. Brief descriptions of the series examined follow.

1. Series 1, standard grout: The standard grout was chosen to be representative of grouts that have been used for many years in the United States. It is a simple mixture of Type II portland cement and water with a water/cement ratio of 0.44.
2. Series 2, commercial antibleed admixtures: This grout also has a normal water/cement ratio (0.45) but contains a commercially available antibleed admixture that has been fairly widely used in recent years (Celtite Inc.'s Celbex 209X).
3. Series 3, high-range water reducer (HRWR): The use of a superplasticizer provides significantly reduced water/cement ratios (15 percent to 30 percent water reduction) while maintaining the same level of fluidity. This series provides reduced water content grouts that are otherwise comparable (from a materials point of view) to the standard grout composition.
4. Series 4 and 10, corrosion inhibitor: The corrosion inhibitor (calcium nitrite) was used in grouts at both normal (Series 10) and reduced (Series 4) water/cement ratios. These series are unique in that it is the only grout that can possibly contribute to an improved resistance to tendon corrosion after the chloride ion has reached the steel.
5. Series 5, HRWR plus fly ash and sand: This series was formulated in an effort to produce a relatively impermeable grout that would function at the same performance level as silica fume grouts while costing less.
6. Series 6, HRWR plus silica fume: Silica fume replacements up to 20 percent of cement weight were evaluated. Superplasticizers are required in these systems to achieve the desired level of fluidity at a reduced water content.
7. Series 8, HRWR plus latex: There is little information in the literature concerning the use of superplasticizers with latex modifiers in portland cement–based systems. In the present investigation, success was achieved in producing low water/cement ratio, latex-modified grouts.
8. Series 11, HRWR plus expansive agent plus antibleed additive: This series was evaluated to learn the effect of the expansive additive on the performance of Grout Series 3 and 12.
9. Series 12, antibleed additive: In this grout series, a water soluble, polysaccharide gum, providing superior antibleed behavior, was evaluated.

Actual components of the grout mixtures used in this study are given in Table 1. Measured properties for several grout mixtures are given in Tables 2–5.

#### *Series 1: Standard Grout Properties and Behavior*

The standard grout used in the investigation is a simple mixture of Type II portland cement and water with a water/cement ratio of 0.44. At a water/cement ratio of 0.44, the standard grout had a unit weight of 118 lb/ft$^3$ (1890 kg/m$^3$) and an initial flow cone efflux time of 18 sec. The grout poured uniformly with no disruption or tearing of the grout stream. The standard grout showed little bleeding at normal atmospheric pressure but did lose almost half of its total water at a pressure (gauge) of 80 psi (552 kPa). It is estimated that the standard grout remains pumpable for more than 3 hr at 73°F (23°C). The standard grout showed good strength gain behavior with a 7-day compressive strength of 6,000 psi (41,370 kPa) and a 90-day compressive strength of almost 10,000 psi (68,950 kPa). Tested at 30 V, the standard grout showed a rapid permeability test current flow of 2400 coulombs in 6 hr.

#### *Series 2: Effect of Commercial Antibleed Admixture on Grout Properties and Behavior*

At an additional rate of 1.5 percent by weight of cement, the commercial admixture had a beneficial effect on the water retention under pressure of the grout and provided a modest

**TABLE 1 Compositions of Grout Mixtures**

| Component | Grout Series | | | | | | | | | |
|---|---|---|---|---|---|---|---|---|---|---|
| | 1 | 2-1 | 3 | 4-1 | 5-1 | 6B | 6D | 8 | 10-1 | 11 |
| Type II, Portland Cement, parts by weight | 100 | 100 | 100 | 100 | 100 | 100 | 100 | 100 | 100 | 100 |
| Water, parts by weight | 44 | 46 | 36 | 34.7 | 40.8 | 39.6 | 43.2 | 12 | 42.7 | 32.7 |
| Conbex 209X, % (based on cement weight) | | 1.5 | | | | | | | | |
| HRWR, fl oz per 100 lb cement | | | 15 | 15 | 40 | 24 | 55 | 15 | | 32 |
| Calcium Nitrite, gal/yd$^3$ | | | | 6 | | | | | 6 | |
| Flyash, parts by weight | | | | | 33 | | | | | |
| Silica Sand, parts by weight | | | | | 52 | | | | | |
| Gum, parts by weight | | | | | 0.05 | | | | | 0.01 |
| Silica Fume, parts by weight | | | | | | 11 | 25 | | | |
| Latex Modifier, parts by weight | | | | | | | | 31.4 | | |
| Al Powder, parts by weight | | | | | | | | | | 0.0075 |

**TABLE 2 Physical Properties: Flow and Bleeding Characteristics**

| Grout Series | Unit Weight, lb/ft$^3$ | Initial Flow Cone Efflux Time[a], sec. | Bleeding[b] Percent | Expansion[b] Percent | Bleeding Under Pressure[c] | |
|---|---|---|---|---|---|---|
| | | | | | Pressure, psi at which water loss first effected | Percent of Total Water Removed at 80 psi |
| 1 | 118 | 18 | 0.1 | 0 | 0 | 48 |
| 2-1 | 115 | 59 | 0 | 1.3 | 30 | 5 |
| 3 | 120 | 19 | 0.15 | 0 | 10 | 38 |
| 4-1 | 121 | 22 | 0.60 | 0 | 0 | 44 |
| 5-1 | 128.6 | 86 | 0 | 0 | 40 | 5 |
| 6B | 116 | 28 | 0 | 0 | 10 | 16 |
| 6D | 117 | 27 | 0 | 0 | 30 | 6 |
| 8 | 117 | 16 | 0 | 0 | 50 | 1 |
| 11 | 126 | 57 | 0 | 0 | 30 | 7 |

[a] ASTM C939
[b] ASTM C940
[c] Gelman pressure filtration procedure

**TABLE 3 Physical Properties: Open and Setting Time and Heat Evolution**

| Grout Series | Grout Open Time, Hr: Min (Estimated Time Grout Remains Pumpable at 74F) | Setting Time[a] | | Heat Evolution Behavior | |
|---|---|---|---|---|---|
| | | Initial Hr:Min | Final Hr:Min | Maximum Temperature, F | Time to Reach Maximum Temperature Hr:Min |
| 1 | 3:20 | 5:15 | 7:00 | 150 | 9:50 |
| 2-1 | 8:00 | 14:00 | 23:30 | 155 | 11 |
| 3 | 4:20 | 8:06 | 10:00 | 180 | 12:00 |
| 4-1 | 3:15 | 6:50 | 8:45 | 157 | 13:00 |
| 5-1 | 5:00 | 16:10 | 18:45 | 132 | 24:00 |
| 6B | 1:53 | 6:50 | 9:00 | 170 | 11:00 |
| 6D | 6:00 | 10:23 | 12:00 | 150 | 15:00 |
| 8 | 5:20 | 9:57 | 11:15 | 155 | 16:00 |
| 11 | 7:30 | 13:00 | 13:50 | ND | ND |

[a] ASTM C953
ND - No Data

**TABLE 4 Mechanical Properties**

| Grout Series | Compressive Strength,[a] psi | | | |
|---|---|---|---|---|
| | 1d | 7d | 28d | 90d |
| 1 | 2700 | 5960 | 7840 | 9860 |
| 2-1 | 155 | 3410 | 5580 | 6530 |
| 3 | 4170 | 8000 | 9530 | 10,980 |
| 4-1 | 1700 | 6225 | 8740 | 9710 |
| 5-1 | 900 | 6450 | 8400 | 13,385 |
| 6B | 3310 | 7130 | 10,030 | 11,620 |
| 6D | 1930 | 6760 | 8830 | 9340 |
| 8 | 1775 | 5710 | 7150 | 9190 |
| 11 | 1850 | 4810 | 5440 | 6225 |

[a] ASTM C942.

**TABLE 5 Rapid Permeability Data[a]**

| Grout | Coulombs | |
|---|---|---|
| | 60 V | 30 V |
| 1 | 33,000 (36,000)[b] | 2,400 |
| 2-1 | 59,000 | 14,500 |
| 3 | 24,000 | 4,300 |
| 4-1 | 32,000 | 4,000 |
| 5-1 | 6,960 | 370 (140)[b] |
| 6B | 270 | 1,000 (910)[b] |
| 6D | 590 | 150 |
| 8-1 | 15,000 | 1,600 |
| 11L | ND | 7,200 |

[a] AASHTO Designation T277-83.
[b] Duplicate specimens.
ND - No Data.

expansion (1.3 percent) with an increase in the time that the grout remained pumpable. At this addition rate, the grout did have an adverse (but acceptable) effect on compressive strength development and a significant adverse effect on the chloride permeability of the grout.

*Series 3: Effect of HRWR on Grout Properties and Behavior*

The use of an HRWR provided for the maintenance of adequate fluidity and working time in the grouts at up to a 20 percent reduction in water content. Relative to the standard grout, the grouts containing the HRWR showed improvements in the rate of strength development and in the water retention capacity under pressure. An expected reduction in chloride permeability brought about by the lower water/cement ratio of the admixed grout (relative to the standard grout) was not seen in the present investigation.

*Series 4 and 10: Effect of Calcium Nitrite Corrosion Inhibitor on Grout Properties and Behavior*

Grouts containing the calcium nitrite corrosion inhibitor were prepared at water/cement ratios of 0.365 (Grout No. 4-1) and 0.44 (Grout No. 10-1). No property data were obtained on Grout No. 10-1. Only ACTM specimens were prepared from this grout. The main objective of property measurements on the corrosion inhibitor-containing grout was to ensure that the inhibitor had no adverse effect on the properties of the grout in the fresh and hardened state while providing the desired corrosion inhibiting function in the hardened grout. A comparison of the grouts with (Grout 4-1) and without (Grout 3) the corrosion inhibiting admixture confirms this desired result. The only exception is a lower 1 day compressive strength for the grout containing the corrosion inhibitor. This was an unexpected result because the calcium nitrite corrosion inhibitor is expected to act as a set accelerator. However, in the present case, the set-retarding function of the HRWR appears to offset this function.

*Series 5: Effect of Fine Aggregate (Sand) Additions on Grout Properties and Behavior*

Sanded grouts containing up to 28 percent sand were prepared with ratios of water/cement and fly ash between 0.27 and 0.32. These grouts had a pourable fluidity and maintained their pumpability for up to 5 hr. Although initially pourable, these grouts were quite viscous; Grout 5-1 showed an initial flow cone efflux time of 86 sec at a water/cement and fly ash ratio of 0.32.

The use of fine aggregate (sand) in these grouts has the potential for reducing overall grout cost without having any adverse effect on engineering properties relevant to the bonded posttensioning application. In fact, properties such as strength development and bleeding behavior may be improved by the sand addition. It is also expected that the volume stability of sanded grouts will be superior to that of unsanded grouts (reduced drying shrinkage strain). The overall pumpability of these relatively viscous, high unit weight grouts remains to be determined.

*Series 6: Effect of Silica Fume on Grout Properties and Behavior*

Grout compositions were studied that contained Type II portland cement and silica fume additions of 5, 10, 15, and 20 percent of cement weight. In all of the silica fume grouts, it was necessary to use the HRWR to achieve and maintain satisfactory fluidity characteristics. Two of the silica fume grout compositions that were studied most extensively in the present investigation were Composition 6B (10 percent silica fume) and Composition 6D (20 percent silica fume).

The time during which the silica fume grouts remain pumpable can be controlled by controlling the quantity of HRWR used. This phenomenon is shown in Figure 3 for a 10-percent silica fume grout (Grout 6B). At the 10 percent silica fume addition, the open time of the grout varied from 1½ hr to 8 hr when the HRWR was increased from 25 oz/cwt (16.2 ml/kg) to 55 oz/cwt (35.8 ml/kg).

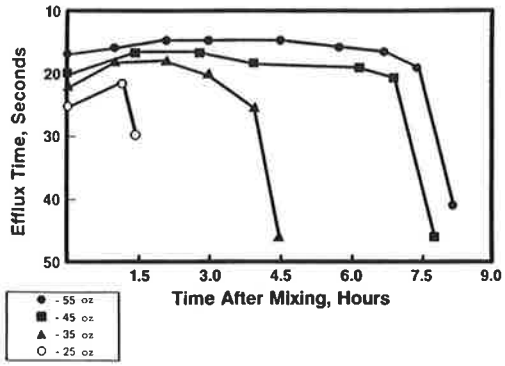


**FIGURE 3 Initial and time-dependent efflux time of Grout 6B (90 percent Type II portland cement, 10 percent silica fume grout) as affected by superplasticizer (M150) (water/cement and silica fume ratio = 0.365).**

Relative to the standard grout, the use of silica fume (10 and 20 percent cement replacement) in conjunction with an HRWR provided significant improvements in water retention capacity (under pressure) and in chloride ion permeability. These benefits were achieved without sacrificing strength and working time characteristics.

*Series 8: Effect of Latex Polymer Modifier on Grout Properties and Behavior*

Acrylic and SBR latex polymer modifiers were evaluated. The SBR latex modifier provided the most stable grout and the most consistent properties. The latex addition was 15 percent (percent of cement weight based on dry latex solids). The use of an SBR latex in conjunction with an HRWR provided significant improvements in grout properties relative to the standard grout in the application of interest. The latex-modified grout showed the best performance of all grouts tested in the pressure filtration test. A pressure of 50 psi (345 kPa) was required before any water was lost from the grout, and at a final pressure of 80 psi (552 kPa) only 1 percent of the total water was removed from the latex-modified grout (Composition 8-1).

*Series 11: Effect of Expansive Additive on Grout Properties and Behavior*

Opinion is divided on the merit of incorporating an expansion-causing additive in grouts for bonded, posttensioned construction. In this program, a grout composition (Composition 11L) was developed to study this variable.

The performance of Composition 11L somewhat paralleled the performance of the grout containing the commercial antibleed admixture (Composition 2-1 at a water/cement ratio of 0.46). Although Composition 11L at a water/cement ratio of 0.34 was initially pourable, it was quite viscous. One interesting and unexpected phenomenon associated with Composition 11L was the nature of the expansion caused by the aluminum powder. In simple cement and water systems, a powdered aluminum additive typically provides some expansion within 15 to 60 min after the contact time between water and cement. For Grout 11L, no expansion occurred in the grout for up to 3 hr after mixing. At that point (3 hr) the grout began to expand and showed a final expansion value of 9 percent after 6 hr.

*Series 12: Effect of Experimental Antibleed Admixture on Grout Properties and Behavior*

A number of antibleed and thickening admixtures were evaluated in the program. After initial screening tests, most of the work was done on grouts containing a polysaccharide gum. The principal intended function of the gum was as an antibleed/antisegregation additive. The cumulative water loss in the pressure filtration test from grouts with and without antibleed additives is shown in Figure 4. The polysaccharide gum not only increases the pressure required to first force water from the grout but also limits the total amount of water forced from the grout at the highest pressure (80 psi or 552 kPa). The best result was obtained using 0.20 percent of the gum in silica fume grout Composition 6D. Here, 70 psi (483 kPa) was required before any water was forced from the grout and at 80 psi (552 kPa) only 0.5 percent of the total water was removed from the grout.

At increasing levels of polysaccharide gum (to a maximum of 0.20 percent), the fluidity of the grout is adversely affected. However, at the highest addition rate (0.20 percent of cement weight), the grout is still pumpable.

**Accelerated Corrosion Test Method**

Typical results from ACTM are shown in Figure 5, and results for all of the grouts tested are summarized in Table 6. More detailed data are found in FHWA Report FHWA-RD-91-092 (*1,2*). It is important to note that a poor grout with a high water/cement ratio (0.65) gave, by far, the worst results, which indicates that ACTM can differentiate good from poor grout. The addition of HRWR (and corresponding decreases in water/cement ratio), fly ash and sand, silica fume, and latex modifier all improved the corrosion performance over Grout 1. Grout 5-1, containing the HRWR, sand, and fly ash, provided the longest time to failure.

Using the specified ACTM test, Grout 10-1, which was the same as Grout 1 with the addition of an inhibitor, indicated a decrease in corrosion performance when compared with Grout 1. This was unexpected; these results were further examined. It is believed that ACTM is too severe for evaluating inhibitor performance and that the 0.6 V (SCE) applied potential exceeds the breakdown potential for steel in an inhibited grout. Therefore, the ACTM masked the inhibiting ability of the grout. To examine this problem, ACTM was modified to use an applied potential of 0.0 V (SCE). The 0.0 V potential is sufficient to accelerate corrosion once $Cl^-$ reaches the steel surface, but will not unrealistically break down protection provided by an inhibitor of the type utilized in this study. The data presented in Table 6 show the results for the modified ACTM for Grout 1 (standard) and Grout 10-1 (standard plus inhibitor). The time to failure for Grout 1 is similar for both

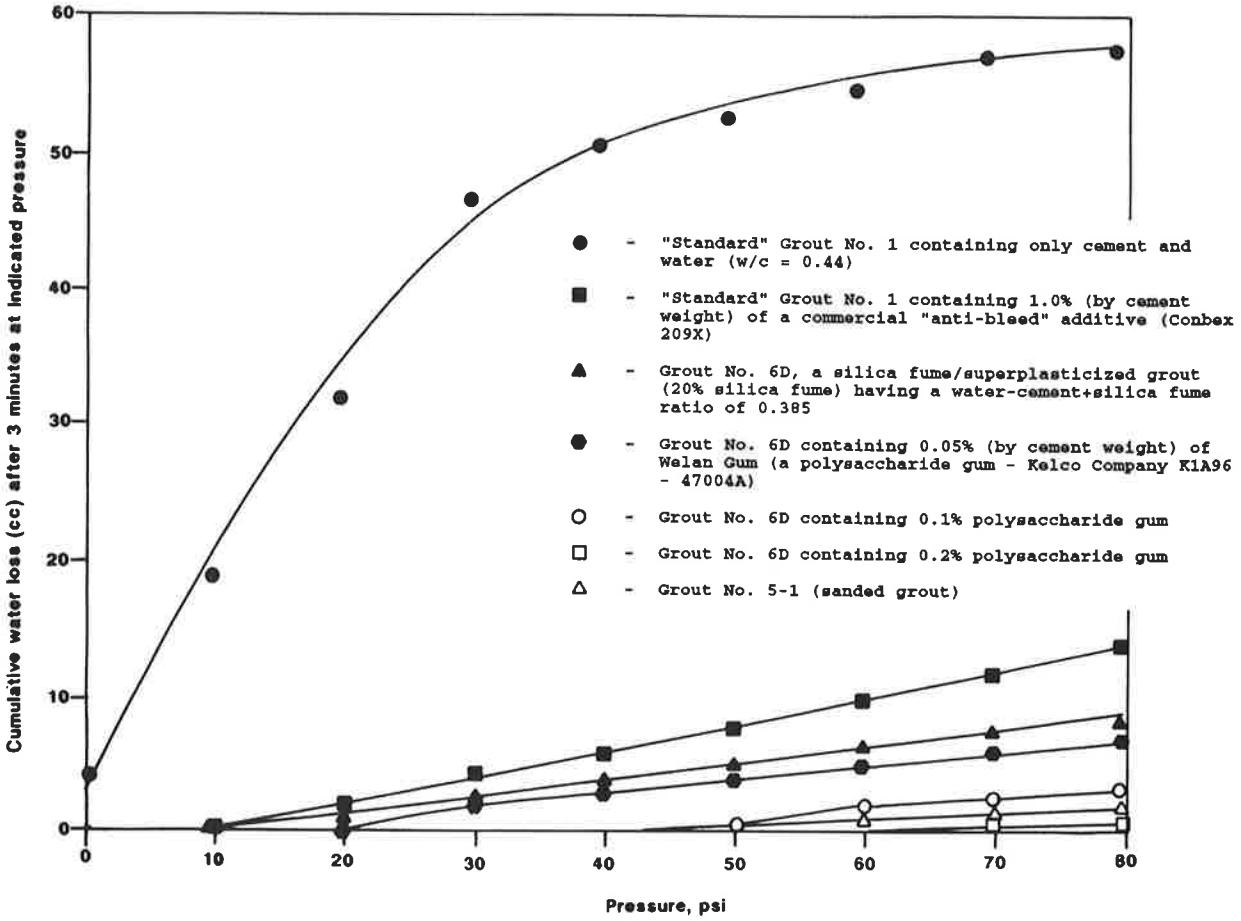


**FIGURE 4 Cumulative water loss from indicated grouts (from 0 to 80 psi) using Gelman pressure filtration funnel.**

the 0.6 V applied ACTM and the modified 0.0 V applied ACTM. This indicates that the modified ACTM is adequate to examine corrosion performance. A significant improvement in the corrosion performance was realized when an inhibitor was added to the grout (time to failure increased from 177 up to 713 hr) based on the modified ACTM results. Although the data are limited, the improvement in corrosion performance is significant. Therefore, when an inhibitor is added, the modified ACTM must be used. Typical plots for current and time for the rapid $Cl^-$ permeability tests are shown in Figure 6. When a 60 V applied voltage was used, overheating occurred and extrapolation of the data was required. In a few instances the overheating resulted in cracking of the grout specimen. A comparison of rapid $Cl^-$ permeability results for the 60 V and 30 V applied voltage is presented in Table 5. The only discrepancy in the data is with Grout 6B. The 30 V tests were repeated; it is believed that these data are correct, which indicates that the 60 V data may be in error.

The ACTM results and the AASHTO rapid $Cl^-$ permeability results for several grouts are compared in Table 7. For the five grouts for which both sets of data are available, there is a reasonable correlation between the two sets of data. As permeability increases, the time to corrosion initiation decreases. This correlation suggests that if $Cl^-$ permeation is the major contributor to corrosion initiation, the rapid $Cl^-$ permeability test may be sufficient to characterize a grout's corrosion performance. Therefore, in the absence of inhibitors, a specification of time to corrosion initiation may include only the rapid $Cl^-$ permeability test. However, initial test results using a modified (0.0 V, SCE, polarized) ACTM indicates that the addition of an inhibitor significantly increases the time for corrosion initiation. It was not expected that the rapid $Cl^-$ permeability would have indicated this result. Therefore, when an inhibitor is incorporated in the grout, the modified ACTM test is required to characterize the corrosion performance. It should also be recalled that ACTM provides an indication of the rate of corrosion following corrosion initiation.

## CONCLUSIONS

1. The results of investigations to date indicate that, in general, bonded posttension concrete structures exhibit excellent performance. However, in at least one instance, corrosion of the duct material and subsequent corrosion and failure of individual strands of a tendon have been reported.
2. Present specifications are inadequate for ensuring optimum corrosion protection of the prestressing steel based on state-of-the-art grout technology.
3. It is possible to achieve and control a specified level of grout fluidity and acceptable open time through the use of controlled dosage rates of HRWR.

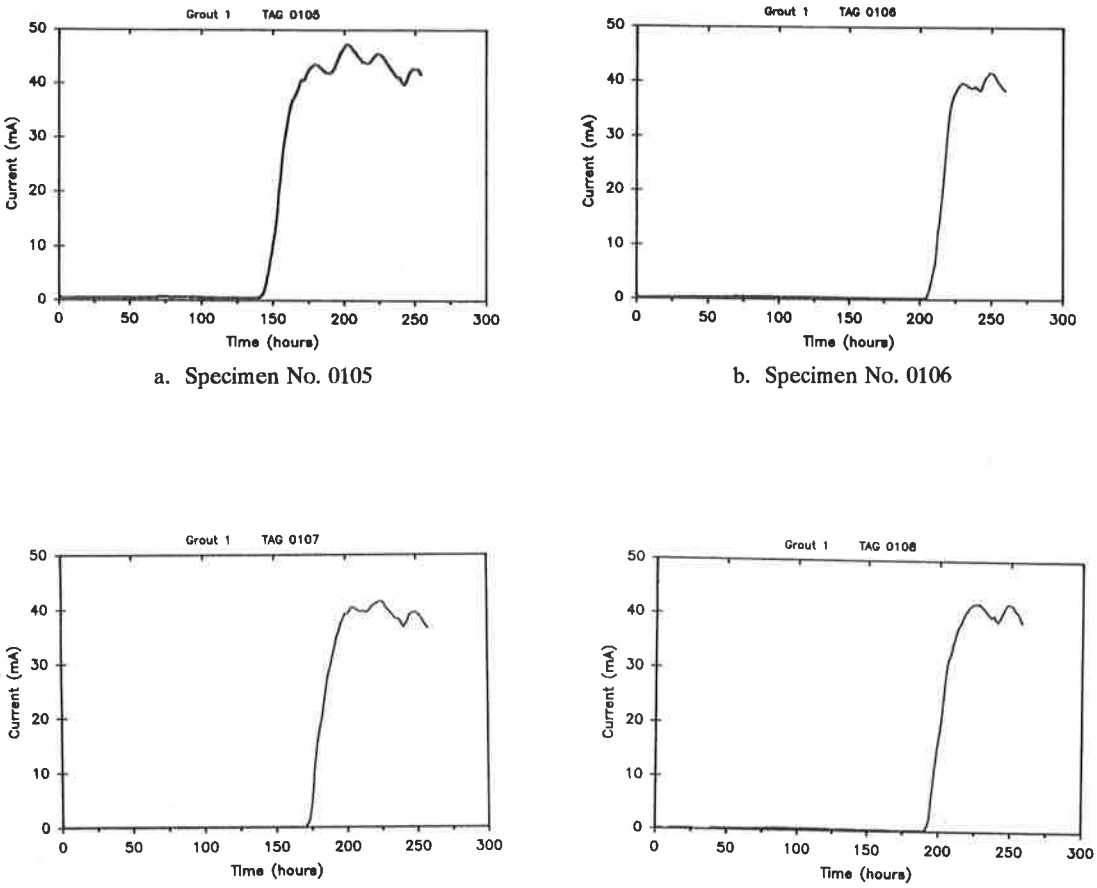


a. Specimen No. 0105

b. Specimen No. 0106

c. Specimen No. 0107

d. Specimen No. 0108

**FIGURE 5 ACTM current-time data for replicate standard specimens for Grout 1 (standard grout).**

**TABLE 6 Summary of ACTM Results**

| Grout Identification | Standard Specimens, (0.6V, SCE, Polarized) Time-To-Failure, Hours[a] | Standard Specimens, (0.6V, SCE, Polarized) Current Following Failure, mA[a] | Standard Specimens, (0.0V, SCE, Polarized) Time-To-Failure, Hours |
|---|---|---|---|
| No. 1 Standard | 164 | 41 | 177 |
| No. 1B Standard/ High w/c | 30 | 46 | - |
| No. 10-1 Standard/Inhibitor | 129 | 26 | 713 |
| No. 5-1 HRWR/ Flyash/Sand | 418 | 8 | - |
| No. 6B HRWR/ Silica Fume | 295 | 18 | - |
| No. 8-1 HRWR/ Latex Mod. | 237 | 14 | - |
| No. 11L HRWR/ Expansive/Anti-Bleed | 168 | 32 | - |

[a] Mean Value

4. Use of modifiers and additives provided improved resistance to pressure-induced grout bleeding:
   - Reduction in water/cement ratio had a marginal beneficial effect,
   - Silica fume combined with low water/cement ratio had a significant beneficial effect,
   - SBR latex polymer modifier produced a significant reduction in pressure-induced bleeding, and
   - Antibleeding admixtures were effective in reducing pressure-induced bleeding.
5. On the basis of results from this investigation, the use of expansive additives for grouts designed for bonded, posttensioned construction should be reconsidered.
6. A test protocol (ACTM) was developed that provides a relatively fast evaluation of the ability of grouts to delay the onset of corrosion in prestressing steel, which simulates bonded posttensioned bridge exposures while accelerating the corrosion process.
7. Evaluation of corrosion performance is accomplished by two performance tests: the ACTM developed in this study and the modified AASHTO rapid $Cl^-$ permeability test method (30 V applied voltage).

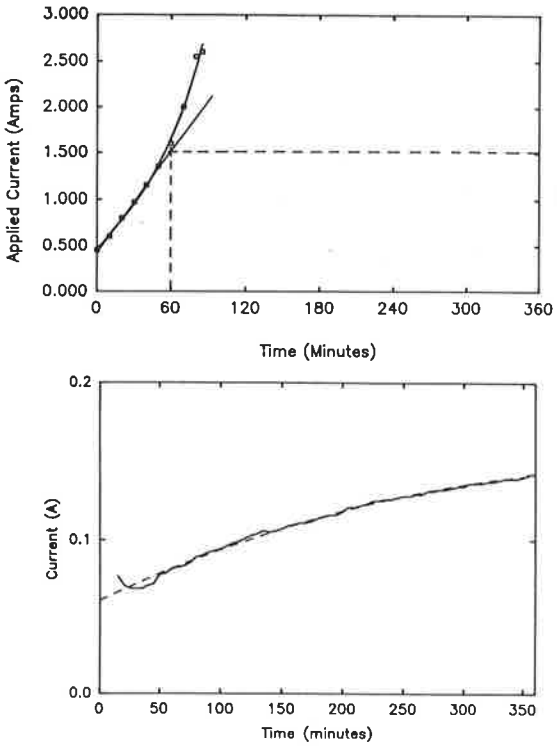


**FIGURE 6 Rapid $Cl^-$ permeability test results for Grout 1 for 60 V (*top*) and 30 V (*bottom*) applied voltage.**

8. Rapid $Cl^-$ permeability test gives similar ranking of grout performance as ACTM when $Cl^-$ permeability is the primary mechanism controlling corrosion initiation. ACTM provides more detailed information (time to corrosion initiation and current following initiation) than rapid $Cl^-$ permeability test.

9. A modified version of ACTM must be used when inhibitors are added to the grout, and in these cases ACTM may be the only method for evaluating corrosion performance.

10. On the basis of ACTM results, grout additives and modifiers that significantly reduce $Cl^-$ permeation also significantly increase the time to corrosion of embedded steel tendons.

11. Grout 5-1, containing 33 percent (cement weight) fly ash, provided a threefold increase in the time to corrosion relative to the standard grout.

12. Grout 6B, containing 10 percent (cement weight) silica fume addition, provided a twofold increase in the time to corrosion relative to the standard grout.

13. Based on limited comparison data from the modified ACTM, the calcium nitrite corrosion inhibitor provided improvement in corrosion performance.

**TABLE 7 Comparison of ACTM Results (0.6 V, SCE, Polarization) with AASHTO Rapid $Cl^-$ Permeability Test**

| Grout Identification | ACTM (0.6V, SCE, Polarized), hours | AASHTO Rapid Permeability Test (6h at 30V), coulombs |
|---|---|---|
| No. 1 Standard (w/c = 0.44) | 164 | 2,400 |
| No. 11L HRWR/ Expansive/Anti-Bleed | 168 | 7,200 |
| No. 8-1 HRWR/Latex Mod. | 237 | 1,600 |
| No. 6B HRWR/Silica Fume | 295 | 1,000 (910)[a] |
| No. 5-1 HRWR/Flyash/Sand | 418 | 370 (140)[a] |

[a] Duplicate Specimens

## REFERENCES

1. N. G. Thompson et al. *Grouting Technology For Bonded Tendons in Post-Tensioned Bridge Structure.* Report FHWA-RD-90-102. FHWA, U.S. Department of Transportation, Nov. 1990, pp. 1–39.
2. D. R. Lankard et al. Grouts For Bonded Post-Tensioned Concrete Construction: Protecting Prestressing Steel From Corrosion. 1990 Fall Convention, American Concrete Institute, Philadelphia, Pa., Nov. 11–16, 1990.
3. D. G. Moore et al. *NCHRP Report 90: Protection of Steel in Prestressed Concrete Bridges.* HRB, National Research Council, Washington, D.C., 1970, pp. 1–86.
4. J. Ryell and B. S. Richardson. *Cracks in Concrete Bridge Decks and Their Contributions To Corrosion of Reinforcing Steel in Prestressing Cables.* Ontario Ministry of Transportation and Communications Report IR51, Toronto, Canada, Sept. 1972, pp. 1–30.
5. T. J. Bezouska. *Field Inspection of Grouted Post-Tensioning Tendons.* Post-Tensioning Institute, Phoenix, Ariz., March 1977, pp. 1–16.
6. M. Schupack. *A Survey of the Durability Performance of Post-Tensioning Tendons.* Post-Tensioning Institute, Phoenix, Ariz., 1978, pp. 1–10.
7. J. R. Libby. *Three Chloride-Related Failures in Concrete Structures.* Concrete International, Detroit, Mich., June 1987, pp. 29–31.
8. V. Novokshchenov. *Salt Penetration and Corrosion in Prestressed Concrete Members.* Report FHWA-RD-88-269. FHWA, U.S. Department of Transportation, July 1989, pp. 1–212.
9. M. Schupack. Water Retentive Admixtures For Grouts Serve Post-Tensioning Needs. *Concrete Construction,* Addison, Ill., Jan. 1984, pp. 7–51.
10. N. G. Thompson et al. *Improved Grouts For Bonded Tendons In Post-Tensioned Bridge Structures.* Report FHWA-RD-91-092. FHWA, U.S. Department of Transportation, Oct. 1991.

*Publication of this paper sponsored by Committee on Corrosion.*

*Abridgment*

# Laboratory and Field Corrosion Test Methods for Highway Metals Exposed to Inhibited Rock Salt

RONALD J. SMITH, DONALD W. PFEIFER, J. ROBERT LANDGREN, BERNIE BUITTKE, AND DAVID MCDONALD

Corrosion-inhibited rock salt as an alternative deicing material has been extensively researched through laboratory and field tests of exposed structural steels, aluminum, and galvanized steel. Because ASTM corrosion test methods G4, G31, and B117 do not address this area of corrosion, a series of specifically designed corrosion tests in the laboratory and at bridge and highway sites was undertaken. Realistically sized metal coupons were used in tests undertaken to explore the role of chloride ion concentration in the deicing solution, the ratio of wet/dry time, and the difference between immersion tests and spray tests to achieve wetting with solutions of inhibited and normal rock salt. Test results indicate that a particular inhibited rock salt can cause reductions in weight loss from 25 to 98 percent, with average corrosion reductions of 55 to 70 percent in the laboratory tests. Results from field tests on the Dan Ryan Expressway and the Chicago Skyway during the 1990–1991 winter suggest a similar corrosion reduction of about 65 percent based on the wire resistance change per weight of chloride collected at six highway and bridge sites. Results of the test series during a 2-year period point toward realistic accelerated corrosion test methods to ensure that alternative deicing materials that show good laboratory performance also provide good performance on highways and bridges.

The deterioration of bridge systems and other metal structures along highways has prompted investigations of alternative deicing chemicals to provide reduced corrosion of embedded reinforcing bars in concrete or exposed metals on highway structures. Evaluation of alternative deicing chemicals involves laboratory testing, for both product development and evaluation by potential customers. The purpose of laboratory tests is to evaluate and select materials performing effectively under actual field conditions. Laboratory tests are necessary to avoid the high costs, in terms of both dollars and time, of large-scale field tests made under relatively uncontrolled conditions.

A cyclical wetting and drying procedure for accelerated laboratory testing of deicing chemicals on reinforced concrete specimens, as reported in FHWA and NCHRP studies (*1–10*), is becoming well established. Similar procedures for evaluation of exposed metals are not as well defined in terms of the relationship between laboratory results and actual field performance. Akzo Salt, in cooperation with Wiss, Janney, Elstner Associates, Inc. (WJE), initiated a program for evaluation of corrosion of bare metal specimens exposed to deicing chemicals by laboratory procedure that could be directly related to relative field performance.

Test practices and methods for studying the corrosion of exposed metal specimens are published by ASTM and the National Association of Corrosion Engineers. Chief among these are ASTM G4, corrosion coupon testing; ASTM G31, laboratory immersion corrosion testing; and ASTM B117, salt spray test. Many investigators have used these ASTM procedures, or variations of them, to compare the corrosion performance of deicing chemicals. Although they provide relative performance in the laboratory, these procedures do not reproduce parameters that may be critical to corrosion reactions in the field. As a result, and as noted in ASTM G31, laboratory evaluation may provide misleading results or results that cannot be used to predict actual field performance.

This Akzo/WJE investigation examined, with the use of realistically sized metal coupons, the role of the ratio of wet/dry time, salt concentration, and cycle length with respect to laboratory corrosion performance relative to actual field performance. In addition, the use of the resistance wire method of measuring field corrosion as a replacement for costly steel coupon mass loss methods was evaluated. The resistance wire method provides the advantage of nondestructive measurement, allowing cumulative data to be obtained from a single specimen over long periods of time at considerably reduced cost.

The referenced ASTM laboratory tests generally use thin steel coupons having small volume/surface (v/s) ratios. As noted in ASTM B117, G4, and G31, the specifics of the corrosion test conditions cannot be standardized because accelerated corrosion testing has so many variables. It is also stated in ASTM G31, "In designing any corrosion test, consideration must be given to the various factors discussed in this practice, because these factors have been found to affect greatly the results obtained." In this Akzo/WJE investigation, the geometry of the test coupon was selected to more closely represent the v/s ratio found in structural members. Typical wide flange beams and plates have v/s ratios from 2 to 40 times greater than the thin specimens commonly used in ASTM

R. J. Smith, Akzo Salt Inc., Abington Executive Park, P.O. Box 352, Clarks Summit, Pa. 18411-0352. D. W. Pfeifer, J. R. Landgren, B. Buittke, and D. McDonald, Wiss, Janney, Elstner Associates, Inc., 330 Pfingsten Road, Northbrook, Ill. 60062.

corrosion testing, but only 1 to 5 times that of the selected ½- × ⅝- × 4-in. specimen. Thus, the selected test specimen is more reasonable when compared with structural shapes.

Field exposure can be divided into three periods: wet time, drying time, and dry time. The authors hypothesized that the relative lengths of wet time and drying time provide the controlling influence on total corrosion of the specimen. That is, corrosion takes place when a corrosive solution is present, and little corrosion occurs during the dry period. Accelerated testing could be better achieved by defining the proper ratio of wet and drying times to dry time to represent actual field conditions and accelerating the test by shortening or eliminating the dry period. Data generated from these tests and tests currently under way indicate that this may be correct.

The accelerated laboratory tests and field tests are discussed here. The actual data and a more detailed discussion are presented in a supplemental document available from Akzo Salt Inc.

## 1989 TEST SERIES ON A36, A572, AND A588 STEEL, GALVANIZED 36 STEEL, AND 6061-T6 ALUMINUM

Two different corrosion inhibition materials (Numbers 1 and 2) were used in a 15 percent NaCl solution. The uninhibited NaCl solution strength was also 15 percent. Two 30-day accelerated corrosion test procedures were used. One test method addressed the cyclical wet and dry environment; the second addressed the partial immersion environment. The mean percent improvement in weight loss for the A36, A588, and A572 steels for Solutions 1 and 2 for the wet/dry test method ranged from 40 to 54 percent.

## 1990 TEST SERIES ON A36 STEEL WITH 11 DIFFERENT DEICER FORMULATIONS

This test series used the same wet/dry test cycle. Eleven different deicing solutions were evaluated. All solutions used 15 percent NaCl. Ten solutions contained corrosion inhibitors; one was uninhibited.

Test results showed that the 10 formulations increased the effectiveness of the inhibitors tested in 1989 from the 40 to 54 percent range to the 81 to 94 percent range.

## 1990 TEST SERIES ON ASTM STEEL AND ASTM A615 GRADE 60 REINFORCING BAR STEEL

The objective of this series was twofold: to determine (a) if 15 percent salt solutions containing the inhibitors would be equally effective on A36 prisms and A615 reinforcing steel and (b) if immersion of the specimens in alkaline salt solutions similar to the pH found in concrete would have a passivating effect. A review of the data indicates the following:

- The specimens in 11 different inhibited salt solutions (normal pH of 7) showed a decrease in percent metal loss over those specimens exposed to plain salt solutions. The magnitude of improvement ranged from 36 to 94 percent for A36 steel and from 86 to 98 percent for A615 rebar.
- The use of $Ca(OH)_2$ in the salt water solutions (pH = 12) produced a remarkable 98 percent reduction in the metal loss during the laboratory test series with both steels. This decrease in the metal loss was due solely to pH change.

## 1990 TEST SERIES ON ASTM A36 STEEL WITH VARIOUS SOLUTION STRENGTHS AND VARIOUS SALT SPRAY/DRY TEST PERIODS

A new 30-day accelerated corrosion procedure and apparatus were developed. Previously, the laboratory test specimens were totally immersed for 60 min during each 6-hr cycle. This total immersion did not allow high oxygen availability during the wet period. The new method used a salt spray instead of total immersion. The salt spray times and number of spray cycles per day were also varied.

Four different deicer solutions were evaluated with six series. The inhibited and uninhibited solutions used NaCl concentrations of 3 and 15 percent. In Series 4–6, one 15-min fresh water rinse each day was used to simulate one short period of daily precipitation.

These data indicate that the inhibitor is effective at both concentrations when the steel surfaces are sprayed for 50 to 80 percent of the test period, with improvement in weight loss ranging from 46 to 90 percent and averaging 70 percent. When sprayed for 25 percent of the total cycle period, the improvement in weight loss ranged from 25 to 84 percent and averaged 54 percent. These data suggest that the average improvement in a typical bridge environment subjected to an inhibited salt spray concentration between 3 and 15 percent could be between 55 and 70 percent.

These test results suggest that as the concentration strength decreased from 15 percent to 3 percent the corrosion-induced weight loss increased from 1.3 to 2.6 times, averaging 1.95 times. This suggests that as highway agencies use less salt or dilute the salt with other materials, the concentration strength of the solutions splashed onto these bridges is probably decreasing, which in turn allows for much greater corrosion-induced weight loss.

## FIELD TESTS IN CHICAGO DURING WINTER 1990–1991

The concentration of salt solutions applied on bridge structures and pavements remains largely unknown. Thus, laboratory corrosion experiments may not be representative of actual highway conditions. For this reason, a field study of A36 steel coupons under both inhibited and normal salt environments was initiated. The tests continued through the winter of 1991–1992.

Seven sites were chosen by WJE and the cooperating agencies. As a control measure, three sites (1–3) exposed to normal deicing salts were chosen along I-94 on the Dan Ryan Expressway. Three other sites were deiced with the corrosion inhibiting salt. These sites (4–6) were on the Chicago Skyway. Great care was taken to ensure that the six sites appeared to be similar, although traffic volumes are not equal. The I-

94 sites certainly have much greater traffic volume. All six highway and bridge sites are within a 10 mi radius. A seventh site, on the roof of a WJE building, was chosen to allow an investigation of steel coupons not exposed to deicing salts.

At the end of each month during the 3 months of exposure, a single coupon was collected and tested from each of the six highway sites, and three coupons were collected from the WJE building roof. A prototype test method for determination of corrosion rates in the field was also developed by WJE. Six wire specimens were mounted at each of the seven sites and their electrical resistance measured using a fine-scale ohm meter.

To quantify the salt exposure at each site, a salt spray and water collector was mounted near the steel coupons. The salt solutions were collected at each site at the end of each month and analyzed. The weight losses after three months of winter weather for the atmospherically corroding specimens were 30 to 37 percent of the two other exposures where deicer salts were applied. The relationship between theoretical coupon weight loss and theoretical wire resistance shows a good correlation between theory and field measurements. The amount of wire resistance change per gram of collected inhibited salt in the collectors is 31 percent of that of the normal salt after the 3-month period.

Chloride-induced corrosion, defined as the weight loss at each exposure that is over and above that caused by normal atmospheric corrosion, was calculated by subtracting the average weight loss at Site 7 (WJE) from the average from the other exposures. The average chlorine-induced weight loss per gram of collected inhibited salt is 35 percent of that for the normal salt after the 3-month period. This conclusion is based on the reasonable assumption that the amount of weight loss due to chloride ions is proportional to the quantity of chloride exposure at the site.

## CONCLUSION

Extensive laboratory and field tests on exposed steels, aluminum and galvanized steel were undertaken during a 2-year period. These tests were directed toward establishing realistic, accelerated test methods to ensure that alternative deicing materials that provide good corrosion reduction in laboratory tests also exhibit these properties on highway and bridge systems.

Certain corrosion-inhibited rock salt materials achieved reductions in weight loss in laboratory and field tests that averaged about 55 to 70 percent, with some laboratory tests achieving as much as 98 percent weight loss reductions when compared with normal rock salt.

Tests are continuing, and future tests will focus on the role of oxygen and variable chloride concentrations during wet and drying times, as well as the role of the dry time in the corrosion process. Future tests will use automatic data-logging of corrosion activity under bridge site and laboratory conditions to better understand this complex process.

## ACKNOWLEDGMENTS

The authors acknowledge the guidance and cooperation of the Chicago Skyway Toll Bridge agency and the Illinois Department of Transportation and their staff during field testing.

## REFERENCES

1. K. C. Clear. *Time-to-Corrosion of Reinforcing Steel in Concrete Slabs: Vol. 1, Effect of Mix Design and Construction Parameters.* Interim Report FHWA-RD-73/52. FHWA, U.S. Department of Transportation, 1976.
2. K. C. Clear. *Time-to-Corrosion of Reinforcing Steel in Concrete Slabs: Vol. 3, Performance After 830 Daily Salt Applications.* Report FHWA-RD-76/70. FHWA, U.S. Department of Transportation, 1976.
3. K. C. Clear. *Time-to-Corrosion of Reinforcing Steel in Concrete Slabs: Vol. 4, Galvanized Reinforcing Steel.* Report FHWA-RD-82/028. FHWA, U.S. Department of Transportation, 1981.
4. D. W. Pfeifer and M. J. Scali. *NCHRP Report 244: Concrete Sealers for Protection of Bridge Structures.* TRB, National Research Council, Washington, D.C., Dec. 1981.
5. Y. P. Virmani, K. C. Clear, and T. J. Pasko. *Time-to Corrosion of Reinforcing Steel in Concrete Slabs: Vol. 5, Calcium Nitrite Admixture or Epoxy-Coated Reinforcing Bars as Corrosion Protection Systems.* Report FHWA-RD-83/012. FHWA, U.S. Department of Transportation, Sept. 1983.
6. D. W. Pfeifer, J. R. Landgren, and W. F. Perenchio. Concrete, Chlorides, Cover and Corrosion. *Journal of Prestressed Concrete Institute,* Vol. 31, No. 4, July – Aug. 1986.
7. *DCI Performance in Cracked Concrete.* Technical Bulletin TB DCI-87-02. W. R. Grace and Co., Cambridge, Mass., 1987.
8. D. W. Pfeifer, J. R. Landgren, and A. B. Zoob. *Protective Systems for New Prestressed and Substructure Concrete.* Final Report FHWA/RD-86/193. FHWA, U.S. Department of Transportation, April 1987.
9. B. B. Hope, and A. K. C. Ip. Chloride Corrosion Threshold in Concrete. *American Concrete Institute Materials Journal,* July/Aug. 1987.
10. W. F. Perenchio, J. Fraczek, and D. W. Pfeifer. *NCHRP Report 313: Corrosion Protection of Prestressing Systems in Concrete Bridges,* TRB, National Research Council, Washington, D.C., Feb. 1989.

*Publication of this paper sponsored by Committee on Corrosion.*

# Measuring the Chloride Content of Concrete

STEPHEN E. HERALD, RICHARD E. WEYERS, AND PHILIP D. CADY

The deterioration of reinforced concrete due to the corrosion of the reinforcing bars may be expressed as the sum of three time events: time to initiation of corrosion, time to first spalling, and time to failure. Three corrosion processes have to be characterized to determine the corrosion state of the concrete within the three events. The three processes are the rate of chloride diffusion and present level of chloride contamination, rate of corrosion, and rate of maintenance activities from first spalling to failure. Thus, measuring the chloride content of concrete as a function of depth is critical to determining the chloride contamination state and the rate of chloride diffusion into concrete. The present standard methods are too arduous, time-consuming, and costly for use in the field and for measuring the chloride content of the relatively large number of samples needed to characterize the chloride contamination level of concrete bridges. The laboratory work in the development of a field-worthy method of measuring the chloride content of reinforced concrete structures was addressed in this study.

A literature review was performed, and four methods were selected for the laboratory study: Quantab chloride titrator strips, specific chloride ion electrode, spectrophotometer, and argentometric digital titrator. The laboratory study was composed of the determination of the accuracy of the method with respect to the AASHTO T-260 standard method and the effect of cement content and temperature. In addition to the control with no additional chlorides added to a concrete mixture, contamination levels of 0.2, 0.4, 0.8, 1.6, 3.2, 6.4, 8.6, 10.8 and 12.8 lb chlorides/yd$^3$ of concrete were tested. On the basis of accuracy, cost, speed, and level of expertise required, the specific ion electrode was selected for further evaluation of the effects of cement content and temperature. Cement content was shown to have no effect on the results. However, the reaction temperature does influence the measured chloride content. A correction factor was developed for the effect of the reaction temperature.

The deterioration of concrete bridges from the chloride-induced corrosion of the reinforcing steel in the United States is well known. A recent projection estimated the financial liability of corrosion-induced deterioration in bridges at $20 billion, increasing at a rate of $0.5 billion annually (*1*). To optimize the cost-effective solution to the protection, repair, and rehabilitation of concrete bridges, one must identify the present corrosion state of the bridge components. The corrosion state of a bridge component will be within one of the three time events: time to initiation of corrosion, time to first spalling, or time to failure. The three processes associated with the time events are the rate of chloride diffusion and the present level of chloride contamination, the rate of corrosion, and rate of maintenance activities from first spalling to failure. Thus, measuring the chloride content of concrete as a function of depth is critical to identifying the present corrosion state and predicting the future contamination level using the rate of chloride diffusion.

The present standard methods of measuring the chloride content of concrete, AASHTO T-260 and ASTM C114, are too arduous, time-consuming, and costly for use in the field and for measuring the chloride content of the relatively large number of samples needed to characterize the chloride contamination state of concrete bridges. The laboratory work in the development of a field-worthy method of measuring the chloride content of reinforced concrete structures was addressed in this study.

## BACKGROUND

Methods to use to determine the chloride ion content of concrete may be classified as nondestructive and destructive techniques. Nondestructive techniques include the dual neutron-gamma ray and the neutron-gamma ray spectroscope. Destructive methods, requiring a drilled powdered sample, include the AASHTO standard method, x-ray fluorescence, gas chromatograph, Quantab chloride titrator strips, specific ion electrode, spectrophotometer, and argentometric digital titrator.

The dual neutron-gamma ray technique was developed for FHWA by Columbia Scientific Industries (*2,3*). The instrument is capable of measuring chloride content with respect to depth; its detection limits are 0.04 to 0.08 lb/yd$^3$ and depth resolutions are 0.40 to 8 in., depending on the calibration model. The choice of the wrong calibration model ($Cl^-$ depth distribution model) will result in significant measurement errors. Calibration models would have to be developed for specific types of bridges (e.g., concrete or steel beams, varying deck thickness, varying overlay thickness, coastal or inland bridges) (*3*). The method is relatively fast, 2 to 3 measurements per hour with a 10-min data acquisition time. Instrument operation is straightforward and requires little training. However, instrument calibration and setup must be done by qualified scientists. Although operational costs are relatively low, capital costs are high. Also, the equipment is large and is mounted on a self-contained vehicle and thus is limited to use on bridge decks.

S. E. Herald and R. E. Weyers, Civil Engineering Department, Virginia Polytechnic Institute and State University, Blacksburg, Va. 24061. P. D. Cady, Civil Engineering Department, Pennsylvania State University, University Park, Pa. 16802.

Neutron-gamma ray spectroscopy also uses a californium-252 neutron source for composition measurements, but uses a high-resolution, high purity germanium detector rather than a NaI (T1) crystal gamma-ray detector (*4–6*). The instrument has been used to measure the relative difference with regard to surface position of the chloride content of a masonry wall by normalizing the chloride intensities to the value of silicon ($Cl^-$/Si ratio). The procedure assumes the value of silicon remains relatively constant throughout the material. Portability problems, calibration requirements, and equipment costs significantly limit the usefulness of the device for determining the chloride content of concrete bridge components.

X-ray fluorescence and gas chromatography analysis methods of powder samples offer no advantage over other powder analysis methods because of the related power requirements (x-ray fluorescence requires approximately a 100-kV source), cost (between $25,000 and $100,000 for equipment only), and level of expertise required. These limitations restrict the use of the instruments to the laboratory.

Quantab chloride titrator strips are simple and fast to use and are applicable to field measurement techniques of powder samples. Simplified procedures for the Quantab method were developed by the Building Research Station, Garston, Wartford, for analyzing the chloride content in portland cement concrete. The analysis procedure developed for the Quantab titrator strips consists of an acid digestion of a 5 g sample of powdered concrete. Fifty mL of 1 N nitric acid solution were used to digest the chloride followed by neutralization of the acid using 5 g of anhydrous sodium carbonate. Chloride concentration of the sample was then determined using the Quantab titrator strips (*7*).

The Building Research Station, Garston, Wartford, also developed a simplified procedure for the chloride determination in portland cement concrete using the (argentometric) test method. In this procedure, the 5-g powdered concrete sample is acid digested with 50 mL of 1 N nitric acid. While the sample mixture is being stirred, 5 g of sodium bicarbonate is added to the sample mixture. Once completely dissolved, the mixture is allowed to stand for 1 to 2 min. Finally, the mixture is filtered into a beaker using Whatman 41 or an equivalent filter paper. The filtered solution is then titrated by pouring 5.75 mL of the filtrate into a mixing bottle. One capsule of potassium chromate powder indicator is added to the sample. A silver nitrate solution is added drop by drop and the sample is swirled after each drop. The sample is titrated from a bright yellow to faint reddish brown color, and the number of digits required to complete the titration is recorded (*7*).

The development of the specific ion probe method for measuring the chloride content of concrete was first conducted at The Pennsylvania State University (*8*). The procedure was further developed for field use by James Instruments (*9*). The method digests a 3-g powered sample in a chloride extraction solution. A combination specific chloride ion electrode connected to a voltmeter is inserted into the sample mixture, and the millivolt reading is recorded. The chloride content is determined by using a calibration equation, which in turn is determined every time the instrument is turned on.

The spectrophotometric method compares the color difference of a chloride extracted mixture with a standard reference solution. The chloride content is a direct digital readout in parts per million (*10*).

The most promising methods, on the basis of initial equipment cost, level of expertise required, and portability (which may be adapted to the rapid field measurement of the chloride content of reinforced concrete using powder samples), are the specific ion electrode, spectrophotometric, and argentometric digital titration methods, and Quantab titrator strips. Subsequently, these methods were selected for laboratory investigation.

## EXPERIMENTS

The laboratory investigation of the four test methods consisted of three phases: accuracy of the four test methods as compared with the AASHTO standard test method, the effect of cement content, and temperature on the performance of a best select test method.

For the accuracy, cement content, and temperature tests, concrete specimens 1 $ft^2$ × 6 in. thick were cast at 10 chloride contamination levels. Specimens were cast at chloride additive rates of 0.0, 0.2, 0.4, 0.8, 1.6, 3.2, 6.4, 8.6, 10.8 and 12.8 lb $Cl^-/yd^3$ of concrete using a sodium chloride solution. Concrete slabs were cast at a water/cement ratio (w/c) of 0.40, 0.47, and 0.50 with Type I cement contents of 658, 640, and 552 lb/$yd^3$ of concrete, respectively, at each of 10 chloride contamination levels. The fine aggregate was a natural sand and the coarse aggregate was a nominal 1-in. crushed limestone. The specimens were moist cured for 46 days. A rotary hammer drill with a ¾-in. carbide drill bit was used to sample each of the concrete slabs. The extracted powder from the multiple drill holes in a single contaminated slab was combined, dried, and sieved over a number 50 sieve, and the retained 50 sieve material was discarded.

Bridge deck class concrete specimens (w/c = 0.47) were used in the initial series of chloride content tests to determine the accuracy of the four methods. The substructure and superstructure mixtures (w/c = 0.50 and 0.40, respectively) were used to determine the effects of cement content. A single chloride contamination level (1.4 lb $Cl^-/yd^3$) was used to determine the effects of chloride extraction reaction temperature.

## LABORATORY TESTING

The standard potentiometric titration method was used to standardize the 0.01 N silver nitrate and sodium chloride solutions used for the analysis of chloride in accordance with the standard AASHTO procedure. Tests for chloride content using the four select methods were performed on standardized solutions to verify their accuracy before the specimens were tested. The test results for all four selected methods were within the range of accuracy specified by the manufacturers.

### Specific Ion Probe

A deviation from the recommended calibration procedure involved a regression analysis of the calibration measurements instead of determination of the calibration equation graphically. This deviation was used to allow more precision in the test results.

A plot of the results obtained using the specific ion probe as a function of the potentiometric titration results and the 95 percent confidence limits for the prediction interval are presented in Figure 1.

### Spectrophotometric

Samples analyzed using the spectrophotometer were also compared with the results obtained from the potentiometric titration procedure. A plot of the spectrophotometer and the potentiometric titration results and the 95 percent confidence limits for the prediction interval are presented in Figure 2.

### Digital Titrator

Samples analyzed using the digital titrator were also compared with the results obtained from the potentiometric titration procedure. A plot of the digital titrator as a function of the potentiometric titration results and the associated 95 percent confidence limits are presented in Figure 3.

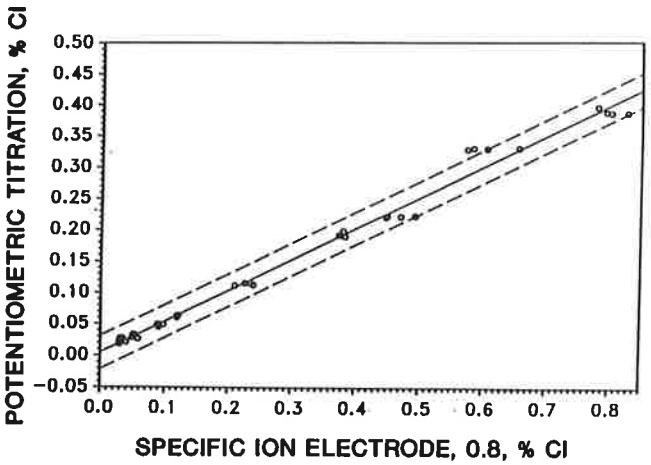


**FIGURE 1 Potentiometric titration versus specific ion probe.**

### Quantab Titrator Strips

Acid digested samples analyzed using the Quantab titrator strips were compared with the results obtained from the potentiometric titration procedure. A plot of the Quantab titrator strips number as a function of the potentiometric titration results and the 95 percent confidence limits for the predicted value are presented in Figure 4.

## COMPARISON OF TEST METHODS

As indicated from an analysis of the results obtained from the first series of tests for chloride, the highest accuracy is achieved using the specific ion probe followed by the digital titrator, spectrophotometer, and the Quantab titrator strips (see Table 1). These are considered the most important criteria for selecting the appropriate method because errors in measuring the chloride content of bridges may influence the results obtained in estimating the extent of chloride contamination and in predicting the time to depassivation.

The initial cost of the specific ion probe was greater than the other selected methods. It should be noted that hidden costs are associated with the spectrophotometer, digital titrator, and the Quantab titrator strips. Items such as filter paper, beakers, stirring rods, nitric acid, and deionized water are required for all three methods. Additional items such as funnels, a funneling apparatus, and pipets are required for the spectrophotometer and the digital titrator. Finally, a magnetic stirrer and magnetic stirring rods are desirable when using the digital titrator.

No special sample preparation is required for the specific ion probe. The probe can be calibrated in less than 10 min, after which samples can be weighed and analyzed in less than 10 min. This allows the operator 7 min to weigh the sample before testing.

The procedure for weighing and preparing the sample for the spectrophotometer and the digital titrator requires the same amount of time. Once the samples are prepared, the analysis procedure using the spectrophotometer requires a little less than the digital titrator. The operator must pay

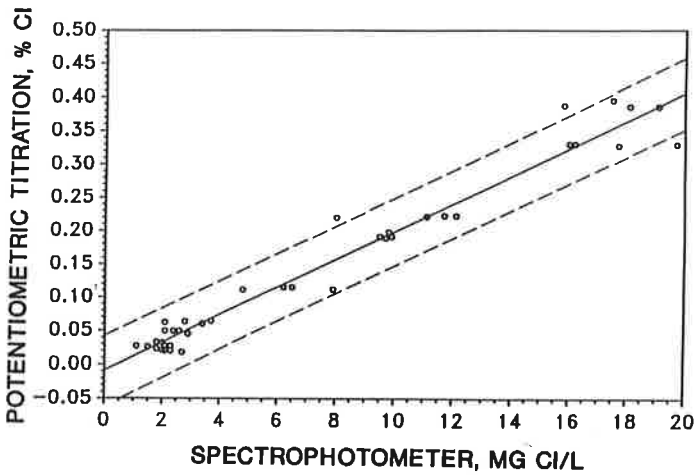


**FIGURE 2 Potentiometric titration versus spectrophotometer.**

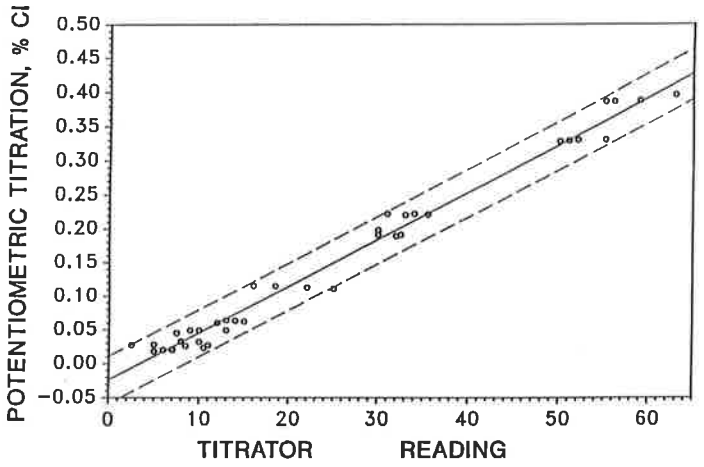


**FIGURE 3 Potentiometric titration versus digital titrator.**

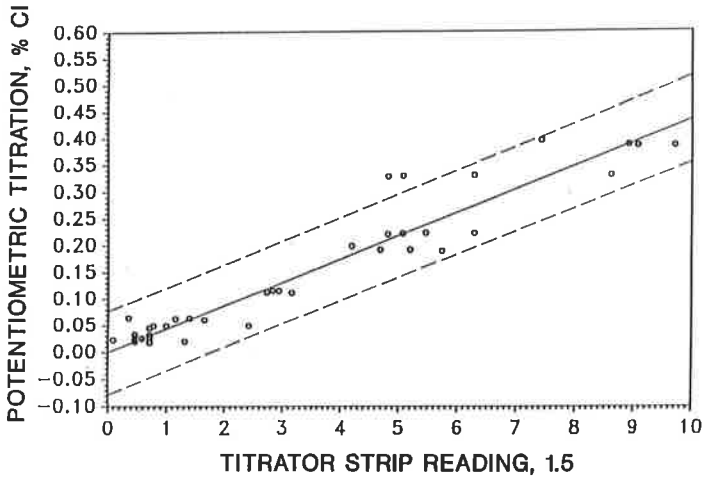


**FIGURE 4 Potentiometric titration versus Quantab titrator strips.**

**TABLE 1 Comparison of Test Methods**

| Method | Accuracy R-sq (Adj) | *Cost | **Speed | *** Level of Expertise |
|---|---|---|---|---|
| Specific Ion Probe | 99.0% | $1860.90 | 1 | Simple |
| Spectrophotometer | 96.3% | 1363.57 | 2 | Medium |
| Digital Titrator | 98.3% | 156.74 | 3 | Medium |
| Quantab Titrator Strips | 91.2% | 49.30 | 4 | Simple |

*Cost represents the initial cost of the equipment and the chemicals necessary for analyzing 40 specimens.

**Speed represents the order in which samples may be weighed, prepared, and tested using each method.

***Level of expertise gives an indication of how complicated each procedure is to use.

particular attention during the titrating procedure when using the digital titrator so the midpoint of the titration will be recognized.

The procedure for weighing and preparing the sample to be analyzed using the Quantab titrator strips does not require as much time as for the spectrophotometer and the digital titrator. However, sometimes the operator may be required to wait as long as 20 min before the results may be read using the Quantab titrator strips.

The analysis procedure for the specific ion probe was simplified for the operator when compared with the original procedure developed by James Instruments (*9*). Essentially, the operator records readings displayed by the electrometer while following a step-by-step procedure. Two precautions must be followed in using this procedure to obtain accurate results. Otherwise, the procedure is simple, quick, and straightforward. Procedures for the spectrophotometer and the digital titrator are a little more complicated than those for the specific ion probe. The operator not only must realize the importance of following the procedure completely, but also must be able to detect interferences and compensate for them. The analysis procedure for using the Quantab titrator strip is a little more complicated than the procedure for the specific ion probe, but it requires little technical expertise.

Considering each of the criteria, which are summarized in Table 1, for selecting the method for determining the chloride content of concrete, the specific ion probe was determined to be most suitable for the purpose intended. First, the apparatus required for the spectrophotometer and the digital titrator is more suited for use in the laboratory than in the field. Second, both of those procedures require a certain level of expertise to achieve meaningful results. Finally, the Quantab titrator strips do not provide the accuracy that is desirable for determining the time to depassivation and, at times, may require an excessive amount of time for analysis.

## EFFECTS OF CEMENT CONTENT

A comparison of the results for the effects of cement content on the specific ion electrode method encompassed using the accuracy test results (w/c = 0.47) along with the results of the testing of 0.50 and 0.40 w/c slab series. As shown in Figure 5, it appears that there is no significant effect of cement content on the performance of the specific ion probe. In addition, a statistical analysis of the results indicated there was no correlation between the results obtained for chloride content using the specific ion probe and cement content.

## EFFECTS OF REACTION TEMPERATURE

The results obtained for the specific ion probe during this series of tests were compared with the results obtained for the specimen from the first series of tests to determine the effects of temperature.

Figure 6 shows the relationship between the correction factor for the specific ion probe suggested by the results of the regression analysis relative to the reaction temperature.

## SUMMARY AND CONCLUSIONS

The objective of this study was to identify a field procedure for determining the chloride content of concrete. This objective was accomplished by a preliminary investigation of four select methods to determine their effectiveness in measuring the chloride content of concrete followed by a subsequent analysis of the select method to determine the effects of cement content and reaction temperature. Ultimately, a field procedure for determining the chloride content in concrete will be validated.

Results from the initial phase of the investigation indicated that the Quantab titrator strips would provide a rough estimate of the chloride content in a concrete specimen.

The results of the tests using the spectrophotometer indicated that reasonable estimates of chloride content could be obtained particularly for low levels of chloride.

The digital titrator may also be used to obtain good estimates of chloride content in concrete specimens. This procedure allows for accuracy in measuring the chloride content

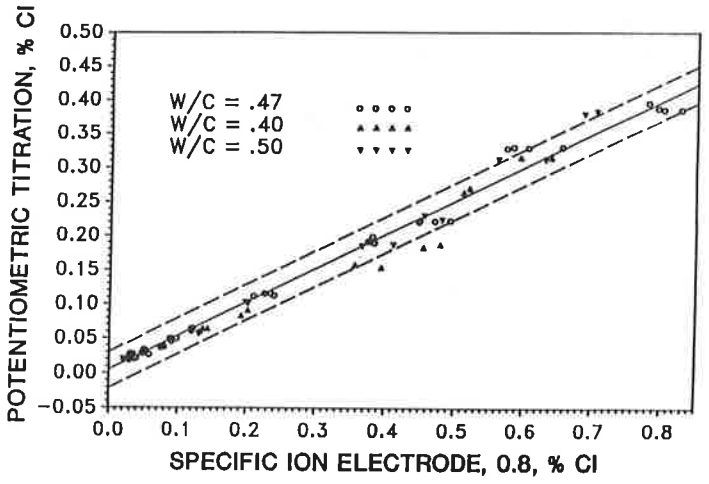


**FIGURE 5 Potentiometric titration versus specific ion probe for different cement contents.**

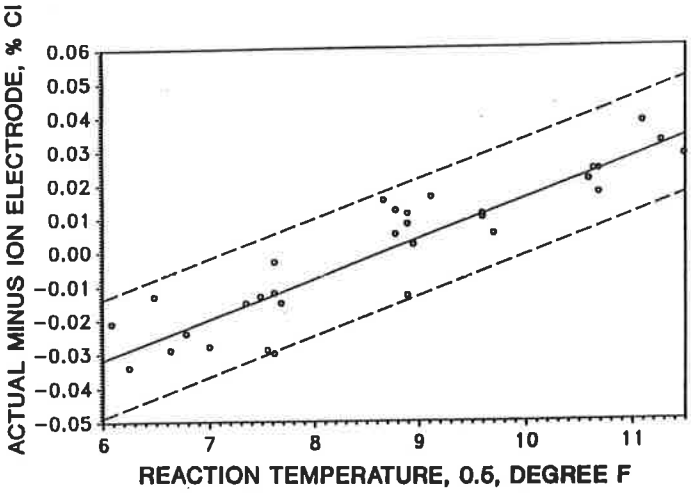


**FIGURE 6 Temperature correction for specific ion probe.**

over a broader range of contamination levels than with the spectrophotometer.

The specific ion probe provided more accuracy in measuring chlorides in concrete than the previous methods tested. In addition, less than 5 min per specimen was required for the analysis procedure during the laboratory investigation.

The second and third phases of the investigation indicated the specific ion probe test results were not affected by different cement contents but were affected by changes in chloride extraction temperature. Consequently, a correction factor for temperature was developed.

## ACKNOWLEDGMENTS

The research reported here was funded by the Strategic Highway Research Program under contract C-101. The authors are indebted to John P. Broomfield, the SHRP project technical contract manager, for his sound advice.

## REFERENCES

1. *Strategic Highway Research Program: Research Plans.* TRB, National Research Council, Washington, D.C., May 1986, pp. TRA 4.1–4.60.
2. J. R. Rhodes et al. *In Situ Determination of the Chloride Content of Portland Cement Concrete in Bridge Decks—Feasibility Study.* Report FHWA-RD-77-26. FHWA, U.S. Department of Transportation, Feb. 1977, p. 114.
3. J. R. Rhodes et al. *In Situ Determination of the Chloride Content of Portland Cement Concrete in Bridge Decks.* Report FHWA-RD-80-030. Aug. 1980, p. 59.
4. R. A. Livingston. X-Ray Analysis of Brick Cores from the Powell-Waller Smokehouse, Colonial Williamsburg. *Proc., Third North American Masonry Conference,* June 1985, pp. 61/1–16.
5. L. G. Evans et al. Neutron/Gamma Ray Techniques for Investigating the Deterioration of Historical Buildings. *Nuclear Instruments and Methods in Physics Research,* A242, 1986, pp. 346–351.
6. L. G. Livingston et al. *Diagnosis of Building Condition by Neutron-Gamma Ray Technique.* ASTM STP 901. ASTM, Philadelphia, Pa., 1986, pp. 165–180.
7. Building Research Station. Determination of Chloride and Cement Content in Hardened Portland Cement Concrete. *Building Research Establishment Information Sheet,* IS 13/77, July 1977.
8. T. D. Larson, P. D. Cady, F. P. Browne, and N. B. Bolling. *Deicer Scaling Mechanism in Concrete.* Pennsylvania State University, University Park, Dec. 1970, pp. 87–100.
9. *CL Test Model CL 500 Instruction Manual.* James Instruments Inc., Chicago, Ill., 1988, p. 11.
10. *DR/2000 Spectrophotometer Procedure Manual,* 2nd ed. Hach Company, Loveland, Colo., Sept. 1988, p. 395.

*The opinions, findings, and conclusions are those of the authors and not necessarily those of the sponsoring agency.*

*Publication of this paper sponsored by Committee on Corrosion.*

# Recent Research on Alternative Deicers at Chevron

C. D. BUSCEMI, K. A. HOENKE, AND K. L. EKLUND

A calcium magnesium acetate (CMA)–based deicing product has been tested as an alternative to salt-based deicers, which are corrosive to steels used in the construction of bridges, roadways, and automobiles. The CMA-based deicer showed much lower corrosion rates than salt-based deicers in alternative immersion tests. Electrochemical testing of steels in CMA-based deicer suggests that although similar corrosion potentials to salt-based deicers occur with the CMA-based product, corrosion currents, and thus corrosion rates, are greatly reduced. Results of alternative immersion and electrochemical testing are presented.

Substantial corrosion of roadways and bridges due to the application of deicing salts has come to be recognized as a major problem. Today's road salts contain chlorides, which are responsible for the corrosion of bridge and roadway steels. Substitute deicing chemicals have been formulated and are being tested in various forums for their ability to remove snow and ice without causing further infrastructure damage.

Two classes of deicers are undergoing testing currently. One class uses small amounts of inhibiting chemicals added to plain road salt; in this case the chloride-containing road salt is still the deicer, but the chemical additions cause reduction of metal corrosion rates as long as the inhibiting chemical remains in contact with the steel.

Another class of deicer relies not on chlorides, but on low-corrosion chemicals, which are deicers themselves. These deicers have the potential to eventually allow removal of destructive chlorides entirely from the infrastructure.

## CURRENT RESEARCH ON DEICERS

Research has been focused on three primary areas: corrosion of bare metal, corrosion of steel rebar in concrete, and deterioration of concrete. In all cases, solutions of varying concentration have been tested. Representative concentrations range from 3.5 percent to more dilute values, which simulate what might be encountered on a roadway following deicer spreading and melt runoff.

Bare metal testing is a straightforward way to evaluate the effects of deicing solutions on structural metals, can be done quickly and cheaply, and has provided much of the information known about deicer corrosivity. Although corrosion rates for bare metal do not necessarily indicate corrosion rates for reinforcing steel in concrete, bare metal tests allow comparisons of the relative effects of deicing solutions on structural highway metals.

To determine the effects of deicing solutions on reinforcing steel bar in concrete, tests have been done on concrete slabs containing rebar. These tests take longer to complete, so less data are currently available on rebar in concrete.

Tests on the effects of deicing solutions on concrete have also been performed. In these tests, concrete slabs are usually cyclically ponded with deicing solutions, so that they go through wetting and drying cycles that simulate actual road conditions. Freeze-thaw cycles are a common test on concrete to determine if use of alternative deicing chemicals leads to increased cracking and pothole damage during the winter.

## WHAT IS KNOWN ABOUT BARE METAL CORROSION BY CALCIUM MAGNESIUM ACETATE?

Most corrosion testing of calcium magnesium acetate (CMA) to date has been on structural steels. CMA has been found to reduce corrosion of highway steels by five to fifteen times compared with plain road salt.

Extensive coupon weight loss work by Locke and Kennelley, sponsored by FHWA, concluded that corrosion of steel in CMA is about two to five times less than in salt solution (*1,2*). The corrosion rate of A-36 steel in CMA was found to be only 1 mil per year (mpy) in a 2 percent CMA solution.

Another large study on the effects of CMA has been performed by the Michigan Department of Transportation (DOT) (*3*), which tested a variety of structural steels, including ASTM A-36 bridge steels, A-588 weathering steel rebar, and galvanized steel, along with several galvanic couples of stainless steel with carbon steel and with aluminum. Welds were also tested, as were some common aluminum alloys. Test solutions included CMA, various CMA/NaCl mixtures, NaCl with a commercially available $MgCl_2$ corrosion inhibitor, simulated acid rain, and distilled water.

Steel specimens in CMA corroded at only 1/4 to 1/15 the rate of steel specimens in NaCl (5–10 mpy for CMA versus 30–60 mpy for salt). CMA also caused less pitting. Additions of one part CMA to two parts NaCl also greatly reduced corrosion rates over plain salt. Steel welds were dramatically less corroded in CMA as well. Aluminum was attacked aggressively in neither CMA nor salt, but pitting was less in CMA. CMA was only slightly more corrosive than distilled water, and was less corrosive than simulated acid rain.

The Minnesota and Washington DOTs have also seen reduced corrosion of highway steels by CMA. Minnesota

C. D. Buscemi, Materials Unit, Chevron Research and Technology Co., 100 Chevron Way, Richmond, Calif. 94802-0627. K. A. Hoenke, Chevron Chemical Co., 6001 Bollinger Canyon Road, San Ramon, Calif. 94583-0956. K. L. Eklund, Department of Materials Science, Carnegie-Mellon University, Pittsburgh, Pa. 15213.

reported that out of seven deicers sprayed on steel three times daily over a period of about 250 days, a 20/80 mix of CMA/salt showed the least corrosion, actually less than water alone (unpublished data). The CMA/NaCl mix corroded steel six times less than plain salt, and two times less than its closest competitor. Washington DOT reported corrosion five to seven times less in CMA solution (about 4 mpy) than in salt solution (*4*).

Southwest Research Institute (SwRI) reports corrosion rates for steel in pure CMA to be near zero (*5*). SwRI found that additions of about 20 percent CMA to NaCl solutions reduces corrosion by up to 80 percent more than plain salt.

In another comprehensive FHWA report (*6*), CMA was found to be less corrosive than salt to automotive steels, stainless steels, aluminum alloys, automotive and road paints, brake linings, and portland cement concrete. CMA did no damage to plastics, elastomers, ceramics, rubbers, sealants, adhesives, and asphalts.

## WHAT IS KNOWN ABOUT CORROSION OF REBAR IN CONCRETE BY CMA?

Locke and Kennelley performed electrochemical measurements of corrosion potential for rebar in concrete (*1,2*). They concluded that although an active corrosion potential is measured for rebar in concrete exposed to CMA solutions, the actual corrosion rate is small compared with that in salt solution. Another important conclusion was that "galvanic type" corrosion cells can be set up when corrosion potential differs from one area of a reinforced concrete mat to another.

Locke and Kennelley found that CMA solutions ponded on reinforced concrete can change local corrosion potentials; however, their work did not measure corrosion current, which would have yielded a clearer picture of the amount of corrosion that was occurring. The finding that CMA causes active corrosion potentials for rebar in concrete, but that actual corrosion is small, has been reproduced by Chevron. It will be discussed in more detail in the section dealing with Chevron's electrochemistry work.

Two European studies, one by British Petroleum (*7*), the other sponsored by the Danish Ministry of Transport (*8*), have concluded that corrosion by salt solutions of steel embedded in concrete can be slowed down or terminated once the use of salt is discontinued and the concrete is exposed to CMA solution. The Danish study concluded that ponding a 50/50 CMA/salt mix "has a retarding effect on the corrosion of steel in concrete."

The most current work on rebar in concrete is being performed by Peart at FHWA. Peart's unpublished data show that ponding of either clean or chloride-contaminated concrete by CMA solutions results in minimal corrosion current and passive corrosion potentials, whereas ponding of the same slabs with salt solutions results in higher corrosion currents and active corrosion potentials.

## WHAT IS KNOWN ABOUT THE EFFECTS ON CONCRETE OF CMA?

In several major studies, CMA caused the least damage to concrete of all deicers tested, including the road salt commonly used today. Michigan DOT found freeze-thaw damage from salt to be dramatically decreased when CMA was added to NaCl and to be eliminated by plain CMA (*9*). A salt-based deicer containing phosphates, tested at the same time, caused more concrete spalling as well as more corrosion to rebar than even plain salt.

A study by Nadezhdin et al. found that CMA caused less freeze-thaw damage than any of the other deicing chemicals tested, including $CaCl_2$, sodium formate, urea, and NaCl (*10*). CMA accounted for far less spalled concrete material than plain road salt in a 100-cycle test.

Chollar and Virmani found that salt ponded on concrete slabs caused rust-filled surface cracks to develop (*11*). Over time, cracks grew wider and deeper. CMA, on the other hand, showed no evidence of concrete cracking. Electropotential measurements of rebars embedded in concrete showed CMA-ponded specimens lie in the passive (noncorroding) range, whereas salt-ponded specimens lie in the active (corroding) range.

An interesting side effect of spreading CMA on roadways has been the observation by several state DOTs that CMA has a residual effect on concrete. That is, once CMA is applied to a roadway, it tends to be less susceptible to being washed away, so that subsequent applications need not be as frequent. A recent thesis published at Michigan Tech explains that CMA actually is absorbed into limestone and diffuses into some types of rock, thereby creating a reservoir of deicer in the roadway surface that is available at the next snowfall (*12*).

## CHEVRON'S CURRENT RESEARCH ON CMA

This part of the report is divided into three sections. Results of a 3-month planned interval test utilizing alternative immersion testing of plain carbon steel (ASTM A-36) in solutions of CMA and other deicers are summarized in the first section.

The second section concerns alternative immersion testing of a weathering steel commonly used for bridges (ASTM A-588). The weathering steel was subjected first to immersion in salt solutions and then to alternative deicers to determine the effect of deicers on precorroded bridge steels.

Results of subsequent electrochemical testing which was performed to further explore the corrosion phenomena observed in the immersion tests are summarized in the third section.

### Alternative Immersion Testing of Plain Carbon Steels

#### *Background*

A 3-month planned interval test was used to determine steel corrosion rates after longer-term exposure to solutions of Chevron CMA-based deicer and several other deicers. The advantage of such testing is that both the liquid corrosiveness and the metal corrosivity can be measured. Not only were corrosion rates determined, but pH, solution conductivity, corrosion potential, metal surface appearance, corrosion product composition, acetate concentration, and microbiological activity of Chevron CMA-based deicer also were measured.

In a planned interval test, samples are placed in test solutions for different durations and at different times as shown in Figure 1 (*13*). Comparison of the corrosion rates observed in the first month ($A_1$) with those in the third month (B) shows changes in the corrosiveness of the liquid. Comparison of $A_2$ (the corrosion rate of only the final month of the 3-month immersion) with B gives information on changes in metal corrodibility with time. Metal corrodibility is affected by such factors as corrosion product formation and other changes to the metal surface.

### *Procedure*

Six ASTM A-36 carbon steel coupons (½ × 4 × 1/16 in.) were hung from nylon rods and immersed in several different deicing solutions and distilled water at ambient temperature (Table 1) for 10 min, then raised into ambient air for 50 min. This cycle was repeated throughout the 3-month testing period using an automatic hydraulic system controlled by an electronic timer.

Corrosion potentials, conductivity, and pH of the solutions were recorded twice a week in each of the test solutions. Two samples from each solution were removed at the end of each exposure period (1, 2, and 3 months), and their corrosion rates determined. Corrosion products and scale on certain samples were analyzed.

### *Corrosion Rate Results*

Figure 2 shows average corrosion rates after 1, 2, and 3 months for each of the test solutions. The CMA-based products, and urea, showed low corrosion rates (less than 5 mpy)—about the same as water. By far the highest corrosion rate was that of pure salt (30–60 mpy); 10 percent Chevron CMA-based deicer or CMA added to salt solutions reduced the corrosion rate to about ⅓ that of NaCl alone.

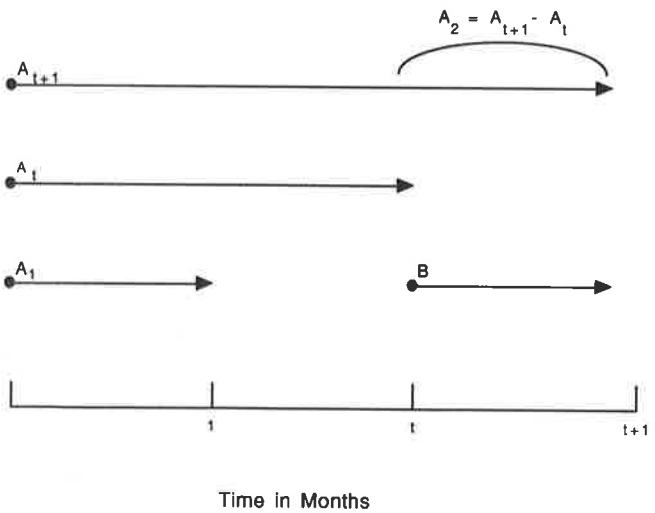


**FIGURE 1 Planned interval test design. Each arrow represents immersion of corrosion coupons in solution for duration shown ($t$ = 2 for 3-month test).**

**TABLE 1 Solution Chemistries for 3-Month Planned Interval Testing**

| Solution | Composition | Concentration |
|---|---|---|
| Water | Distilled Water | 100% |
| NaCl | Sodium Chloride | 3.5 wt% |
| Chevron CMA-Based Deicer | CMA-Based | 3.5 wt% |
| NaCl/Chevron CMA-Based Deicer | 9 g. Sodium Chloride<br>1 g. Chevron Deicer | 3.5 wt% |
| Reagant Grade CMA | 7 moles Mg Acetate<br>3 moles Ca Acetate | 3.5 wt% |
| NaCl/Reagant Grade CMA | 9 g. Sodium Chloride<br>1 g. Reagant Grade CMA | 3.5 wt% |
| Urea | Chevron Chemical Urea | 3.5 wt% |
| NaFo | Commercial Grade Sodium Formate | 3.5 wt% |

For the Chevron CMA-based deicer, some samples displayed a passive film with zero corrosion rate and underwent minimal active corrosion. There appear to be two stable corrosion potentials for CMA: one active with a corrosion rate of about 5 mpy, and one passive with zero corrosion. It is not statistically correct to average the corrosion rates in such cases. For this reason, only the nonzero (active) corrosion rate has been used in determining average corrosion rates. A more detailed explanation of the dual corrosion potential for CMA is given in the next section.

In most cases, average corrosion rate decreased with exposure time. Figure 2 shows that the highest corrosion rates generally occurred in the first month of testing. This could be a result of either a decrease in metal corrodibility or an increase in liquid corrosiveness. In most cases, it was found that metal corrodibility decreased over time. This is because scale formation tends to act as a barrier that decreases the availability of corrodent species at the metal surface.

A detailed analysis of metal corrodibility and solution corrosivity is beyond the scope of this paper, but interested readers can obtain more detailed information from the Chevron Materials Laboratory.

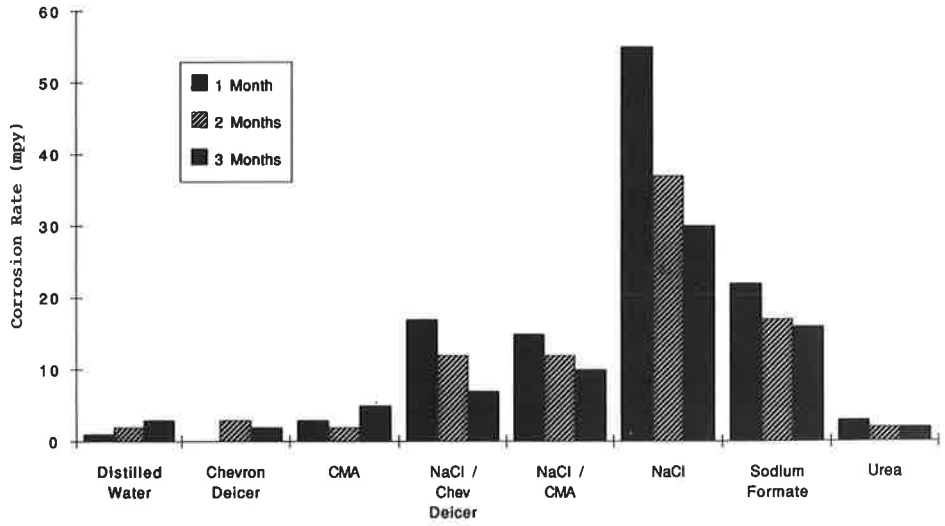


**FIGURE 2 Summary of results from A-36 carbon steel alternative immersion corrosion testing.**

*Corrosion Coupon Surface Analysis*

After a 4-week exposure, representative metal samples from each solution were cleaned per ASTM G1-88 and analyzed using a scanning electron microscope. Samples tested in NaCl were the most corroded. Chevron CMA-based deicer, CMA, and urea samples showed little surface attack. Surface appearances correlated well with the corrosion rates measured during the test.

*Corrosion Coupon Scale Analysis*

Scales from all samples were typically iron oxide and iron hydroxide corrosion products, such as $Fe_3O_4$ (magnetite) and various forms of FeO(OH). Precipitation deposits were also found in scales. Examples of this are $CaCO_3$ (calcite) in Chevron CMA-based deicer and CMA-containing solutions, and NaCl in salt solutions.

How the corrosion mechanisms for CMA-based solutions are affected by scale formation is described in the second section. As mentioned previously, the presence of scales can decrease metal corrodibility.

*Conclusions from Carbon Steel Tests*

- CMA-based solutions cause minimal corrosion (less than 5 mpy) to A-36 carbon steel, even when tested in alternative immersion conditions, which are more severe than constant immersion because of the ample supply of oxygen. Urea also showed minimal corrosion of A-36 carbon steel.
- Addition of 10 percent CMA or Chevron CMA-based deicer to salt lowered the corrosion rate to roughly that of plain salt (10 – 20 mpy for the mixtures versus 30 – 60 mpy for plain salt).
- CMA-based solutions show corrosion behavior that can be either passive, indicating zero corrosion, or active, which accounted for corrosion of about 5 mpy or less. Potentials can change from passive to active and back within the same test.

**Alternative Immersion Testing of Weathering Steels**

*Introduction*

For this test, ASTM A-588 weathering steel was chosen because it is commonly used on bridges because of its increased corrosion resistance.

The test was designed to simulate changes in corrosion phenomena that would occur if alternative deicers were applied to previously corroded and chloride-attacked bridge steel. Samples were thus first subjected to salt solutions and then to deicing solutions. To our knowledge, this is first time such a test program was carried out.

*Procedure*

The procedure for these tests was essentially the same as for those described in the previous section. Samples of weathering steel were immersed in ambient temperature solution for 10 min, followed by drying in ambient air for 50 min. The cycle was continued for the duration of the 6-week tests. For the first 2 weeks samples were immersed in salt solution; for the next 4 weeks samples were immersed in the same 10 deicing solutions and distilled water as in the previous section.

Samples were removed at various intervals, and corrosion rates were measured. Some samples were removed after just 2 weeks to determine corrosion rate in salt solution only; others were left in for 6 weeks to determine if corrosion rate was lowered after the switch from salt to alternative deicer.

A mixture of 10 percent Chevron CMA-based deicer and 90 percent NaCl was also tested following salt solution immersion to determine whether Chevron CMA-based deicer has inhibitor capabilities when added to salt on precorroded weathering steels.

*Results of Testing on Weathering Steels*

Figure 3 shows the results of tests on weathering steel. For simplification, only the final corrosion rates (those that occurred during the 4 weeks of immersion in deicing chemicals) are shown.

As anticipated, corrosion rates were highest for the samples exposed to NaCl only (about 28 mpy). As in the tests on carbon steel, CMA-based solutions (including reagent grade CMA and Chevron CMA-based deicer) performed the best, with corrosion rates dropping to 2 – 6 mpy.

Corrosion in urea was slightly higher in these tests (about 8 mpy), suggesting that for steel previously exposed to NaCl, urea does not slow corrosion as fast as CMA.

Corrosion rates in plain water were also significantly higher than in CMA solutions (about 9 mpy), showing that switching to alternative deicers such as CMA can limit further damage to steel previously exposed to chlorides. The corrosion rate for the 10/90 Chevron CMA-based deicer and NaCl mixture dropped to 12 mpy versus 28 mpy for the plain salt solution.

*Conclusions from Weathering Steel Tests*

- When applied to precorroded samples of weathering steel, CMA-based solutions reduced the corrosion rate to ⅕ to 1/10 that in NaCl solution after 4 weeks (3 – 6 mpy for the CMA-based deicers versus 28 mpy for plain salt).
- Addition of 10 percent CMA or Chevron CMA-based deicer to salt reduced corrosion by about half versus plain salt (12 mpy for the mixture versus 28 mpy for plain salt).

## Electrochemical Testing

*Summary*

Both the tests on carbon steel discussed in the first section and those on weathering steel discussed in the second section indicated the possibility that carbon steels were passivated in the presence of CMA-based solutions, such as the Chevron CMA-based deicer. To explore the mechanisms at work behind these two product types, electrochemical tests (potentiodynamic scans) were conducted on carbon steel (ASTM A-36) and weathering steel (ASTM A-588) in Chevron CMA-based deicer and in pure CMA.

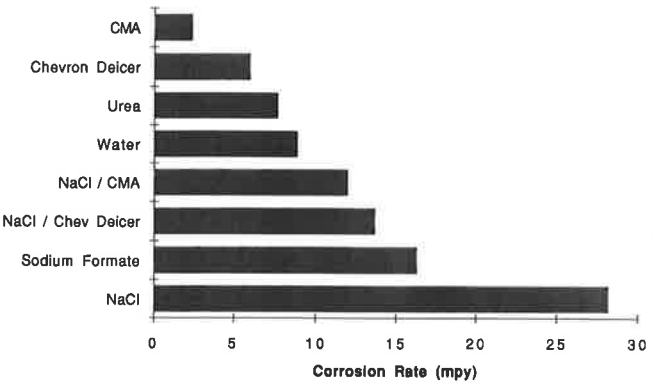


**FIGURE 3 Summary of results from A-588 weathering steel alternative immersion corrosion testing.**

*Procedure*

Potentiodynamic scans were run per ASTM standard G5. Test solutions of 3.5 wt percent concentration were made from pure CMA, Chevron CMA-based deicer, and salt. To ensure an oxygen concentration similar to that of the alternative immersion tests, air was bubbled through the solutions for 15 min before sample immersion. Solution temperatures were held at 30°C throughout the test using a constant temperature bath.

The working electrodes were machined from ASTM A-36 carbon steel and ASTM A-588 weathering steel. Surfaces were wet-sanded with 600 grit emery cloth, rinsed, dried, and stored in a desiccator for 1 hr before testing. Average surface area of several samples (4.55 $cm^2$) was used for consistency in calculations. The platinum auxiliary electrodes were cleaned with hot aqua regia and electrolyzed in 10 percent sulfuric acid. A saturated calomel electrode was used for the reference electrode such that all potentials can be referred to as versus standard calomel electrode (SCE).

Each sample was degreased with trichloroethane and rinsed with distilled water immediately before immersion in the test solution. After 1 hr of exposure, the rest potential (Ecorr) was recorded. Samples were cathodically cleaned by applying a potential of −800 mV (versus SCE) for 10 min. The potential was then swept through a range of −800 mV to 1200 mV (noble) at a rate of .6 V/hr and the corresponding currents recorded. To obtain a hysteresis effect, the scan was then run in the negative (active) direction. The potential was held at 1200 mV for 10 min, then driven from 1200 mV to −800 mV.

All data were collected and plotted using EG&G PARC Model 332 Softcorr Corrosion software. Calculations of corrosion rates by the Polarization Resistance and Tafel Extrapolation methods were also completed by the computer.

*Potentiodynamic Testing*

Potentiodynamic testing can be used to determine the behavior of metal in a corrosive solution. As it corrodes, the metal (anode) transfers electrons to the cathode. This reaction, being electrochemical, occurs at a given potential ($E$). The amount of corrosion is directly related to the number of electrons transferred. This, in turn, sets the corrosion current ($i$).

Metal in solution can be forced to change potential by supplying an additional current to the sample. When this process is done progressively, a graph of $E$ versus $i$ results (a potentiodynamic scan). The behavior of the metal during such a test typically takes one of two forms, as shown in Figure 4 (*14*).

In Curve A the corrosion current, and thus the corrosion rate, increases for every increase in potential. Such behavior is active, with corrosion of steel by NaCl being an example. Curve B, however, shows an increase in corrosion with an increase in potential up to a critical point, where the corrosion

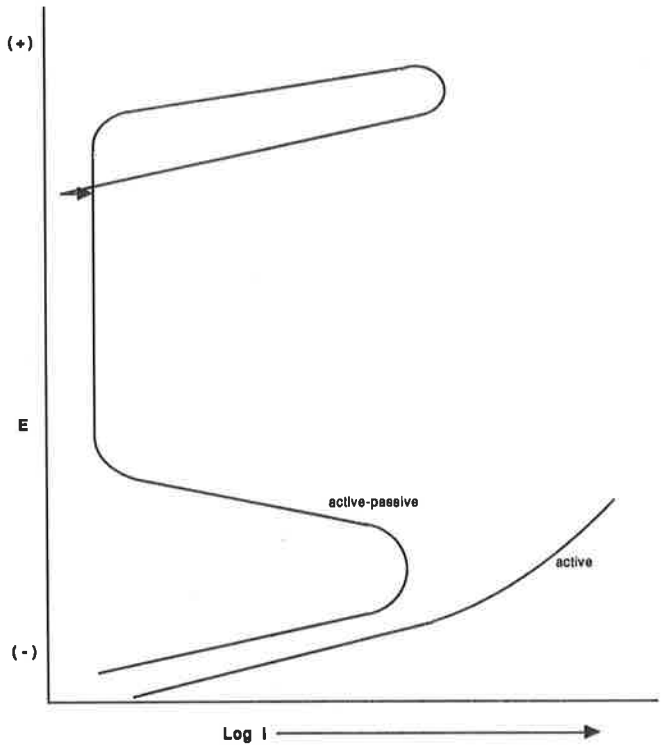


**FIGURE 4 Anodic polarization curves.**

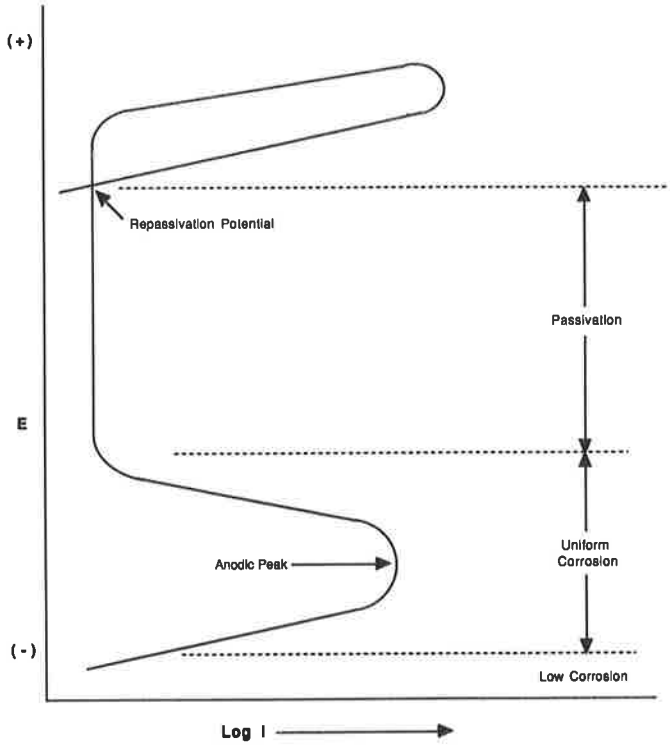


**FIGURE 5 Typical active-passive polarization curve, showing regions of varying corrosion rate and type.**

rate drops dramatically to a passive state. As $E$ is further raised, $i$ eventually increases again in a transpassive region.

Figure 5 shows a summary of the behaviors possible for a metal/solution combination that displays active-passive behavior (*14*). Active-passive behavior is typical of stainless steels that passivate by forming an adherent, protective chromium oxide scale that prevents future corrosion of the metal beneath.

Just as there is an anodic curve for the corroding metal anode, there is a corresponding cathodic curve for the cathodic metal area to which electrons are flowing. Figures 6 and 7 show some typical cathodic curves and the effect they have on the corrosion behavior of the metal (*14*).

In Figures 6 and 7, the curves on the left are true polarization curves. These curves represent the actual relationship of potential to current for the anode and for the cathode, if they could be separated. In the laboratory, potentiodynamic tests yield the experimental curves shown on the right. These curves measure net current only; wherever the cathodic and anodic curves intersect, the measured net current is zero because their signs $(+/-)$ are opposite. True corrosion current is determined by extrapolating the slopes of the anodic and cathodic portions of the experimental curve in the vicinity of the intersect point. The true corrosion current for any of the experimental curves is denoted by the bull's-eyes in Figures 6 and 7. A bull's-eye also denotes the true corrosion potential for any curve—the potential at which the magnitude of the anodic current equals that of the cathodic current, and the net experimental current becomes zero.

The complete shapes of the true polarization curves on the left can be surmised by analyzing the experimental polarization curves on the right. Figures 6 and 7 will be discussed later when actual tests with deicing products are evaluated.

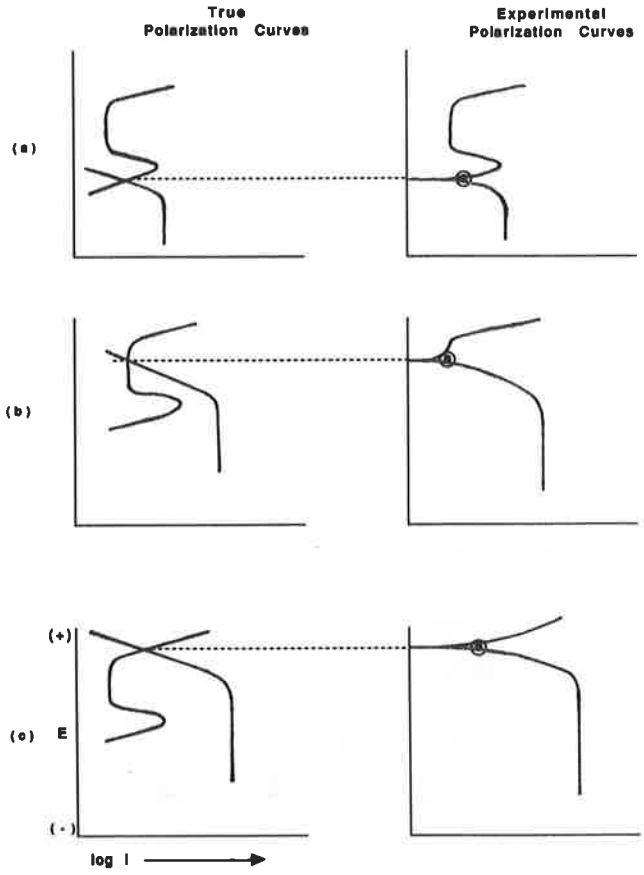


**FIGURE 6 Various shapes of experimental polarization curves caused by changing locations of anodic and cathodic curves.**

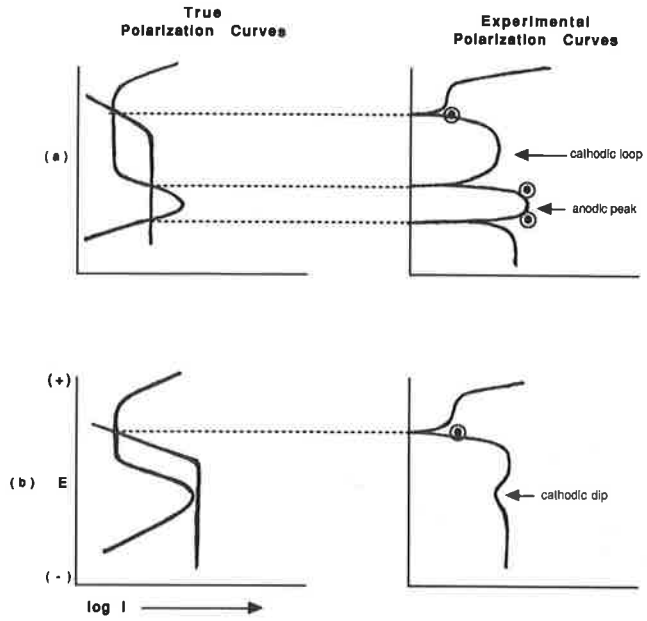


**FIGURE 7 When the anodic and cathodic portions of the true polarization curves intersect (or nearly intersect) in more than one location, the experimental curve is subject to so-called double loop behavior (a). This phenomenon has been seen for steel in Chevron CMA-based deicer.**

*Electrochemistry Results on CMA and Chevron CMA-Based Deicer Solutions*

All of the CMA-based products showed active-passive behavior (Table 2). The solid-line scan in Figure 8 is a forward potentiodynamic scan performed with A-36 steel in a 3.5 percent CMA solution, which shows active-passive behavior. The dashed line is a reverse scan showing three distinct stable (one metastable) corrosion potentials. This behavior has been referred to previously as double-loop behavior (*2*). The phenomenon is well known, as noted in Figure 7a, and is indicative of an unstable passive film (*14*).

In such cases, the metal may either be passive or actively corroding, corresponding to the highest and lowest intersection points where the anodic and cathodic curves meet. This explains the fact that some CMA-based samples tested in the past have shown no corrosion (passive), whereas identical samples in the same test container have shown corrosion of 2 – 5 mpy (active). This theory is supported by the fact that CMA showed a dual corrosion potential in electrochemistry tests. Measurements typically fell either between 0 and −200 mV, or between −500 and −700 mV.

Figure 9 shows how corrosion potential for CMA can be nearly equivalent to that for plain salt, whereas corrosion rate is an order of magnitude less. In Figure 9, $E_{NaCl}$ is about −650 mV, whereas $E_{CMA}$ is about −610 mV. These are representative of active potentials found in this study, which have been duplicated in other studies.

It is a fact that the corrosion rate for CMA is less than that for NaCl. This is because the corrosion current of CMA ($i_{CMA}$) is less than that of NaCl ($i_{NaCl}$). In Figure 9, for example, the corrosion current for CMA is about 5 uA/cm², whereas that for the salt solution is 10 – 50 uA/cm². This explains how

**TABLE 2 Results of Potentiodynamic Scans, 3.5 wt Percent Unstirred Solutions**

| Sol'n/Sample | Rest* Potential | E corr** | Corr. Rate | I cc uA/cm² | E cc | Pasv'n? |
|---|---|---|---|---|---|---|
| Chevron CMA-Based Deicer/ A588 | 192 mV | -554 mV<br>-550 mV | 2.7 mpy<br>2.7 mpy | Note 1 | Note 1 | yes |
| CMA 7:3/ A588 | -513 mV | -676 mV<br>-666 mV | 6.9 mpy<br>6.6 mpy | 1837 | -430 | yes |
| Chevron CMA-Based Deicer/ A588 | -75 mV | -322 mV<br>-326 mV | 0.86 mpy<br>0.16 mpy | 2.03<br>Note 1 | Note 1 | yes |
| CMA 7:3/ A36 | -700 mV | -705 mV<br>-696 mV | 6.0 mpy<br>4.3 mpy | 2378 | -480 | yes |

* Rest potential after one hour in solution.

** Potential where $i_{corr}$ equals zero (by computer).

Upper value calculated by Tafel Extrapolation method.

Lower value calculated by Linear Polarization method.

Note 1: Full passivation (anodic nose does not exist).

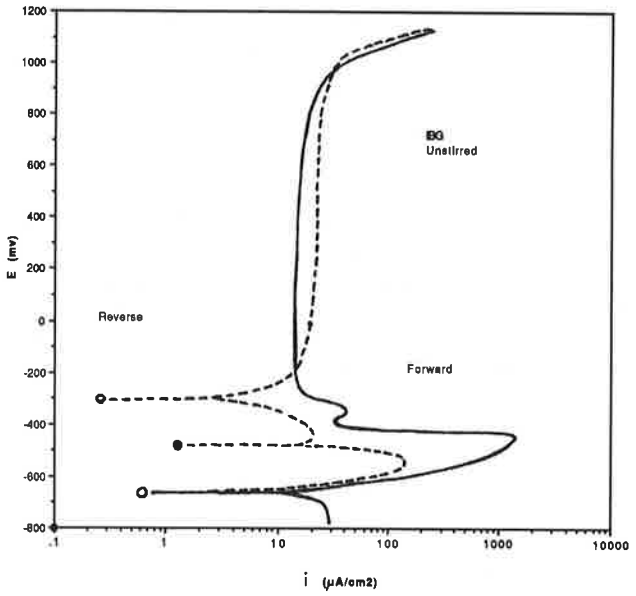


**FIGURE 8 Active-passive behavior observed in CMA solution with A-36 steel, typical of behavior exhibited by all CMA-based deicers on both A-36 and A-588 steels. The dashed-line reverse scan showing one metastable (●) and two stable (○) corrosion potentials is shown in Figure 7a and results from an unstable passive film.**

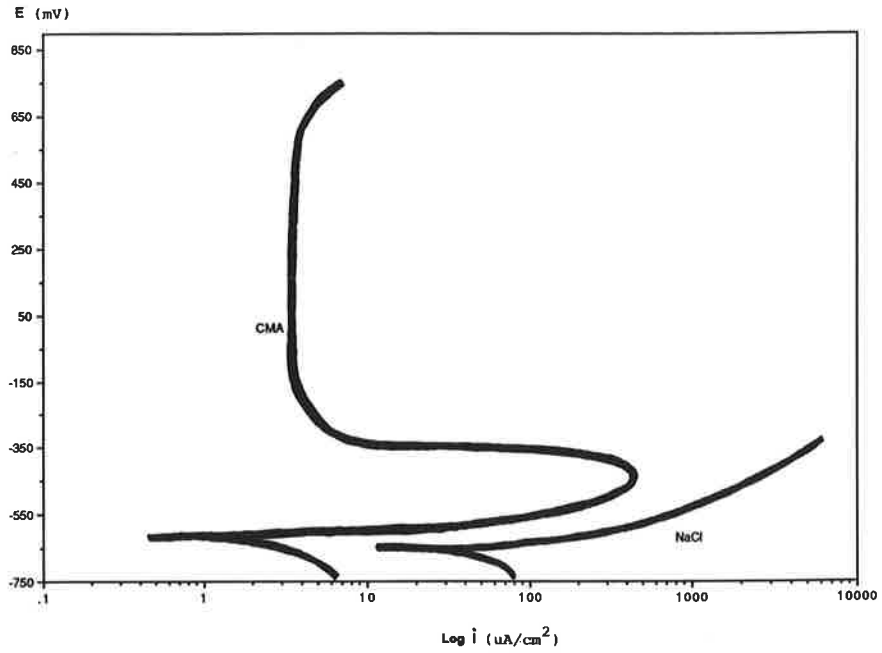


**FIGURE 9 Representative *E* versus *i* curves for CMA and salt solutions. Corrosion potential is similar, but corrosion current is significantly greater for salt solution. Both curves were generated using mild steel.**

measured corrosion rates for CMA-based solutions can be less than 5 mpy, whereas those for plain salt reach about 20 – 60 mpy.

For any solution it is the corrosion current ($i$), not the potential ($E$), that indicates corrosion rate. Because corrosion involves the transfer of ions and electrons from metal to solution, the amount of current generated is directly related to the amount of corrosion that is occurring. For alternative deicers, therefore, it is imperative that corrosion current be measured along with corrosion potential. Erroneous conclusions can be reached if corrosion potential alone is considered as a measure of corrosion rate.

As discussed earlier, Chevron CMA-based deicer can also display both passive and active corrosion behavior. Even in the active potential range, however, corrosion rates are exceedingly low. Table 2 presents corrosion currents for Chevron CMA-based deicer that are in the neighborhood of −300 to −700 mV. Although such a low potential indicates active corrosion, in the case of the Chevron CMA-based deicer, that active corrosion is occurring at the rate of only about 3 mpy—much less than the 20 – 60 mpy that has been typically measured for salt.

### *Conclusions From Electrochemistry Testing*

- CMA-based products (including Chevron CMA-based deicer) exhibit an active/passive behavior, causing identical samples in the same corrosive environments to show either passive corrosion or active corrosion with low corrosion rates.
- In CMA-based solutions passive behavior occurs at a corrosion potential of 0 to −200 mV with essentially no corrosion. Active behavior occurs at a corrosion potential of −500 to −700 mV and with corrosion rates of 2 – 5 mpy.
- Active and passive corrosion behavior can occur on identical samples in the same environment; this mechanism is understood and documented in the literature.
- Tests of alternative deicers should include measurement of both corrosion currents and potentials because it has been shown that corrosion potentials for CMA-based solutions can be similar to those for salt solutions, whereas measured corrosion currents and corrosion rates are markedly different.

## REFERENCES

1. C. E. Locke, and K. J. Kennelley. *Corrosion of Highway and Bridge Structural Metals by CMA*. Report FHWA-RD-86-064. FHWA, U.S. Department of Transportation, June 1986.
2. K. J. Kennelley, and C. E. Locke, Jr. Electrochemical Behavior of Steel in Calcium Magnesium Acetate. *Corrosion,* Vol. 46, No. 11, Nov. 1990, pp. 888–895.
3. R. L. McCrum. Corrosion Evaluation of Calcium Magnesium Acetate (CMA), Salt (NaCl), and CMA/Salt Solutions. NACE Corrosion '89, Paper 127, New Orleans, April 17–21, 1989.
4. T. Wieman, D. Komac, and S. Bigler. *Statewide Experiments with Chemical Deicers*. Washington State Department of Transportation, 1989.
5. W. J. Machowski, and F. F. Lyle, Jr. *Comparative Evaluation of Deicer Corrosion*. Project 06-2033-001. Southwest Research Institute, San Antonio, Tex., March 18, 1988.
6. D. S. Slick. *Effects of Calcium Magnesium Acetate (CMA) on Pavements and Motor Vehicles*. Report FHWA-RD-87-037. FHWA, U.S. Department of Transportation, April 1987.
7. M. C. M. Man, mL. KB. Hazell, and KR. P. Smith. On-Line Measurement of Simulated Reinforcement Corrosion in Concrete Under Action of De-Icers. In *Third International Symposium on Corrosion of Reinforcement in Concrete Construction, Society of Chemical Industry,* Elsevier Applied Science, New York, N.Y., May 1990.
8. Danish Corrosion Centre. *Effect of CMA on Corrosion Properties of Rebars in Concrete* (English translation). National Agency of

Environmental Protection, Copenhagen Airports, Ministry of Transport, Road Directorate. Copenhagen, Denmark, Dec. 1990.
9. R. L. McCrum and J. V. Heffernan. *Evaluation of United Salt's Corrosion Inhibitor Intended for Use with Sodium Chloride Deicing Salt.* Project 89 G-271. Michigan Transportation Commission, Lansing, June 1991.
10. A. Nadezhdin et al. The Effects of Deicing Chemicals on Reinforced Concrete. In *Transportation Research Record 1157*, TRB, National Research Council, Washington, D.C., 1988.
11. B. H. Chollar and Y. P. Virmani. Effects of Calcium Magnesium Acetate on Reinforced Steel Concrete. *Public Roads,* Vol. 51, No. 4, March 1988, pp. 113–115.
12. R. Valverde. *A Comparative Study of the Influence of CMA with Other Deicing Chemicals on Pavement Aggregates.* M.S. thesis. Michigan Technological University, April 1991.
13. M. G. Fontana *Corrosion Engineering* (3rd ed.). McGraw-Hill Book Co., New York, N.Y., 1986, pp. 163, 445–480.
14. E. L. Liening. *Electrochemical Corrosion Testing Techniques.* Dow Chemical Co., Midland, Mich., pp. 88–96.

*Publication of this paper sponsored by Committee on Corrosion.*